# Properties and application of PdCu membranes for hydrogen separation.

## Camilla Lindgren

# PREFACE

This thesis is submitted as the final part of the Master of Science Degree in Chemical Engineering (MTKJ) at the Norwegian University of Science and Technology (NTNU). It is a result of experimental work and study of literature. The scientific work was carried out over 20 weeks in the spring semester 2014.

First of all I would like to thank my supervisor Professor Hilde J. Venvik for the guidance and support during the work. The frequent meetings with discussion and follow up, and the fact that she is an enthusiastic supervisor, have been an appreciated motivation in this work.

Further I would like to thank co-advisor PhD. Nicla Vicinanza for all her help during the work. I would also thank SINTEF Materials and Chemistry in Oslo for the membranes that were studied in this work. At NTNU, many thanks to Karin Wiggen Dragsten for answering and helping with all my questions, big or small. Building the setup as fast as we did would not have been possible without Jan-Morten Roel, Mikael Hammer and Bendik Sægrov, thus I would like to direct a thank you to you as well.

I would also like to express my gratitude to Bengt Arild Johannesen for the collaboration during the work this semester. You have been very patience with me and our frequent talks have been invaluable. Finally I want to thank my fellow students, friends and family for the support during this work. Especially I would like to thank Jørgen Nordbø and Kaia Andersson Jenssen, this experience had not been the same without you.

I declare that this is an independent work according to the exam regulations of the Norwegian University of Science and Technology (NTNU).

Trondheim, June 27, 2014                                    Camilla Lindgren

# ABSTRACT

Hydrogen is one of the most important chemicals used in the industry today. The energy in hydrogen molecules can be converted into electric energy in fuel cells, and hydrogen is thus considered an energy carrier for the future. A membrane of palladium and certain Pd-alloys absorb and diffuse hydrogen in the solid, and give 100 % separation selectivity. Alloying palladium with silver leads to an increase in the hydrogen permeability, but pure Pd and Pd-Ag alloys are vulnerable for Co and sulfur poisoning which leads to reduced permeability. Membranes of palladium alloyed with copper are known to be more chemically resistant than pure Pd and Pd-Ag alloys and has thus received a lot of attention lately. They are also lower in costs. The main objective in this work has been to study the fundamental properties of the $Pd_{1-x}Cu_x$ membranes, such as hydrogen permeation and solubility. These properties depend on different factors as structure and composition of the alloy, the temperature and the total pressure difference over the membrane. The membranes used in this study are manufactured by SINTEF Materials and Chemistry in Oslo, by a sputtering technique.

Hydrogen permeance and permeability for $Pd_{1-x}Cu_x$ membranes in the range of 5.8 at% - 55.1 at% copper have been obtained upon stabilization under hydrogen and sweep gas, and under pure hydrogen and total differential pressure in absence of sweep gas. A significant part of this master thesis was building the setup where these experiments were performed. A trend of decreasing permeability with increasing copper content for the membranes was observed. However, the permeability is not constant for a specific composition. This could indicate that there are deviations in the microstructure due to the sputtering technique, and that impurities, time and contamination during the storages can influence the permeability

Hydrogen solubility through the $Pd_{1-x}Cu_x$ membrane was measured by volumetric chemisorption, and shows a decreasing trend with temperature and copper content. Moreover, the absorption isotherms showed a non-linear trend at high pressure, which increase with increasing copper content and it affects the reproducibility. This trend could be a result of the phases present in Pd-Cu alloys depending on the conditions and composition.

The lattice parameter of the $Pd_{1-x}Cu_x$ membranes was studied by X-ray diffraction, and was estimated to be lower than for pure Pd. This indicates that alloying Pd with Cu decreases the unit cell volume.

# SAMMENDRAG

Hydrogen er en av de viktigste kjemikaliene som er brukt i industrien i dag. Energien i et hydrogenmolekyl kan bli omdannet til elektrisk energi i brenselsceller, og hydrogen er derfor sett på som en energi bærer for fremtiden. Hydrogen absorberes og diffunderer gjennom membraner laget av palladium og noen spesielle palladium-legeringer, og gir 100 % selektivitet. Ved å legere palladium med sølv øker permeabiliteten av hydrogen, men både ren Pd og Pd-Ag legeringer er sårbare for CO og $H_2S$ forgiftning som fører til redusert permeabilitet. Membraner av palladium-kobber legeringer er kjent for å være mer kjemisk motstandsdyktige enn ren Pd og Pd-Ag, og har derfor fått mer oppmerksomhet i det siste. Denne legeringen er også billigere en rein Pd og Pd-Ag. Hovedformålet med denne oppgaven var å studere de fundamentale egenskapene til $Pd_{1-x}Cu_x$ membranene, slik som hydrogen permeasjon og løselighet. Disse egenskapene avhenger av ulike faktorer som membranens struktur og sammensetning, temperatur og total trykkforskjell over membranen. Membranene brukt i dette forsøket er av SINTEFF ved bruk av en sputtering teknikk.

Hydrogen permeansen og permeabiliteten for $Pd_{1-x}Cu_x$ membraner i området 5.8 at% - 55.1 at% kobber har blitt målt over stabiliseringen med hydrogen og sveipegass, og under ren hydrogen og et totalt differensialtrykk uten sveipegass . En vesentlig del av denne oppgaven har vært å bygge oppsettet som disse eksperimentene har blitt utført på. Det har blitt observert en synkende trend for permeabilitetene ved økende kobber innhold i membranene. Imidlertid er ikke permeabiliteten konstant for hver sammensetning. Dette kan indikere at det er avvik i mikrostrukturen forårsaket av sputtering teknikken, og at forurensinger, tid og kontaminering i løpet av oppbevaringen kan påvirke permeabiliteten

Hydrogen løseligheten gjennom $Pd_{1-x}Cu_x$ membranen ble målt med volumetrisk kjemisorpsjon, og viser en synkende trend i sammenheng med økende temperatur og kobber innhold. Absorbsjons isotermene viste en ikke-lineær trend ved høyt tykk, som øker ved høyere innhold av kobber i membranen. Dette kan være et resultat av fasene som er tilstede i Pd-Cu legeringer avhengig av betingelsene og sammensetningen, og det påvirker reproduserbarheten.

Gitterkonstanten for $Pd_{1-x}Cu_x$ membranene ble studert med røntgendiffraksjon, og var estimert til å være lavere enn for ren Pd. Dette indikerer at enhets celle volumet minker ved å legere palladium med kobber.

# CONTENT

Chapter 1

# INTRODUCTION

## 1.1 HYDROGEN PRODUCTION

Hydrogen is one of the most important chemicals used in the industry today. It is the raw material for both refining and petrochemical industry, and can be utilized in small- and large-scale energy applications. Hydrogen is not available in the nature, and from a cost and efficiency perspective large scale hydrogen production from natural gas is preferred. It is then normally produced by endothermic methane steam reforming at high temperatures. The main large-scale areas of application are the production of ammonia, the processing of petroleum, and the reducing processes in metallurgy. Another important application of hydrogen is as fuel for fuel cells vehicles and small combined heat and power systems. The energy in hydrogen molecules can be converted into electric energy in fuel cells, and hydrogen is thus considered an energy carrier for the future. The use of hydrogen in these kind of systems can reduce emission of the $CO_2$ generated compared to the fossil fuel based alternatives [1, 2].

The feedstock always has components as $CO$, $CO_2$, $H_2S$ and methane in it, and thus different production and separation technologies have been developed. They are applied to meet the requirements to hydrogen purity or gas mixture composition, depending on the application of the fuel cell. One of the most promising technology for efficiency improvements and costs reduction in the hydrogen production is the use of membranes with high hydrogen permeation and selectivity [2, 3].

Organic polymers are the most used materials in the membranes for gas separation today, but membranes of palladium alloys are also currently in use for gas separation. The polymeric membranes are not favorable at high temperature, which may be a requirement for the production of hydrogen, and the selectivity is moderate. Other membranes of inorganic materials have been developed in the last decade, but the market is small [4, 5].

## 1.2 PALLADIUM MEMBRANES

Palladium membranes and its alloys are known for its high hydrogen permeability and selectivity. They are one of the oldest membranes studied for separation applications and gas permeation. Membranes of palladium and certain Palladium-alloys absorb and diffuse

hydrogen in the solid, and thus give 100% separation selectivity. This gives a direct production of high purity hydrogen [2, 6].

There have been performed extensive studies on how palladium membranes can be used to purify hydrogen [1]. By alloying palladium with different elements, the phase transitions which occur in pure palladium at low temperatures, can be suppressed. Alloying palladium with silver leads to an increase in the stability and hydrogen permeability, but these alloys are vulnerable for CO and sulfur poisoning, which leads to reduced permeability [7, 8]. Membrane of palladium alloyed with copper has lately received attention because they are more chemically resistant than the classic palladium silver membranes, and they are also lower in cost [2, 6].

Palladium is expensive and the permeation of hydrogen decrease with increasing thickness of the membrane [1, 9]. SINTEF Oslo has developed a magnetron sputtering technique to produce thin (1-10$\mu$m) and dense palladium-based membranes [10, 11]. They have produced the membranes investigated in this work.

## 1.3 INDUSTRIAL APPLICATION

Palladium alloyed with silver is well studied [9, 12-15] and have a maximum permeability at ~23% of silver [12]. Reinertsen in collaboration with SINTEF are going to build a pilot plant for $CO_2$ capturing where these kinds of membranes are used. The membranes will capture the $CO_2$ and at the same time produce hydrogen. This is important progress for industrial use of the palladium alloy membranes.

## 1.4 SCOPE OF WORK

The permeation of hydrogen through palladium-based membranes can be measured in a micro dimensional reactor place in a hydrogen permeation setup. An important part of this work has been building a setup like this. Building a setup require a lot of planning and adjusting during the process.

The motivation for the rest of the work has been to learn more about the behavior of the Pd-Cu membranes. This has been done by investigating the permeation and solubility of hydrogen at different temperatures and concentration of copper in the alloy.

The permeability is assumed to be influenced by the grain structure of the membrane and some of the experiments have been done to investigate if XRD could be a usable characterization method.

There have also been done some solubility and XRD experiments on Pd-Ag alloys due to training and as a basis for comparison.

The results have been compared to literature and studies of Pd-Ag membranes done previously in this group [16, 17]. The comparing is manly done between the silver and copper alloys, since those are the most interesting alloys at the time and the Pd-Cu system has been the focus of this work.

Chapter 2

# THEORY

The hydrogen permeation through palladium based membranes follows a solution-diffusion mechanism in different steps, which all influence the rate of permeation [1, 18].
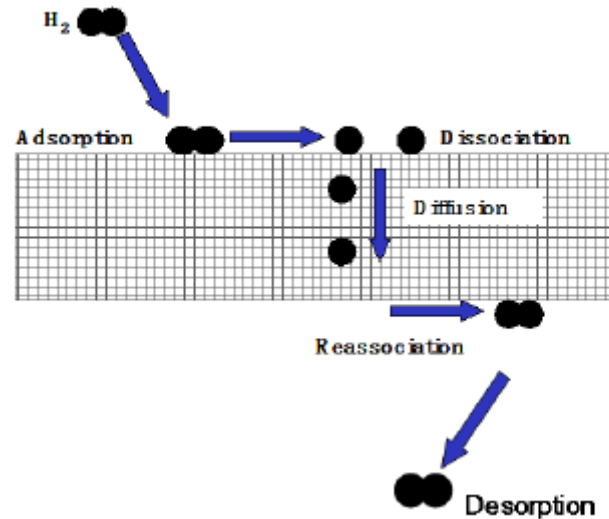


Figure 2.1 – Solution-diffusion transport mechanism [19]

Figure 2.1 shows the steps in the solution-diffusion mechanism from the high pressure side to the low pressure side [18, 19]:

- Gas diffusion from bulk gas to surface
- Dissociative adsorption of hydrogen onto the membrane surface
- Atomic diffusion of hydrogen through the bulk metal
- Re-association of atomic hydrogen to create hydrogen molecules
- Desorption of hydrogen from the surface to the bulk gas

The permeation rate may be limited by one of the steps, or by a combination if there is a substantial difference in the rates.

## 2.1 SIEVERTS' LAW

The steady-state flux is an important parameter that is used to quantify the transfer of hydrogen through the palladium-based membrane. The hydrogen flux ($J_H$) in mol/s m$^2$ can be expressed by Fick's law [20, 21]:

$$J_H = \frac{N}{A} = -D_H \frac{dC}{dx} \qquad (2.1)$$

where $N$ is the flow of hydrogen through the membrane, $A$ is the membrane area, $D_H$ is the diffusion coefficient and $dC/dx$ is the hydrogen concentration gradient through the membrane. The flux can be generalized by integration over the thickness, $t$:

$$J_H = \frac{D_H}{t}(C_1 - C_2) \qquad (2.2)$$

where $C_1$ and $C_2$ is the concentration of hydrogen at the retentate (high pressure) and permeate (low pressure) side respectively. This can also be expressed by the following expression:

$$J_H = \frac{P_H}{t}(p_1{}^n - p_2{}^n) \qquad (2.3)$$

where $P_H$ is the hydrogen permeability. The partial pressures are expressed by $p_1$ and $p_2$, on the retentate and permeate side respectively. The factor $n$ is the dependence factor of the $H_2$ flux on the $H_2$ partial pressure, generally in the range of $1 \geq n \geq 0.5$. It is determined from the rate-limiting step of the transport mechanism described in Figure 2.1 [9, 18, 22]. The permeability, $P_H$, is described as the product of the diffusion coefficient, $D_H$, and the Sieverts constant, Ks,:

$$P_H = D_H \cdot K_s \qquad (2.4)$$

where Sieverts' constant is in mol/m$^3$Pa$^{0,5}$. The diffusion coefficient is expressed by [9]:

$$D_H = D_0 \exp(-\frac{E_a}{RT}) \qquad (2.5)$$

where $D_0$ is a pre-exponential factor, $E_a$ is the activation energy for diffusion, $T$ is the temperature in Kelvin and $R$ is the universal gas constant in J/K mol.

If the bulk diffusion is the rate-limiting step, the hydrogen concentration, $C_H$, is proportional to the square root of $H_2$ pressure in gas phase. This is the case when the equilibrium is reached between the $H_2$ molecules in the gas phase and hydrogen atoms at the gas/solid interphase. At these conditions will the $n$-value be set to 0.5 [1, 18]. Then the hydrogen concentration can be expressed by Sieverts' law:

$$C_H = K_S p_{H_2}{}^{0,5} \qquad (2.6)$$

This equation is only valid for a very low value of *n*, which is the case at low pressure and for relatively thick membranes. Hydrogen-hydrogen interactions within the palladium bulk are not negligible at high pressure, and the surface-reactions will be the rate-limiting step for thinner membranes. The value of *n* will then increase towards one, 1, [1, 18].

## 2.2 THERMODYNAMICS

The molar enthalpy, $\Delta H°$, and the standard molar entropy, $\Delta S°$, of desorption gives an expression of the temperature dependence of the Sieverts' constant, $K_s$ [23]:

$$lnK_S = -\frac{\Delta H°}{2RT} + \frac{\Delta S°}{2R}$$ (2.7)

under the assumption of low hydrogen content in the lattice. Equation 2.7 express that the solubility is inversely proportional to the temperature.

The hydrogen permeability and solubility depend on the copper content in the alloy and the alloy crystal structure. The thermodynamics of the Pd-Cu system and system and Pd-Cu-H has been well investigated [24-27]. Phase diagrams for the systems are plotted using thermodynamic data in comparison with experimental data. Figure 2.1 is an example of a phase diagram of a Pd-Cu system, were an ordered body-centered cubic (bcc) B2 phase is formed at low temperatures and Cu concentrations in the range 35-75% [26].
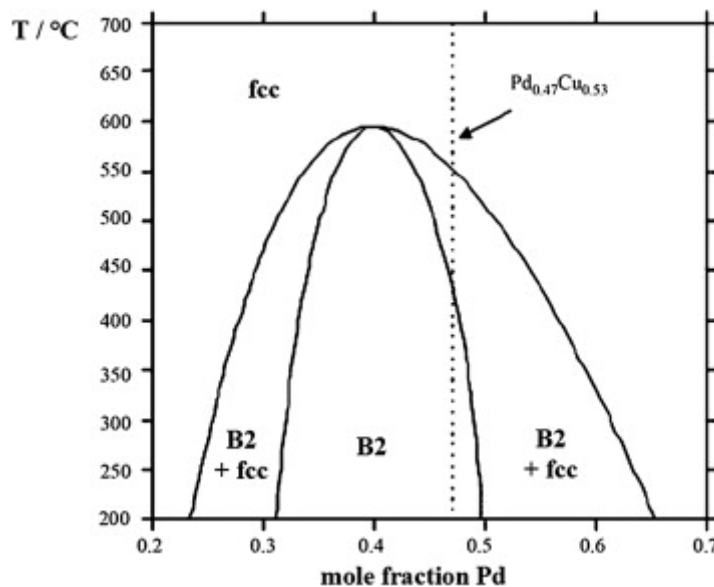


Figure2.1 - Phase diagram of the Pd-Cu system, were B2 refers to bcc phase [26].

As the figure describes can both the body-centered (bbc) and the face-centered (fcc) cubic phase occur in the Pd-Cu alloys at different conditions and concentrations. The fcc structure occurs below 600℃ at low concentrations of Cu (α-phase) and the bbc phase occurs in alloys in the range of 30-60% of Cu (β-phase). In alloys with a copper content of 25-30% and 50-60% do the phases co-exist [28-32].

The system described in this figure does not take the hydrogen interactions into consideration. That is done by combining experimental investigation, first-principles calculations and thermodynamic modeling by Weiming et al [24]. They study the hydrogen interactions with the $Pd_{x-1}Cu_x$ B2 alloys through the thermodynamic modeling of binary Cu-Pd, Pd-H, Cu-H and ternary Cu-Pd-H systems [24].

## 2.3    EXPERIMENTAL METHODS

### 2.3.1 Magnetron sputtering technique

The membranes studied in this work were created by magnetron sputtering, which is a technique that is used to grow thin films [10, 11]. Figure 2.2 shows a schematic overview of the magnetron sputtering process.
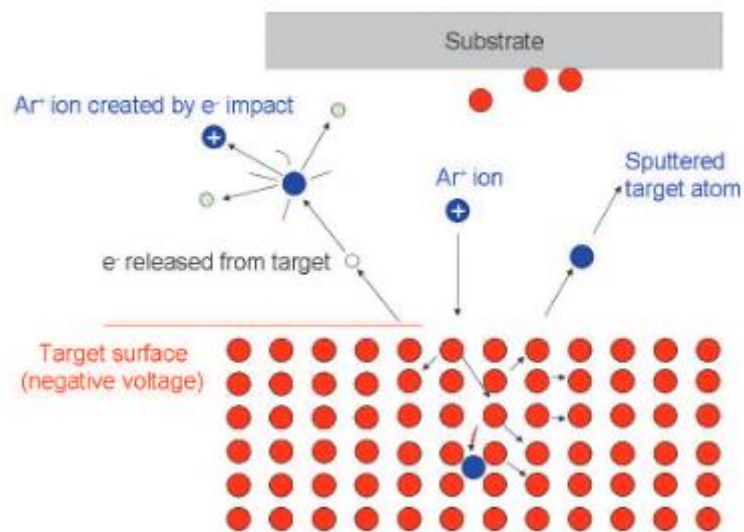


Figure 2.2 - Schematic presentation of magnetron sputtering [33].

An inert gas, usually argon, is ionized by a strong potential difference in the gas, and plasma is created. The ionized gas is accelerated towards the target by the potential difference, and the target atoms are ejected. Then they condense to the substrate, were they grow into a continuous film after some time. The target electrons are also ejected and collide with the gas

atoms. The gas atoms are ionized and the plasma maintains [33, 34]. These technique gives a homogeneous film with controlled thickness from multi-component targets, such as palladium alloys [35]. The thickness can be predicted and manipulated by controlling the sputtering time, and it is deducted that the maximum variation of the membrane thickness on the wafer is 10% [10, 11].

The side of the membrane which is facing the target during the preparation is called the growth/feed side of the membrane, while the other side is called the substrate/permeate side.

This technique is used by SINTEF Oslo and makes it possible to easily remove the membrane from the wafer. Then the film can either be used self-supported or transferred onto a membrane support. The membrane support can have different pore size, geometry or size. This gives a wide range of configurations, scale and conditions, which each have their strength and weaknesses [10, 35]. The silicon wafer has monocrystal line structure with a very smooth surface, and was used as the substrate in the membranes studied in this work [11]. The film was removed from the wafer before examined.

### 2.3.2 Volumetric chemisorption

Volumetric chemisorption is used as a method for characterization of catalyst particles by selective chemisorption of gases by absorption isotherms. The selective chemisorption measure the accessible catalytic component on the surface by noting the amount of gas that absorb per unit weight of catalyst. The absorption isotherm is derived by measuring the amount of absorbed gas on a sample under increasing pressure, while the temperature is maintained constant [36]. In this work, the equilibrium sorption technique is applied to measure the amount of hydrogen dissolved in the Pd-alloy films.

The temperature is measured with a thermocouple attached outside the glass reactor close to the sample. Inert gas, as helium, is used to measure the free space in the sample tube before the measurements with adsorptive gas. A schematic volumetric apparatus is shown in Figure 2.3. $V_1$ and $V_2$ are known volumes, respectively reservoir and sample tube volume. A, B and C are valves that regulate respectively outlet of vacuum, gas flow from tube and hydrogen gas inlet.
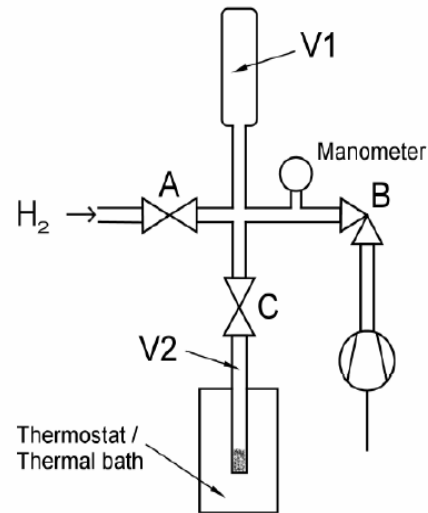


Figure 2.3 – Schematic representation of a volumetric sorption apparatus [31]

The gas will adsorb by dissolution on the sample surface and then absorb in the bulk of the sample. The pressure is monitored and noted when the equilibrium is reached. The absorbed amount of gas is recorded in a stepwise increase in pressure and subsequent equilibrium pressure. The hydrogen uptake can be calculated from [37]:

$$\Delta n = n_i - n_f \qquad (2.8)$$

where $n_i$ is the initial hydrogen amount in the reservoir volume and $n_f$ is the final content of hydrogen in the gas phase. The amount of hydrogen absorbed can be expressed by using the universal gas law [37]:

$$\Delta n = \frac{P_i V_i}{RT} - \frac{P_f (V_1 - V_2)}{RT} \qquad (2.9)$$

where $P_f$ is the final pressure recorded when equilibrium is reached, $R$ is the universal gas constant and $T$ is the temperature. To obtain an isotherm is the process repeated with successive gas expansions for increasing $P_i$. This gives an absorption isotherm were the hydrogen concentration can be expressed by Sieverts' law in equation 2.6.

## 2.3.2 X-ray diffraction

X-ray diffraction (XRD) can be used to determine the sample structure, phase composition and to obtain an indication of the particle size. The crystalline phases inside the membrane can be determined by the means of lattice structural parameters. The XRD technique is based on the observation of how the crystalline atoms cause an incident X-ray beam to diffract in different directions. The diffraction occurs in a periodic lattice and the scattered X-rays that are in phase give a constructive interference [21, 26, 38]. This is satisfied for the so called Bragg's law [38, 39]:

$$sin\ \theta = \frac{\lambda}{2d_{hkl}} \tag{2.10}$$

where $\lambda$ is the wavelength of the X-rays, $d_{hkl}$ is the interplanar distance between two lattice planes, *hkl* are indices for the lattice plane and $\theta$ is the angle between the incoming X-rays and the normal to the reflecting lattice plane, as can be seen in Figure 2.4.
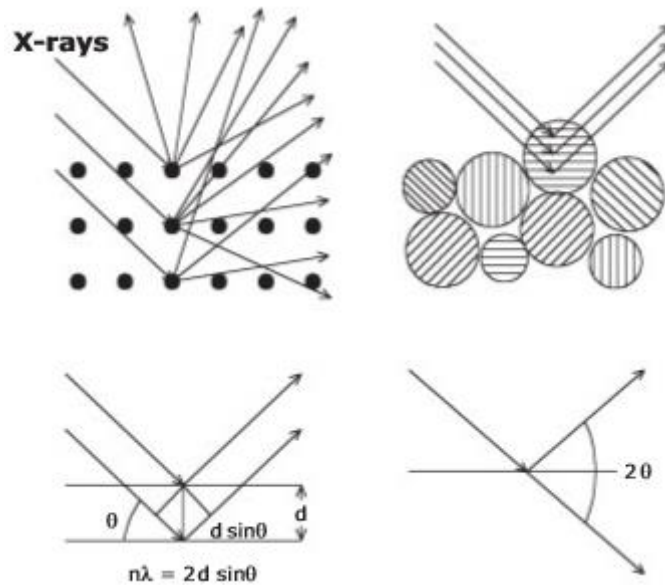


Figure2.4- Schematics of the working principles of Bragg's law, XRD [21]

The top Figure 2.4 shows X-rays scattered by atoms in the ordered lattice at the left side, and the situation if the sample is a polycrystalline powder on the right. The figure at the bottom shows at the right side the incoming X-ray beam and the diffracted beam. The left one describe the Bragg's law for one plane direction of the crystal.

The area of sample illuminated by the divergent primary beam is increasing with the diffraction angle, if the slits are constant. The slit can also be variable and the area illuminated will then be constant [40]. The transmission geometry describes this, and it is shown in Figure 2.5. This gives a diffractogram with Braggs peaks that can be analyzed. Pd and Pd-alloys planes are known to show a preferential orientation with (111) tending to orientate in parallel to the film surface [41]. Diffraction intensities from crystalline planes that are non-parallel to the film surface is studied in [42].



Figure 2.5 – Representation of the Bragg-Brentano and transmission geometries [43].

The interplanar spacing in cubic materials is given by the general equation [38]:

$$d_{hkl} = \frac{a_0}{\sqrt{h^2 k^2 l^2}} \qquad (2.11)$$

where $a_0$ is the lattice parameter that can be calculated from Bragg's law [38]:

$$a_0 = \frac{\lambda \sqrt{h^2 k^2 l^2}}{2 sin\theta} \qquad (2.12)$$

Chapter 3

# EXPERIMENTAL

The risks related to the experimental work were evaluated and a risk assessment for the membrane apparatus and the chemisorption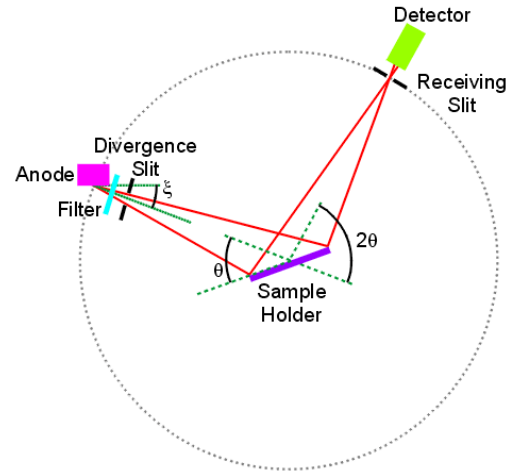 instrument are included in Appendix A. The main risks in this work are leakage, fire and exposure to toxic, flammable and explosive gas, such as CO and $H_2$. The setup is placed in a closed and ventilated glass cage in a chemistry hall. Both the closed cage and the chemistry hall have gas detectors at different levels to detect any leakage. The highest level of gas detector is directly connected to the fire department. The pipes were also manually checked before and during the experiment with soap solution and a hand held detector to detect leakage. The XRD instrument was operated by the responsible for the instrument, and thus it is no major risk associated with the experiment.

## 3.1 PALLADIUM ALLOY MEMBRANES

The membranes studied in this work were made by a magnetron sputtering, described in section 2.3.1, by SINTEF Materials and Chemistry in Oslo [10, 11]. Membranes with different concentrations were analysed, both palladium alloyed with silver and copper. A sample directly pulled off from the silicon wafer is referred to as an *as-grown* sample, and these have been applied for the sorption- and XRD experiments. The membranes examined are listed in Table 3.1.

Table 3.1 - Investigated samples of palladium alloys.

| Alloy | Concentration | Thickness [µm] | Sample |
|-------|--------------|----------------|--------|
| Pd-Ag | 23 wt% Ag | 6.0 | P1 |
| Pd-Ag | 23 wt% Ag | 8.5 | P2 |
| Pd-Ag | 23 wt% Ag | 2.2 | X1 |
| Pd-Ad | 23 wt% Ag | 4.0 | X2 |
| Pd-Ad | 23 wt% Ag | 10.0 | X3 |
| Pd-Cu | 5.8 at% Cu | 2.2 | T1 |
| Pd-Cu | 40.5 at% Cu | 2.1 | T2 |
| Pd-Cu | 5.8 at% Cu | 2.2 | S1 |
| Pd-Cu | 16.8 at% Cu | 1.7 | S2 |
| Pd-Cu | 20.7 at% Cu | 1.8 | S3 |
| Pd-Cu | 36.9 at% Cu | 2.0 | S4 |
| Pd-Cu | 40.5 at% Cu | 2.1 | S5 |
| Pd-Cu | 55.1 at% Cu | 2.1 | S6 |

## 3.2 HYDROGEN PERMEATION MEASUREMENTS

### 3.2.1 Microchannel housing configuration

A sketch of the microchannel housing for the permeation experiments is given in Figure 3.1.
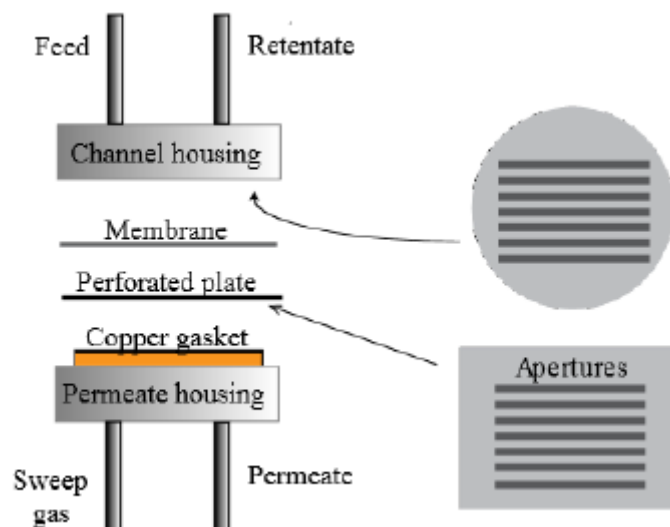


Figure 3.1 – The configuration of the microchannel housing.

The configuration  include the channel housing (feed housing) and permeate housing of stainless steel, a stainless steel plate and a copper gascet, which all were polished by silicon carbide grinding paper and cleaned in methanol befor mounting the membrane. The samples were removed from the silicon-wafer with a scalpel and scotch tape before placed in the microchannel configuration. A detaild mounting procedure is given in Appendix B.

The feed housing contains seven feed channels for gas flow corresponding to a total active surface area of 0.91 $cm^2$. The steel plate has the same configuration, and the membrane is placed between these two parts as shown in Figure 3.1. The permeate housing is an open stainless steel house. The feed side of the membrane is exposed to gas and the permeate side is facing the low pressure side of the membrane during the permeation. The growth side of the membrane is decided to face the feed stream. This is to have a consistency in the result and to be able to compare it to previous work done on similar membrane configuration.

### 3.2.2 Permeation setup

The microchannel housing was placed in a furnace in the hydrogen permeation setup. The setup is shown in Figure 3.2, and a list over the elements and a flow diagram for the setup in respectively Figure 3.3a) and b).



Figure 3.2 – The experimental setup.



Figure 3.3a) – Flow sheet symbol list.

Figure 3.3b) Flow sheet for the hydrogen permeation setup.

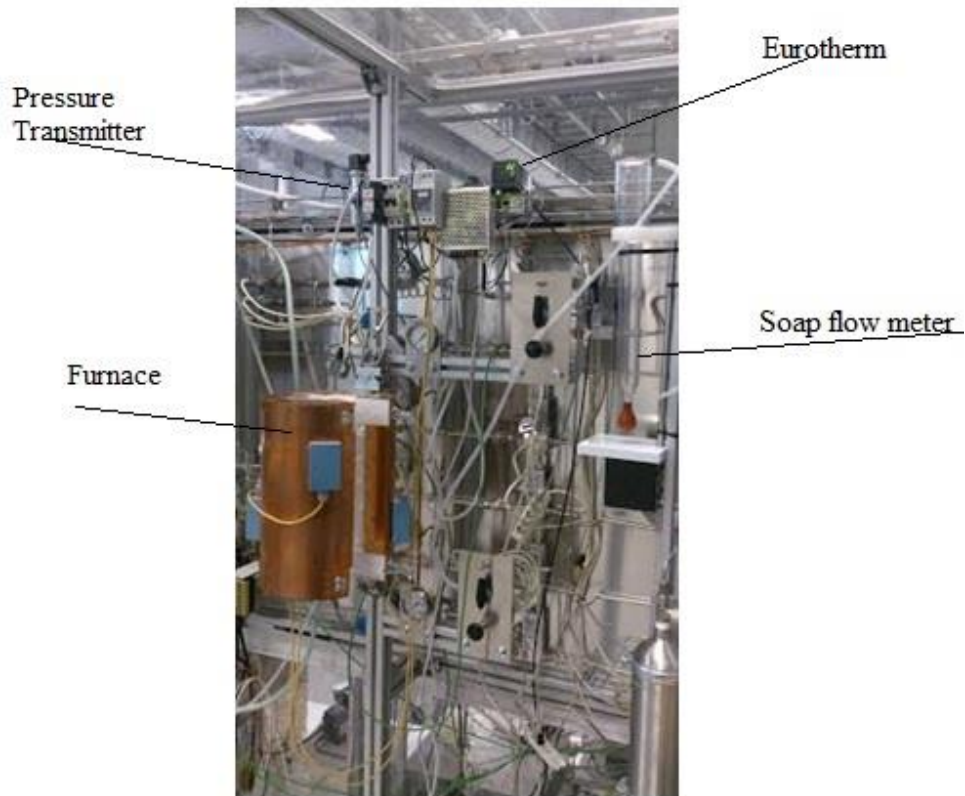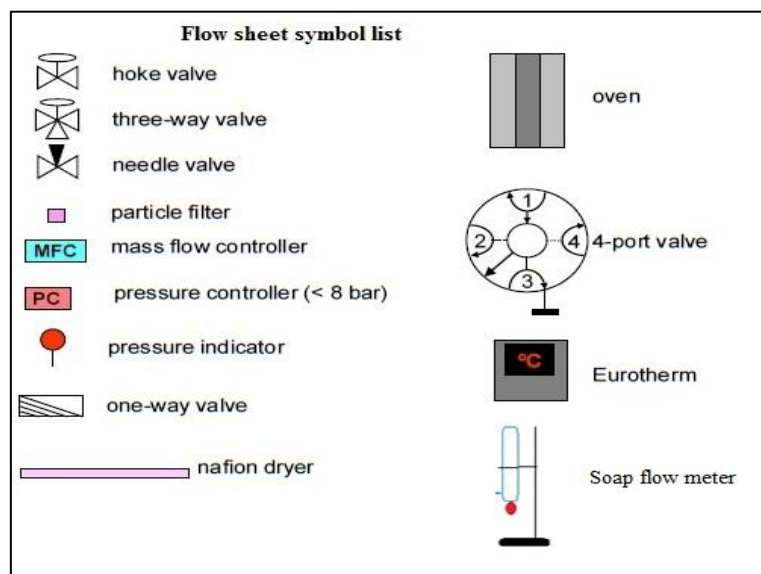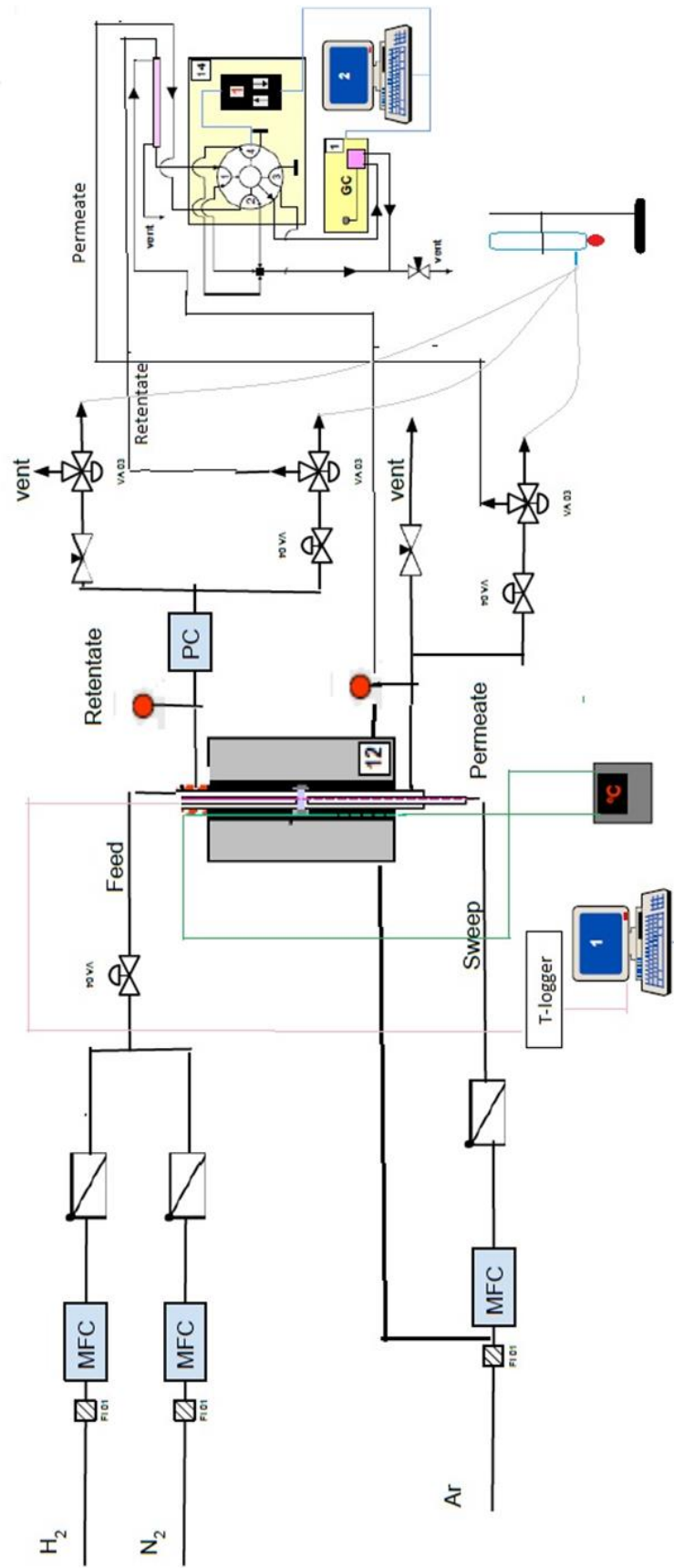The gas flow were controlled by mass flow controllers (MFC) and measured with a soap flow meter. Each gas has a specific MFC, which were calibrated with the soap flow meter. The calibration curves are given in Appendix C. The soap flow meter measure the time a soap film is using between two points in the flow meter, and determines the gas flow rate. Although the distance in the flow meter is fixed can the time taken vary from one observation to another. Thus the human error is approximately ±3%, based on standard deviation calculations. To make the error as small as possible is a mean value calculated from 3-5 time measurements at each point.

The temperature in the furnace is regulated by a K-type thermocouple and the eurotherm. An N-type thermocouple is connected to the computer, to monitor the temperature in the furnace. The K-type thermocouple is placed in the furnace near to the configuration while the N-type is placed as close to the membrane as possible. The N-type thermocouple is used to monitor the temperature, and is used because it measures the temperature more precisely than the K-type and it can be placed closer to the membrane.

A Micro-GC (Agilent), equipped with four columns, was used to detect leakage through the membrane before and during the experiment. Only one of the columns is used for this experiment to detect leakage in the membrane. Channel 1 (MolSieve) has argon as carrier gas and can detect nitrogen, which indicates a broken membrane. The sample speciesare separated and then quantified in the Micro-GC to find the relative amount of each gas component in the mixture. Different species desorb at different times, which gives the quantification based on the different thermal conductivities [44, 45]. The Micro-GC did not need further calibration than done by previous users of the setup, and this channel [9, 31].

### 3.2.3 Hydrogen stabilization

The permeation experiments, to study the behavior of $Pd_{x-1}$-$Cu_x$, were done with different settings as temperature variations, sweep gas and pressure difference. The exact approach for the experiment varies from membrane to membrane because of the difference in the behavior, but the overall procedure was the same.

The membrane was first exposed to nitrogen (purity 99.999%) and argon (99.999%), on the feed side and on the permeate side respectively, while the furnace was ramped, 2℃/min, to the initial temperature. Hydrogen (purity 99.999%) was introduced after reaching a

temperature at 300 ℃. Hydrogen is first introduced at this point to suppress potential phase transitions of the alloys during ramping. Then the membrane was exposed for a feed of 360Nml/min hydrogen and 40Nml/min nitrogen, and a sweep gas of 200Nml/min argon.

The flux through the membrane was measured with the soap flow meter, and monitored over time. The flux of hydrogen was first stabilized at 400℃, 350℃ and then 300℃. The flux was then measured at 400℃ again before nitrogen and argon were slowly removed. Feeding pure hydrogen with no sweep gas applied, a pressure difference was introduced. A differential pressure at max 2 bar was applied at the feed side while the pressure at the permeate side was left at atmospheric pressure. The flux of hydrogen was then studied at various differential pressures in the range from 0.5 bar to 2 bar depending on the membrane. After the pressure measurements were nitrogen and argon again introduced and the temperature raised to 400℃, before measuring the flux once again.

## 3.3 BUILDING THE SETUP

As described in in section 3.2.2 the hydrogen flow was measured directly by using a microchannel membrane module paced in an experimental setup. The configuration of this module and the setup are described in the same section and shown in detail in Figure 3.1-3.3. A significant part of this master thesis was building a separate setup on the same rig as earlier experiments have been performed [9]. This new setup was intended simple experiments, while introducing more complicated gas mixtures to the membrane could be done at the already existing setup. Thus the new setup have the possibility for hydrogen and nitrogen going in on the feed side and argon as sweep gas on the permeate side.

In the planning phase were the setup sketched and it was decided which units that should be included. Some of the units were collected from other setups, not in use at the time, and some new units had to be ordered. The units are listed in Table 3.2.

Table 3.2 – List of Units and how they were obtained

| Unit | |
| --- | --- |
| MFC Hydrogen | Ordered new |
| MFC Nitrogen | Borrowed from another setup |
| MFC Argon | Already existing on the rig |
| Pressure Controller | Borrowed from another setup |
| | (did not work as desired) |
| Pressure Transmitter | Ordered new |
| Pressure indicator | Ordered at the workshop |
| Eurotherm | Borrowed from another setup |
| N-type thermocouple | Already existing on the rig |
| K-type thermocouple | New, but in house |
| Stainless steel tubing | |
|     of different kind | Workshop storage |
| Valves of different kind | Workshop storage |
| Swagelok fittings | Workshop storage |
| Soap flow meter | Already existing on the rig |
| Furnace | New, but in house |
| Particle filter | Workshop storage |

The workshop did the mechanical work and was consulted in how to design the setup in the best way. Gas lines for the new setup were built from a split of the already existing gas lines at the rig. This was done at the same time as the main gas lines at rig were connected to the central gas system instead of bottles. Thus the pipelines were already evacuated and the new lines were built. The new lines were separated from the existing setup with a simple valve, so both setups could operate at the same time without interference.

The existing setup was not operating while the workshop did the mechanical work, due to safety reasons. Thus the planning of the work was important so the building in the glass cage could be done as efficient as possible. Nevertheless some minor problems occurred during the building, but new plans were worked out and fixed in the setup. An example was the system of options around the ventilation, bubble flow and Micro-GC. In the first drawing there was a lack of options, but at the finished setup this is a complex area with a lot of possibilities for directing the gas flows and manipulating pressure differential.

The digital communication at the rig was controlled from the computer in Labview, and the control units for the new setup had to be connected to the program. The connecting and programming had to be done by engineers with a general knowledge about electricity and data communication. The print screen of the operating central for the new setup in Labview is given in Figure 3.3.
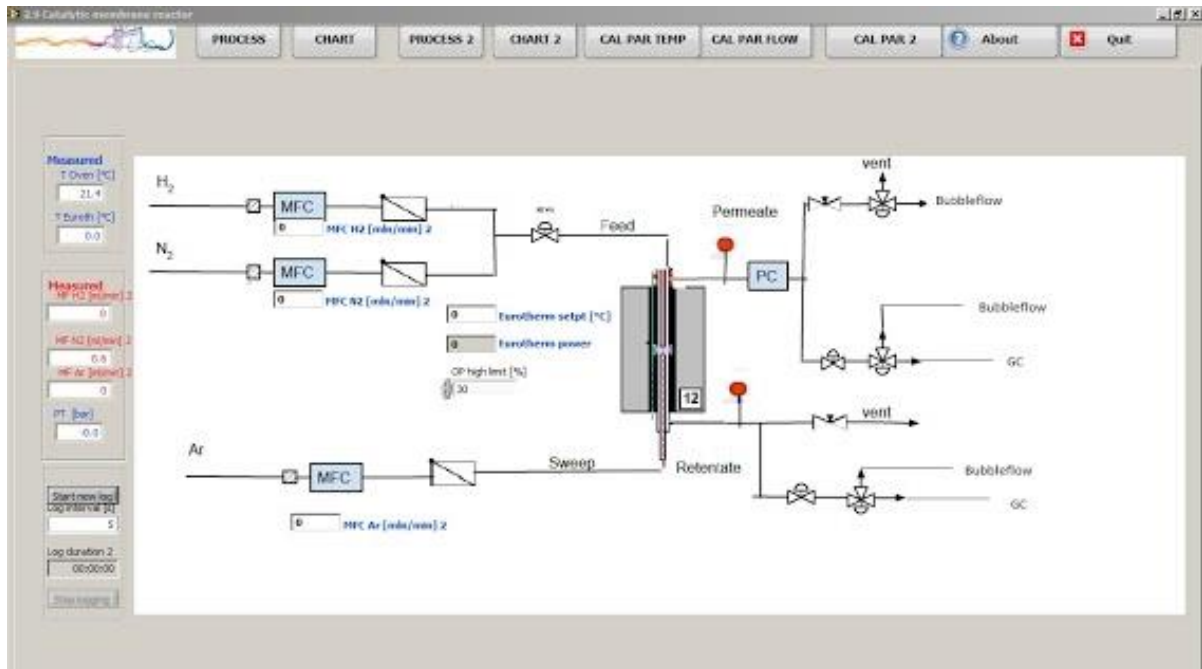


Figure 3.3- Print screen of operating central in Labview

The figure shows the gas flow, the measured parameters and where to type in wanted conditions. There are some deviations between the graphic representation and the actual apparatus that should be corrected in the future. For instance permeate flow and retentate flow is switched and the pressure controller was replaced with a pressure transmitter at a later point.

The testing of the digital communication started when the setup was built and all the control units connected to Labview. One of the mass flow controllers needed a new housing before the connection worked, but there were no further problems with the MFC's so they were calibrated and the correction parameters included in the program. The pressure controller did not work as desired when it was tested. The pressure could be set from the program, but it did not measure and return the actual pressure. It was then decided to order a pressure transmitter

instead. It could not control the pressure, but this was enabled by a needle valve. The pressure transmitter was installed instead of the pressure controller. At last the setup was pressure tested with inert gass.

The digital communication between Labview and the Eurotherm was not functional, but the Eurotherm is a separate unit that not needs to be connected for its use. The connection would have been practical, but is not essential. So due to the limited time it was decided to use the manual function at the Eurotherm, which worked perfectly. It was programed in the same way, with the same parameters as the one on the existing setup. The K-type thermocouple did therefore only communicate with the Eurotherm. The N-type thermocouple was connected to Labview and worked as it should, showing the temperature in the furnace close to the membrane.

## 3.4 SORPTION EXPERIMENTS

The measurements of the equilibrium sorption were carried out by using an ASAP 2020 Chemisorption Analyzer produced by Micromeritics Instrument Corporation.

### 3.4.1 Sample preparation

The membranes that were used for the measurements were removed from the silicon-wafer with a scalpel and tweezers. The experiment was carried out in a glass reactor, and the sample was placed in the rector with quartz wool beneath and above. The reactor and the sample were weighted with a Mettler Toledo XA204 Delta Range Analytical Balance, so that the exact weight of the sample used in the measurement was noticed. The wool and sample were pressed slightly together in the reactor. The glass reactor was also weighted after the experiment to correct for possible weight change in the sample, due to outgassing [31]. The sample mass was close to one gram for each measurement.

### 3.4.2 Hydrogen equilibrium sorption procedure for Pd-Ag

The procedure for the sorption experiment on Pd-Ag membranes was based on an article by Zhang et al. [46]. The sorption experiment was performed at 300℃, 350℃ and 400℃ and the hydrogen pressure was set to be between 0.02 and 90.66 kPa. The experiment was carried out twice at each temperature. The chemisorption analyzer was programed with three different programs according to the temperature examined. The programing is described in Appendix E, and a typical procedure is described in Table 3.3.

Table 3.3 – Sequence performed at 300℃.

| Task | Gas | Temperature [℃] | Rate [℃/min] | Time [min] |
|---|---|---|---|---|
| Evacuation | Helium | 100 | 10 | 30 |
| Evacuation | Helium | 300 | 10 | 15 |
| Evacuation |  | 300 | 10 | 120 |
| Leak test |  | 300 | 10 | - |
| Evacuation |  | 300 | 10 | 60 |
| Analysis | $H_2$ | 300 | 10 | - |

### 3.4.3 Hydrogen equilibrium sorption procedure for Pd-Cu

Two membranes with different concentration of copper, 5.8 at% and 40.5 at%, were studied to find the best programing to examine the Pd-Cu membranes. This was done due to the expected deviation in the behavior of Pd-Cu relative to the Pd-Ag membranes [47]. The goal was to obtain a linear trend of the isotherm according to equation 2.6.

The sorption experiment was carried out at the temperatures of 300℃, 350℃ and 400℃ and the pressure range was set to 0.02 and 90.66 kPa. The chemisorption analyzer was programed with the same basis as for Pd-Ag, but with changes in the evacuation time, the evacuation temperature, the flow temperature and the equilibrium interval time, $t_E$. The order of the temperature was also changed. These program sequences are described in Appendix E.

The Pd-Cu membranes have previously been investigated in permeation experiments, and is found to use some time to stabilize during a permeation experiment [47]. Due to this the equilibrium interval time was increased from 60s, to 120s. It was also decreased down to 20s and 10s, to see if there were any changes in the opposite side of the scale. It is also suspected that there might be some rearrangement of the structure when the temperatures increase [47]. So the evacuation time and flow temperature were also increased.

The sequence of the experiments was changed because of the suspected rearrangement of the structure at increasing temperature. For the membrane with 5.8 at% Cu the measurements was done only at 300℃ and 400℃, and experiments at 400℃ was done before going down to 300℃ again. For the experiment on the membrane with 40.5 at% Cu the sequence was 300℃,

350℃, 400℃ and then down in the opposite order. At one temperature (300℃ on 40.5 at% Cu) the experiment was done with direct repeated sequence, to see if this gave a positive change in the solubility for the second measurement.

The procedure for the sorption experiment on Pd-Cu membranes was done in the same way as for the Pd-Ag membrane, since the changes did not have a significant improvement on the isotherms, which are described and discussed later.

## 3.5 X-RAY DIFFRACTION EXPERIMENTS

The X-ray diffraction measurements were done in a D8 advanced Da Vinci instrument, and the results were analyzed in the program DIFFRAC.EVA. The experiment on Pd-Ag was done to investigate the difference between the growth and permeate side on membranes with different thickness (sample X1-X3), while the experiment on Pd-Cu was done on membranes with different concentration (sample S2 and S5).

The membrane that were used for the measurements were removed from the Silicon-wafer with a scalpel and tweezers before it was attached to a glass plate with high vacuum grease. The glass plate with the sample was placed in the sample holder, showed in Figure 3.3. The experiment was done with a defined programming, different for Pd-Ag and Pd-Cu. The scan time for both alloys was 15 minutes. The angle range for the Pd-Ag measurements was 5-60 degrees with a constant divergence slit on 0.5degrees. The angle range for the Pd-Cu measurements was 35-90degrees with a constant 6mm of sample illuminated at all angles.
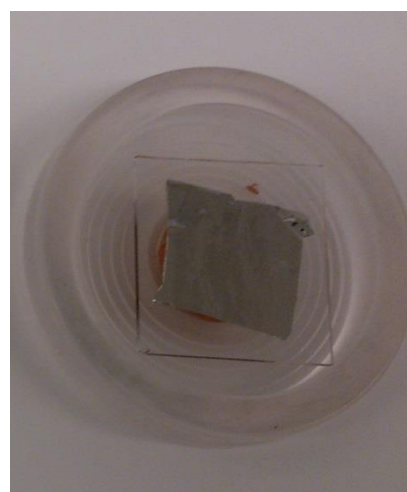


Figure 3.3 – XRD sample

Chapter 4

# RESULTS AND DISCUSSION

The result from the experiments are presented and discussed below.

## 4.1 HYDROGEN PERMEATION

The new setup built for the permeation experiments, worked as preferred. However, some improvements of the setup are desirable in the future. The gas pipelines are not connected to the ventilation between the MFC and the inlet of the channel housing. This could be desirable to avoid sudden pressure difference on the membrane when introducing gas, but it is not certain how important this is. To avoid small leakages that could be present from the 16 inches tubing in the tube transition between the setup and the channel housing, bigger tubing with small inside diameter could be used. This would maintain the small flow in to the membrane, but probably exclude the small leakages. The permeation of hydrogen was investigated for four Pd-Cu membranes with different concentration in the range from 5.8 at% to 55.1 at%. The four membranes and their concentration are given in Table 4.1, extracted from Table 3.1.

Table 4.1 - Investigated samples of palladium alloys

| Alloy | Concentration Cu [at%] | Thickness [µm] | Sample | Experiment |
|-------|------------------------|----------------|--------|------------|
| Pd-Cu | 5.8 Cu | 2.2 | S1 | 1 |
| Pd-Cu | 16.8 Cu | 1.7 | S4 | 3 |
| Pd-Cu | 40.5 Cu | 2.1 | S5 | 4 |
| Pd-Cu | 55.1Cu | 2.2 | S6 | 2 |

### 4.1.1 Stabilization with sweep gas

The hydrogen permeation through the Pd-Cu membranes was first studied under a feed of hydrogen and nitrogen and argon as sweep gas. After the temperature of the channel housing, and thus the membrane, reached $400°C$ was the flux through the membrane measured over time. The development of the hydrogen flux during hydrogen stabilization at $400°C$ for all the membranes are plotted in Figure 4.1.
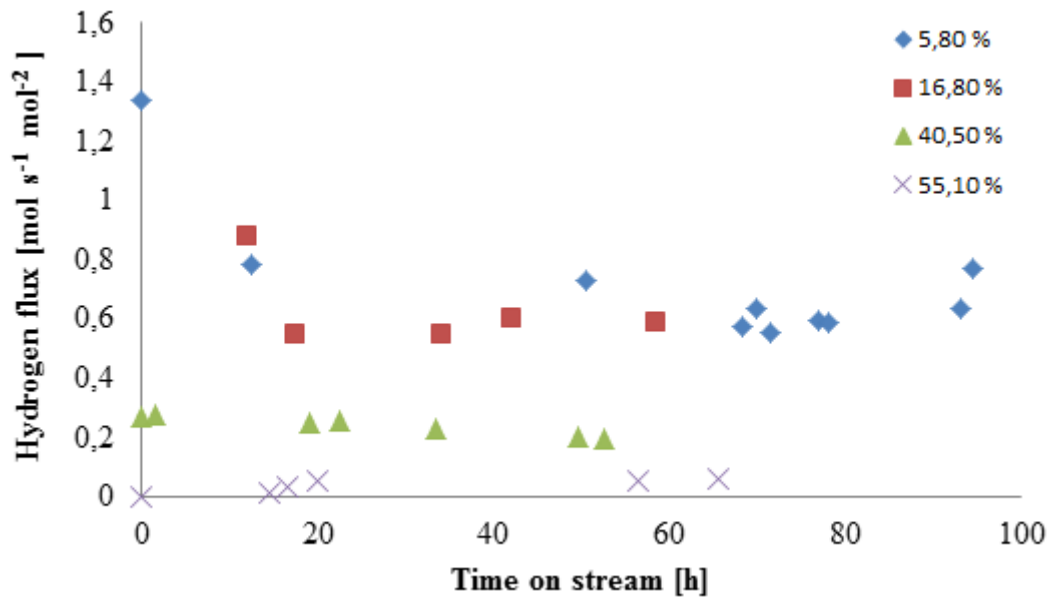
Figure 4.1- Hydrogen flux as a function of time at 400 ℃.

The first experiment was performed on a Pd-Cu membrane with 5.8 at% copper. The stabilization time was expected to be substantial from earlier experience in this group, thus the first membrane was exposed to hydrogen at the same temperature for some time to observe the behavior. After 100 hours of exposure was it decided to attempt to stabilize on the next temperature, and go back to 400 ℃ after the measurements at lower temperatures. This was decided despite the fact that the flux varies again at that point, as can be seen in Figure 4.1. The decision was made in the light of the time limit for this thesis and the fact that the stabilization time was uncertain. The repeatedly measurements of the flux at 400 ℃ through the experiment was manly done to observe how it varies at different conditions, but also to observe the stabilization time.

From Figure 4.1 can it be observed that the flux only have small variation in the time range from 60-90 h, so the stabilization time for the other membranes at 400 ℃ in this work is set to be around 60 h. This is done to have a similar procedure as for all the experiments.

The development of the hydrogen flux through the membrane at 350°C and 300 ℃ are given in Appendix D. The same approach was used: The membrane with 5.8 at% copper was exposed for some time to observe the behavior, and then it was decided that the other membranes should be exposed for around 24h at 350°C and 300 ℃ as a result from the observed stabilization time.

The flux for the membrane at 55.1 at% copper is first measurable after it has been exposed for 15 hours, and it is not measurable at all within the defined exposure time at 350°C and 300°C. The flux measured with the soap flow meter at these points gives a negative value, which should not be possible. Due to this it can be expected that there is a small error in the calibration of the mass flow controller used for argon. If that is the case, there might be a systematic error in all the measured values though the results.

The permeance and permeability for all $Pd_{1-x}Cu_x$ membranes at different temperatures after hydrogen stabilization, with $H_2$ and $N_2$ on the feed side and Ar as sweep gas, are calculated from Equation 2.3 and given in Table 4.2. The permeability is also taking the thickness of the membrane into consideration.

Table 4.2 – Calculated permeance and permeability for all $Pd_{1-x}Cu_x$ samples analyzed upon stabilization in hydrogen.

| Temperature [°C] | Concentration Cu [at%] | Permeance [mol m$^{-2}$s$^{-2}$Pa$^{-0.5}$] | Permeability [mol m m$^{-2}$s$^{-2}$Pa$^{-0.5}$] |
|---|---|---|---|
| 400°C | 5.8 | $4.6 \cdot 10^{-3}$ | $1.0 \cdot 10^{-8}$ |
|  | 16.8 | $4.5 \cdot 10^{-3}$ | $7.7 \cdot 10^{-9}$ |
|  | 40.5 | $1.0 \cdot 10^{-3}$ | $2.2 \cdot 10^{-9}$ |
|  | 55.1 | $0.1 \cdot 10^{-3}$ | $2.7 \cdot 10^{-10}$ |
| 350°C | 5.8 | $3.8 \cdot 10^{-3}$ | $8.3 \cdot 10^{-9}$ |
|  | 16.8 | $3.2 \cdot 10^{-3}$ | $5.5 \cdot 10^{-9}$ |
|  | 40.5 | $0.5 \cdot 10^{-3}$ | $9.9 \cdot 10^{-10}$ |
|  | 55.1 | - | - |
| 300°C | 5.8 | $2.6 \cdot 10^{-3}$ | $5.8 \cdot 10^{-8}$ |
|  | 16.8 | $2.1 \cdot 10^{-3}$ | $3.4 \cdot 10^{-8}$ |
|  | 40.5 | $0.4 \cdot 10^{-3}$ | $9.3 \cdot 10^{-10}$ |
|  | 55.1 | - | - |

The permeance and permeability for the membranes are calculated from an average value of the hydrogen flux in the stable area of the curves plotted in Figure 4.1 and Appendix D. As mentioned there are no measured values at 350°C and 300°C for the membrane with 55.1at% copper. The measured flux, and hence the permeance, at 400°C for this membrane is almost undetectable.

The hydrogen permeability for the Pd-Cu membranes is presented as a function of copper content at different temperatures in Figure 4.2.
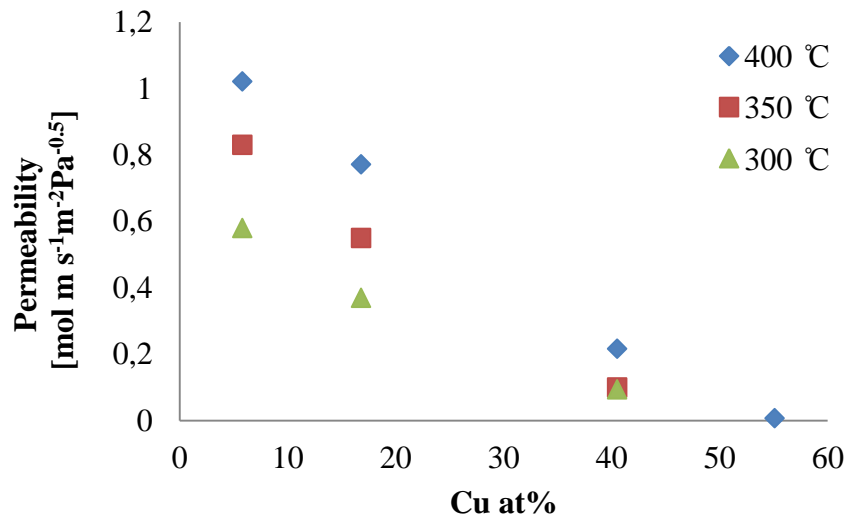


Figure 4.2- Hydrogen permeance as a function of copper content for different temperatures

The permeability, and thus also the permeance, decreases whit increasing copper content and increases with the temperature if the thicknesses are comparable, which is the case in this work. This is expected behavior from the literature and the measured values are comparable [29, 48, 49]. Pd-Cu also follows the same trends as Pd-Ag according to the increased permeability with temperature [13, 31].

### 4.1.2 Stabilization with pressure difference

Nitrogen and argon were slowly removed and a total pressure difference was introduced in absence of sweep gas. A pressure at max 2 bar was applied on the feed side while the pressure on the permeate side was left at atmospheric pressure. The flux of hydrogen was then studied at various total differential pressures in the range 0.5-2 bar, depending on the membrane, at 400℃, 350℃ and then 300℃. The calculated permeance and permeability at 400℃ are presented in Table 4.3.

Table 4.3 – Calculated permeance and permeability for the all $Pd_{1-x}Cu_x$ samples upon stabilization in hydrogen at 400 ℃

| Concentration Cu [at%] | Pressure difference [Pa] | Permeance [mol m$^{-2}$s$^{-2}$Pa$^{-0,5}$] | Permeability [mol m m$^{-2}$s$^{-2}$Pa$^{-0,5}$] |
|---|---|---|---|
| 5.8 | 0.5 | $4.7 \cdot 10^{-3}$ | $1.0 \cdot 10^{-8}$ |
| | 1.0 | $5.1 \cdot 10^{-3}$ | $1.1 \cdot 10^{-8}$ |
| | 1.5 | $7.0 \cdot 10^{-3}$ | $1.6 \cdot 10^{-8}$ |
| 16.8 | 0.5 | $4.3 \cdot 10^{-3}$ | $7.3 \cdot 10^{-9}$ |
| | 1.0 | $4.4 \cdot 10^{-3}$ | $7.5 \cdot 10^{-9}$ |
| | 1.5 | $4.7 \cdot 10^{-3}$ | $7.9 \cdot 10^{-9}$ |
| 40.5 | 1.5 | $1.0 \cdot 10^{-3}$ | $2.0 \cdot 10^{-9}$ |
| | 1.7 | $1.2 \cdot 10^{-3}$ | $2.6 \cdot 10^{-9}$ |
| | 2.0 | $1.2 \cdot 10^{-3}$ | $2.6 \cdot 10^{-9}$ |
| 55.1 | 1.5 | $0.7 \cdot 10^{-3}$ | $1.6 \cdot 10^{-9}$ |
| | 1.7 | $1.5 \cdot 10^{-3}$ | $3.2 \cdot 10^{-9}$ |
| | 2.0 | $2.0 \cdot 10^{-3}$ | $4.3 \cdot 10^{-9}$ |

The permeance and permeability for the membrane with 5.8 at% and 16.8 at% copper content at various differential pressures for 350 ℃ and 300 ℃ is given in Appendix D. The differential pressure varies from 0.5-1.5 bar for these membranes, while it varies from 1.5-2.0 bar for the membranes with 40.5 at% and 55.1 at% copper content. The different pressure range is because the flux at lower pressures for the membranes with high copper content not was measurable, and that it was not desirable to increase the pressure more than necessary for the membranes with lover content of copper due to the possible increase in surface area.

The estimation of permeance and permeability consider the differential pressure, due to Equation 2.3, and thus is a material constant for each membrane. In this work is it not constant, as can be seen from Table 4.3. There could be several reasons for the variation between the values, including experimental uncertainty. The differences can be a result of the time the membrane was exposed to hydrogen at each pressure and thus the fact that the flux was not stable. There may be a gradient in the membrane thickness over the silicon wafer that can affect the permeance, and so could also the time and contamination during ambient storage. It could also be caused by an increase in the surface area, due to increased total pressure [15, 50].

For the membrane with a copper content of 5.8 at% is the permeance increasing with increasing pressure, and there is a considerably difference in the values. An increase of surface area due to stretching of the membrane could influence the flux. It also has to be considered that the flux for this membrane was measured at one pressure difference while changing the temperature, and then repeated for each pressure difference. This was done to avoid the increase of membrane surface, but the time the flux use to stabilize at different temperatures could be longer than assumed. If that is the case, the flux is not stable when measured and the value can differ from the actual value.

The increase in permeance for the membranes with 16.8 at% and 40.5 at% copper with increasing pressure is probably due to the increase in surface area. The variation is small and is further discussed in the context with the other permeance measurements at 400℃.

The permeance through the membrane with a copper content of 55.1 at% was first at a higher level after reaching a differential pressure at 2.0 bar. The values measured before reaching a high differential pressure was small. This is probably due to the long stabilization time and increased surface area as discussed above. This membrane has higher permeance than the one with content of 40.5 at% copper at differential pressures above 1.7 bar. This could indicate that a higher atomic content of copper is more favorable at this temperature and differential pressure, but since this is the highest copper content studied in this work it is not a certainty [28, 31].

The measurements done with different differential pressure at 350℃ and 300℃ for the two membranes with low copper content, given in Appendix D, indicates that the permeance is more stable at lower temperatures, at least with low copper contents, and that the variation of the values for a specific content of copper is smaller than for 400℃.

The permeance at 400 ℃ and 1.5 bar as differential pressure is plotted as a function of copper content in Figure 4.3.
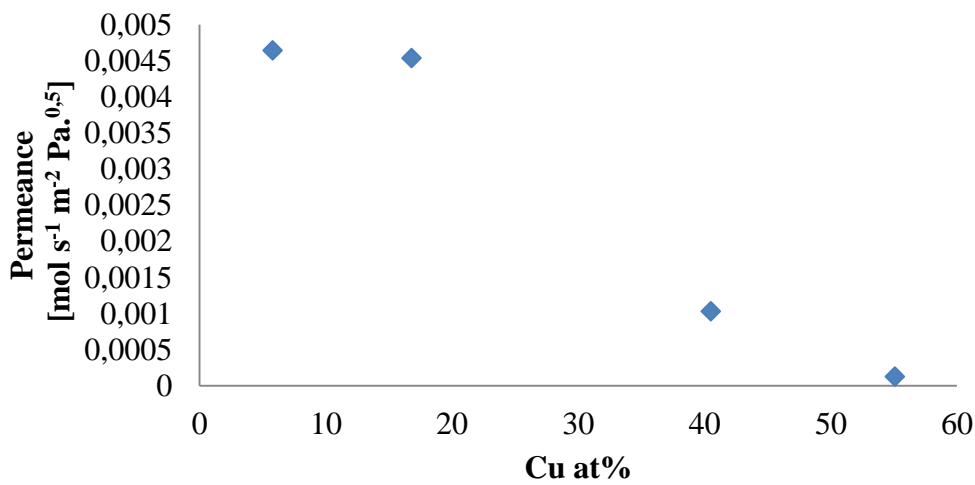


Figure 4.3 – Hydrogen permeance as a function of copper content at 400 ℃ and a pressure difference at 1,5 bar.

Figure 4.3 shows the same trends as Figure 4.2: Decrease in permeance, and thus the permeability in this work, whit increasing copper content and is further discussed in the overview. The measured values at 55.1 at% are small which increase the uncertainty of its credibility.

The permeance can also be estimated from linear regression of the measured flux vs. the difference in the square root of the hydrogen partial pressure. Figure 4.4 gives the linearization and Table 4.4 the permeance for all the membranes.
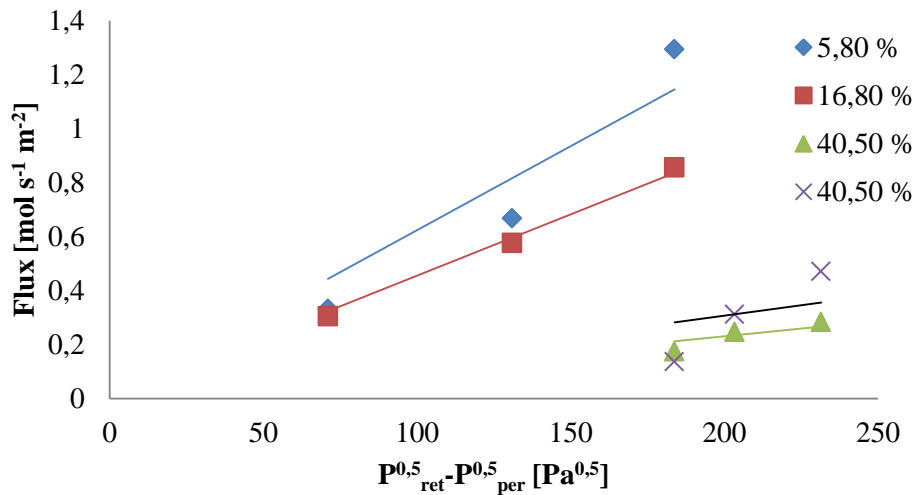
Figure 4.4 – Hydrogen flux as a function of the difference in the square root of the hydrogen partial pressure. Linear fits are represented by colored lines.

Table 4.4 – Permeance calculated from linear regression.

| Concentration Cu [at%] | Permeance [mol m$^{-2}$s$^{-2}$Pa$^{-0.5}$] |
|:---:|:---:|
| 5.8 | $6.2 \cdot 10^{-3}$ |
| 16.8 | $4.5 \cdot 10^{-3}$ |
| 40.5 | $1.2 \cdot 10^{-3}$ |
| 55.1 | $1.5 \cdot 10^{-3}$ |

The linear regression gives a permeance comparable to the value calculated in Table 4.3, and deviations are discussed in the next section. The trends and variation in this figure is the same as discussed above: Decrease in the permeance with increasing copper content except for the one with 55.1 at%, which probably is due to either phase changes, short stabilization time, increased surface area or a combination of them.

### 4.1.3 Overview

The permeance through the Pd$_{x-1}$-Cu$_x$ membranes with sweep gas was studied at 400 ℃ three times during the experiment: first at the beginning of the experiment, then after varying the temperature and then again after pressure difference. It was done a fourth measurement with sweep after varying the temperature a second time for the membrane with copper content of 55.1 at%. The hydrogen permeance was not measured after varying the total differential pressure for the membrane with 16.8 at% copper because of a leakage in the setup, and thus

termination of the experiment. The results for all the measurements at 400℃ in this work are given in Table 4.5.

Table 4.5 – Permeance measured at 400℃ at different stages in the experiment for $Pd_{1-x}Cu_x$

| Concentration Cu [at%] | Permeance $[mol\ m^{-2}s^{-2}Pa^{-0.5}]$ | | | | |
|---|---|---|---|---|---|
| | With sweep | After temp (sweep) | Average ΔP | Linear regression ΔP | After ΔP (sweep) |
| 5.8 | $4.6 \cdot 10^{-3}$ | $2.7 \cdot 10^{-3}$ | $5.6 \cdot 10^{-3}$ | $6.2 \cdot 10^{-3}$ | $2.6 \cdot 10^{-3}$ |
| 16.8 | $4.5 \cdot 10^{-3}$ | $5.0 \cdot 10^{-3}$ | $4.5 \cdot 10^{-3}$ | $4.5 \cdot 10^{-3}$ | - |
| 40.5 | $1.0 \cdot 10^{-3}$ | $1.1 \cdot 10^{-3}$ | $1.2 \cdot 10^{-3}$ | $1.2 \cdot 10^{-3}$ | $1.1 \cdot 10^{-3}$ |
| 55.1 | $0.1 \cdot 10^{-3}$ | $0.2 \cdot 10^{-3}$ $1.5 \cdot 10^{-3}*$ | $1.4 \cdot 10^{-3}$ | $1.5 \cdot 10^{-3}$ | $1.3 \cdot 10^{-3}$ |

*permeance measured with sweep after temperature variation the second time

Table 4.5 describes the already mentioned trend with decreasing permeance with increasing copper content for the membranes. Except from the membrane with a copper content of 5.8 at%, are the variations in the measured permeance during the experiment small. The small increase in the measurements with sweep before and after the temperature variation for the other membranes is probably due to longer stabilization time. The further increase for the two membranes with highest copper content could be due to the same, the increase if surface area or a combination.

The measured value for the permeation through the membrane with 5.8 at% of copper is changing during the experiment. The decrease in the value after the temperature variation could be due to the stabilization time. The value after the variation in differential pressure is almost the same as before. This could indicate that the increase of the value measured under differential pressure is due to other aspects mentioned than the increase of surface area.

The permeance for the membrane with a copper content of 16.8 at% is the same at all points in the experiment except from the increase of the value after the temperature variation. Since the permeance after the differential pressure variation not was measured it is hard to say if the variation in the value is due to experimental uncertainties or other aspects. An aspect can be that there are transport limitations in the gas phase, so called concentration polarization [31].

The last measurement for the Pd-Cu with 55.1 at% was done to see if another change in temperature and thus extended total exposure time would increase the permeance. The permeance is increased after the experiments done without sweep and is further increased after the second temperature variation. This could indicate that there has been a physical change in the material, probably due to increased surface area or to phase changes.

The membranes studied in this work are thin and the variation between them is small, 1.7-2.2 μm. Similar variation in the measured permeance, as the observed in this work, has been observed for Pd-Ag membranes in the same thickness range [50]. As described this could be due to several reasons. The measured permeability for a 2.2 μm Pd-Ag membrane with 23 wt% Ag is comparable with the results in this work [50], at least for the lowest content of copper.

## 4.2  HYDROGEN SOLUBILITY

The solubility of hydrogen is influenced by the temperature, pressure, concentration and the microstructure. These parameters have to be examined isolated from each other, so that the impact of one can be studied without the disturbance from the others. Therefor the temperature is held constant during each experiment, while the pressure is changed.  It is done a linear regression in each measurement, to give the Sieverts' constant as described in section 2.1.

### 4.2.1 Palladium Silver

The isotherm for Pd-Ag with a thickness of 6.0 μm at 300℃ is plotted in Figure 4.5 as an example of the sorption result. The isotherm results for the remaining Pd-Ag samples can be found in Appendix F. The isotherms show the amount of hydrogen adsorbed (μmol/g) versus the square root of the equilibrium pressure ($Pa^{0,5}$) of two measurements done at the same temperature. The equilibrium sorption experiment was performed twice at each temperature.
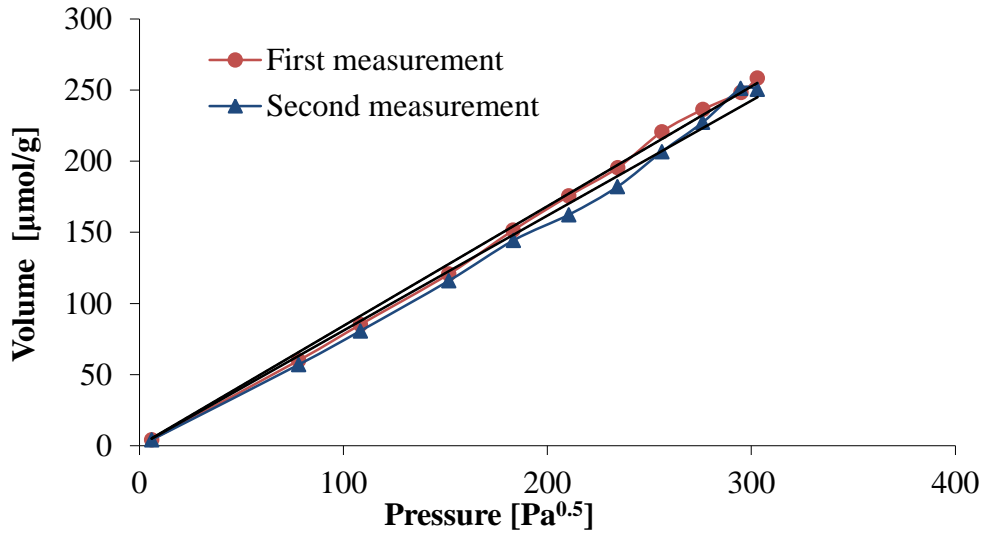
Figure 4.5 – Isotherm result for 6$\mu$m Pd-Ag23wt% (Sample P1) at 300 ℃.

The isotherm plot shows a linear trend, which indicate that the linear solubility dependence of the square root of the equilibrium pressure is maintained. The slope of each graph represents the Sieverts' constant, as described in Equation 2.6. The reported value of Sieverts' constant is an average of the two slopes, due to the limited deviation between the data plot sets at the same temperature. This can be seen in Figure 4.5, and it is a trend through all the data plot sets for the Pd-Ag membranes showed in Appendix F. The Sieverts' constants from these studies are reported in Table 4.6, with results from similar investigation at the same instrument [9, 51]. The difference between the results in the thickness of 8 μm for the membranes studied in [9, 51] is most likely due to different microstructure in the membrane.

Table 4.6- Sieverts' constant calculated in this work and in [9, 51] at different temperature and membrane thickness.

| Temperature | 6 μm | | | 8 μm | | |
|---|---|---|---|---|---|---|
| | Næss | Vicinanza | This | Næss | Vicinanza | This |
| [℃] | [51] | [9] | work | [51] | [9] | work |
| 300 | 0,79 | 0,78 | 0,83 | 0,66 | 0,76 | 0,79 |
| 350 | 0,53 | 0,57 | 0,57 | 0,48 | 0,55 | 0,58 |
| 400 | 0,41 | 0,46 | 0,49 | 0,39 | 0,45 | 0,46 |

The equilibrium sorption experiment was performed twice at each temperature and the isotherms showed that the results for Pd-Ag membranes are reasonably reproducible.

The measurements on Pd-Ag were done to study the reproducibility in the measurements. Especially to see if there is a variation due to the different batches of membranes measured or the operator preforming the experiment.

The hydrogen adsorption for Pd-Ag membranes examined in this work increase with increasing pressure, as expected from equation 2.6, and the solubility decreases with temperature as reported in earlier studies [7].

### 4.2.1 Palladium Copper

**TEST PROCEDURE DEVELOPMENT**

To determine out the best approach to measure the solubility for Pd-Cu, was some tests measurements preformed, as described in section 3.4.3. The isotherm plot is given in Appendix F, and an isotherm for sample for Pd-Cu with 40.5 at% copper at 300℃ is plotted in Figure 4.6 as an example.
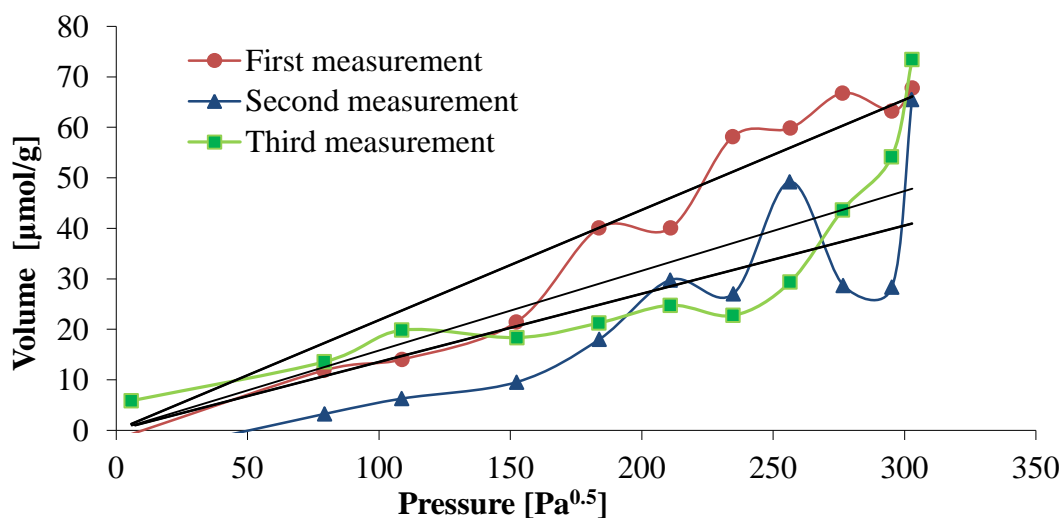


Figure 4.6 – Isotherm result for Pd-Cu with 40.5at% (Sample T2) at 300 ℃. (The first and second measurement; directly repeated with $t_E$=20s, third measurement; after being at 400 ℃ $t_E$=60s.)

From this plots, and the rest of the isotherms in Appendix F, it can be seen that there are no consistent trends that gives the desired linear behavior of the isotherms. This is despite the changes done to try to meet the challenges that are suspected for the Pd-Cu alloy. Thus it was decided to use the same procedure as for the Pd-Ag membranes.

Isotherms Pd-Cu with a copper content of 5.8 at% and 40.5 at% are plotted for Pd-Cu at 300℃ and 400℃ in Figure 4.7. The objective of this figure is to see the influence of the

temperature on the membranes. For closer study, these isotherm plots and the other sample results are shown in Appendix F.
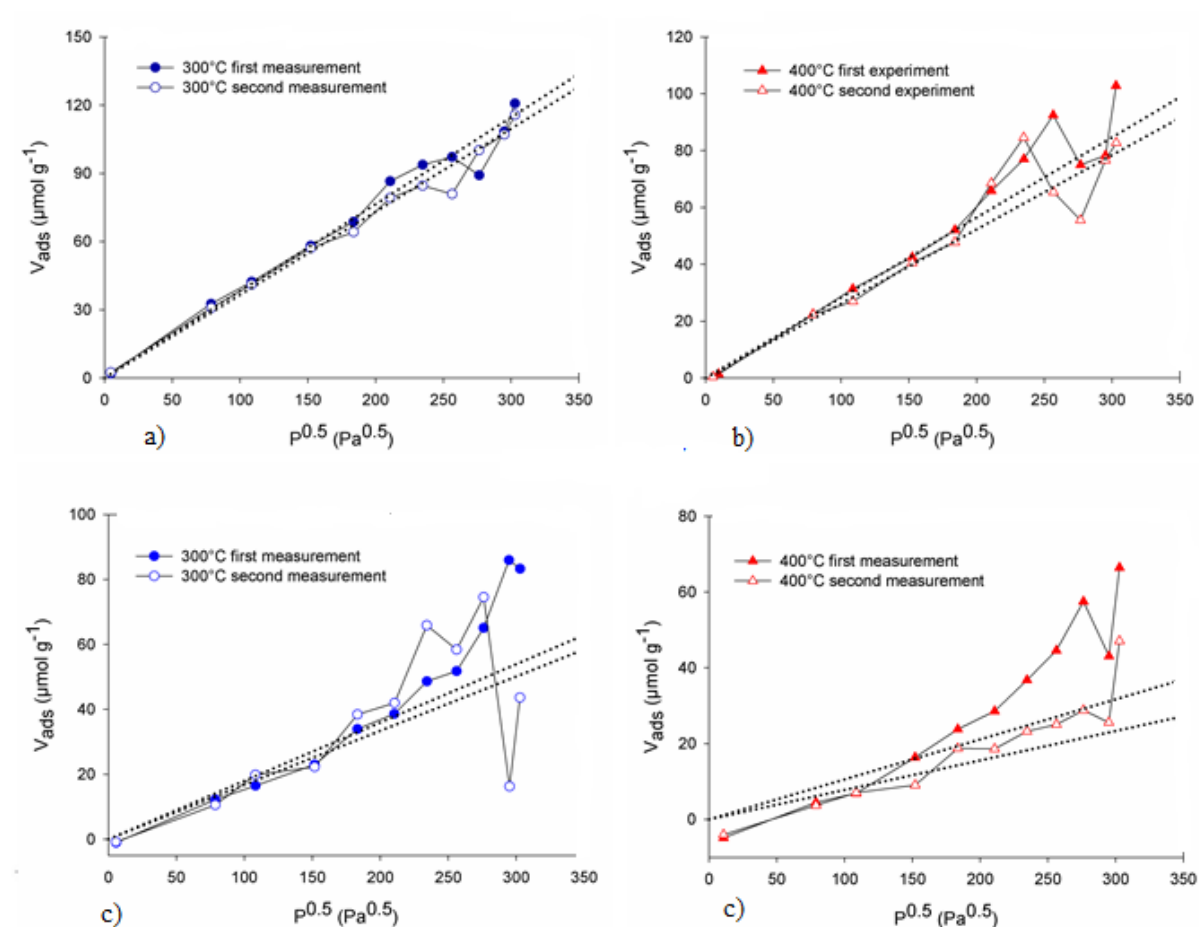


Figure 4.7 – Equilibrium hydrogen isotherms for Pd-Cu sample with 5.8at% (Sample S1) at 300 ℃ (a) and 400 ℃ (b) and for Pd-Cu sample with 40.5at% (Sample S5) at 300 ℃ (c) and 400 ℃ (d)

It can be observed that the deviation from the desired behavior for the isotherm increase with increasing pressure, temperature and concentration of copper. Nevertheless the isotherm result shows a consistent trend of decreasing solubility with increasing temperature and also with increasing copper concentration.

Some of the measurement gives an isotherm with negative adsorption. This will influence the reported solubility. The measurement is not repeated since this is considered an experimental error.

The difference from the linear isotherm increase particularly after the equilibrium reaches approximately 200Pa$^{0.5}$ (14.1Pa). Thus has it been plotted isotherms and calculated Sieverts' constants for the lower part of the isotherm, from now on called *modified fit*. An example is presented in Figure 4.8 for Pd-Cu with 5.8 at% Cu at 300℃. The isotherms for other temperatures and membranes can be seen in Appendix F.
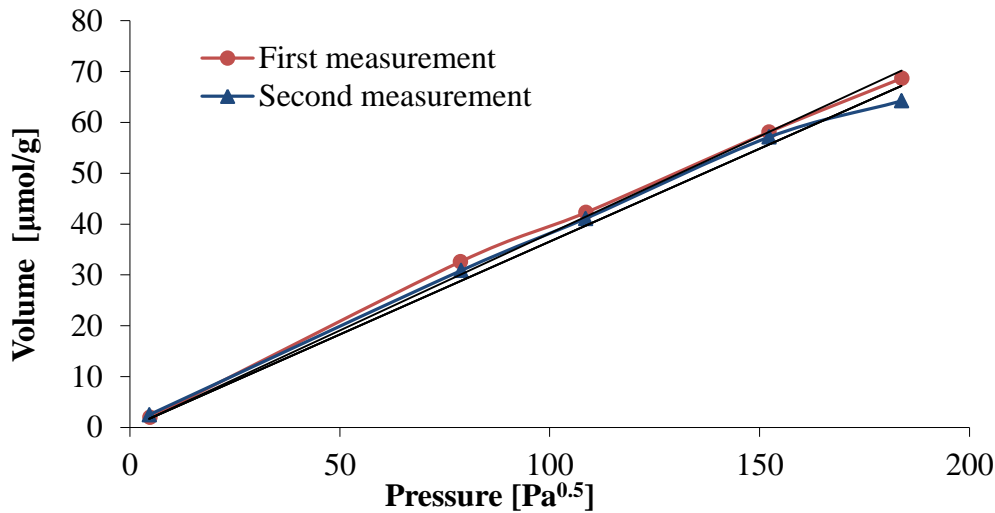


Figure 4.8 – Modified fit isotherm result for Pd-Cu5.8at% (Sample S1) at 300 ℃.

### HYDROGEN SOLUBILITY IN PALLADIUM COPPER FILMS

The thickness of the membranes examined is not constant in this study, as they vary from 1.7-2.2µm. The solubility dependence of the thickness has been studied and is described for thicker membranes of Pd-Ag in [9]. From the result it can be seen that it is a small deviation in a range of 2.2-11.2µm, and for the much smaller range as in this study, it can be assumed that the difference in thickness can be neglected. The equilibrium sorption experiment was performed twice at each temperature.

The result of the plotted isotherms shows that the Pd-Cu membranes behave different from the Pd-Ag membranes, but the trends of decreasing solubility with increasing  temperature and the increasing hydrogen adsorption with increasing pressure, are consistent [2, 7]. The pressure dependence is also due to Equation 2.6, while the temperature dependence is described by equation 2.7. The solubility for the Pd-Cu membrane is all over lower than the solubility for the Pd-Ag membranes, which corresponds with the literature [52].

The isotherms do not behave as desired, since the difference from the linear approach is major at the worst, and affect the reproducibility. The deviation increase with increasing temperature and Cu concentration in the alloy, apart from that it seems to be a random variation in the measurements.

The Sieverts' constant, as the slope of the graph form equation 2.6, is given in Table 4.6 for the original isotherm and for the modified fit isotherm.

Table 4.6- Sieverts' constant at estimated from various Pd-Cu membranes on temperatures 300 ℃, 350 ℃ and 400 ℃ for both the original and the modern fit isotherm.

| | Sieverts' constant [mol/m$^3$Pa$^{0,5}$] | |
| --- | --- | --- |
| | Original isotherm | Modified fit isotherm |
| Temperature [ ℃ ] | 5.8at% Cu | |
| 300 | 0,37 | 0,37 |
| 350 | 0,29 | 0,27 |
| 400 | 0,27 | 0,25 |
| | 16.8at% Cu | |
| 300 | 0,30 | 0,32 |
| 350 | 0,23 | 0,19 |
| 400 | 0,22 | 0,20 |
| | 20.7at% Cu | |
| 300 | 0,31 | 0,29 |
| 350 | 0,18 | 0,16 |
| 400 | 0,17 | 0,13 |
| | 36.9at% Cu | |
| 300 | 0,22 | 0,21 |
| 350 | 0,17 | 0,16 |
| 400 | 0,14 | 0,11 |
| | 40.5at% Cu | |
| 300 | 0,20 | 0,17 |
| 350 | 0,16 | 0,09 |
| 400 | 0,13 | 0,09 |
| | 55.1at% Cu | |
| 300 | 0,22 | 0,19 |
| 350 | 0,15 | 0,12 |
| 400 | 0,15 | 0,12 |

The $K_s$ values are estimated as an average from of the two isotherm measurements done at each temperature. This is due to the varying isotherm measurements result, where it can be seen that measurement 1 and 2 do not appear lower or higher than each other with any consistency. This is supported by the observed trend of a small deviation between the data

plot sets at the same temperature. Overall the solubility for $Pd_{1-x}Cu_x$ membranes is lower than for the Pd77%/Ag23% membranes.

The solubility dependence of the concentration of copper is showed in Figure 4.9 and 4.10. It describes the same trends with decreasing hydrogen solubility with increasing temperature and Cu concentration.
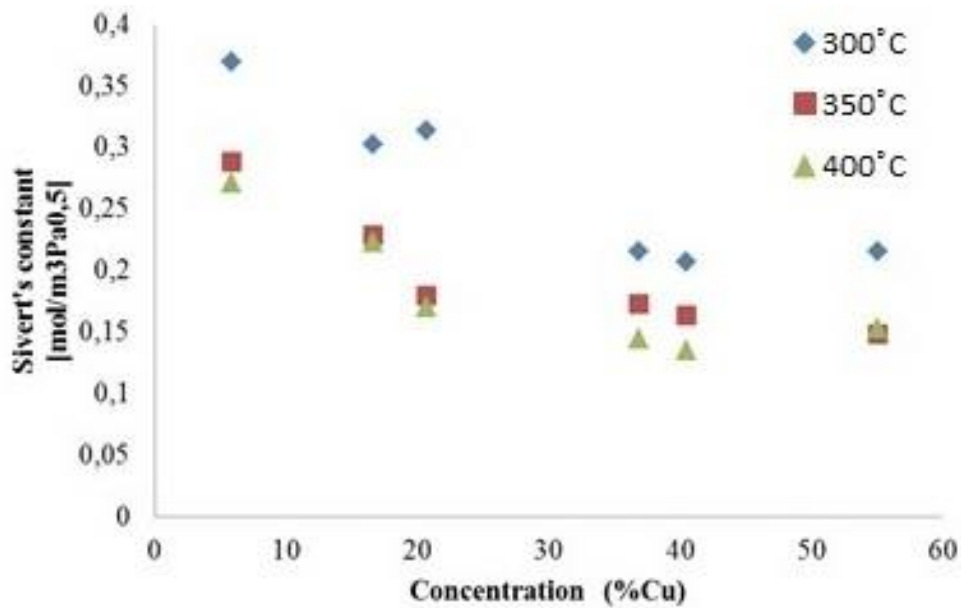


Figure 4.9 – Sieverts' constant for the Pd-Cu membranes of various concentrations
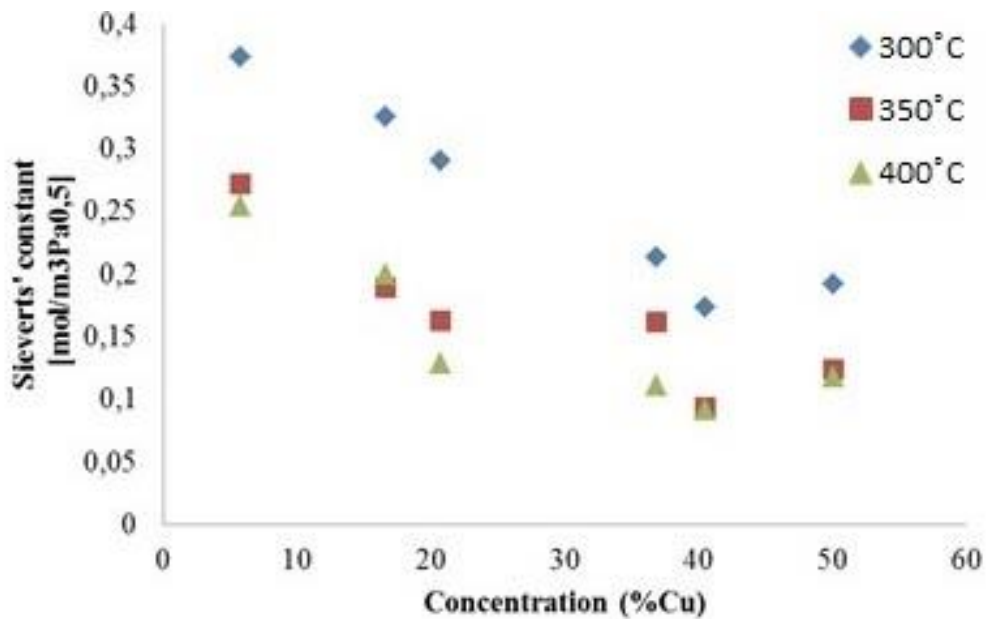from the original isotherm result.



Figure 4.10 – Sieverts' constant for the Pd-Cu membranes of various concentrations
from the modified fit.

There are presented results of two isotherm calculations, with corresponding Sieverts' constants, in this work. The original isotherm describes all the sorption measurements performed, while the modified fit only describes the lower part of the isotherm which seems to behave more linearly. Nevertheless the modified fit isotherm has some drawbacks worth mentioning. In some of the measurements is the noted value of adsorbed hydrogen negative in the start. This will in most cases give a low Sieverts' constant compared to the original value. In the original isotherm is it also possible that some of the deviation will balance each other out, which then can provide a better value for the Sieverts' constant than the modified fit isotherm. Still there is a disadvantage in the unwanted deviation from the linear regression of the original isotherms, and the modified fit is found to give the best representation of the solubility in this work.

It has not been found a concrete reason why the isotherms for the Pd-Cu membranes behave as they do, but this study shows that the expected trends for the system is consistent, yet that does not indicate that the estimated Sieverts' constant are quantitatively correct. Phase transitions in the system is a suggestion to explain the behavior, but the literature found does not describe phase changes in the concentration range studied in this work [24, 25, 27]. In addition a suggestion is that the alloy material changes in long time perspective, due to the long stabilizing time in the hydrogen flux observe in this work and establishment in earlier permeation experiments [47].

## 4.3 DIFFUSIVITY AND ACTIVATION ENERGY FOR THE MEMBRANES

Sieverts' constant from the modified fit isotherms and the permeability of the studied membranes were used to calculate the diffusivity from Equation 2.4. The activation energy, $E_a$, can be determined from an Arrhenius plot of Equation 2.5, were the logarithmic hydrogen diffusivity is plotted against the invers temperature [21]. The Arrhenius plot is given in Figure 4.11.
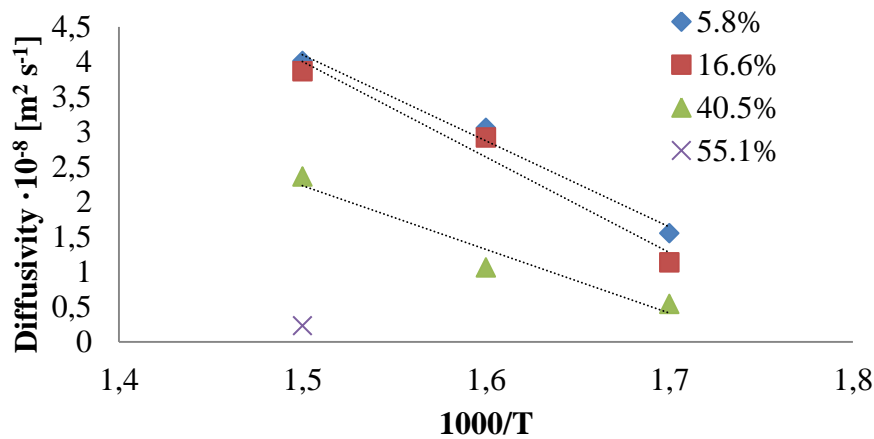
Figure 4.11 – Arrhenius plot of the diffusivity (logarithmic scale) for $Pd_{1-x}Cu_x$ membranes as a function if the inverse temperature. Linear fits are represented by dotted lines.

This figure shows that the diffusivity decreases with increasing content of Cu and temperature. The estimated activation energies are given in Table 4.7 together with activation energies observed for a 2.2 μm Pd77%/Ag23% membrane in this group [16, 17].

Table 4.7 –  comparison of the activation energy in this and previous work

| Concentration of Cu [at%] | Activation Energy [kJ/mol] |
|---|---|
| 5.8 | 31 |
| 16.8 | 39 |
| 40.5 | 47 |
| Pd77%/Ag23% | |
| Vicinanza [17] | 28 |
| Johannesen [16] | 35 |

The activation energy for Pd-Cu with 55.1 at% copper was not estimated due to only one temperature measurement.

The observed values for the activation energy in this work are comparable with values given in the literature [8, 32, 53]. The activation energy for $Pd_{1-x}Cu_x$ membranes are overall higher than the values for Pd77%/Ag23%, this reflects the higher diffusivity measured in this work. The high diffusivity is due to the much lower solubility constant for $Pd_{1-x}Cu_x$ membranes.

Although there is slightly lower permeability for the Pd-Cu, this would not balance the solubility increase between the alloys.

The fact that the permeability is varying for each membrane in this work could be a result of changes in what controlling the transport mechanism described in the theory. Thick Pd-Ag membranes (<20µm) are known to be limited by bulk diffusion while the transport mechanism might be controlled by surface effects for membranes thinner than 5 µm under conditions relevant to this work [15, 50, 53]. The surface limitations for the Pd-Cu membranes are less investigated, but it is likely that these appear at lower thickness as the diffusivity reduces with increasing Cu content. If the surface limitation is considerable should the n-value used to calculate the permeability in Equation 2.4, be increased [15, 53]. In this work is the pressure range to narrow to investigate this further [13].

## 4.4 GRAIN STRUCTURE

In this section is the result from X-ray diffraction measurements on the Pd-alloys described.

### 4.4.1 Palladium Silver

The Pd-Ag membranes were investigated to observe the difference between the growth and substrate side for membranes with different thickness. The grain (crystallite) size and lattice plane was studied. The membranes studied in this work had a thickness of 2.2 µm, 4.0 µm and 10.0 µm. Figure 4.12 presents the XRD pattern of a 4.0µm Pd-Ag membrane.
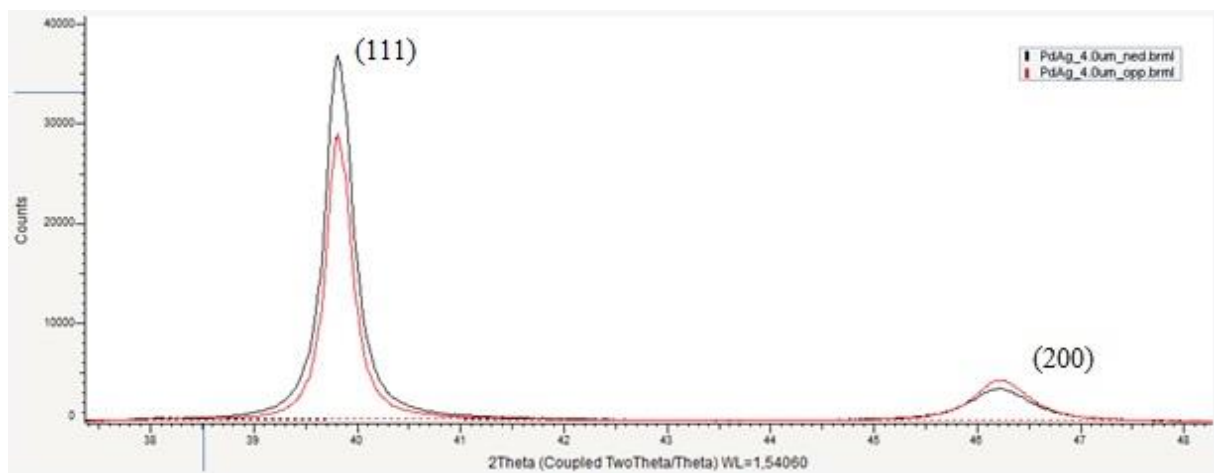


Figure 4.12 – XRD pattern for Pd-Ag, 4.0µm.

The XRD patterns for the other membranes are given in Appendix G. The lines are refined and fitted in the program, DIFFRAC.EVA. The broadened (111) peak indicates that the grains

at the growth side are larger than on the substrate side. This can also be observed for the diffractogram for 4.4µm, but not for the 2.2µm. The difference in grain size for thinnest membrane (2.2µm) is low and it also seems to increase from the growth side to the substrate side. This could be because of the X-rays penetration depth is comparable to the thickness [35].

The (111) peak is also used to determine the lattice parameters from Equation 2.11 and 2.12, and the average lattice parameter constant for Pd-Ag measured in this work is 3.92Å. This is comparable with the previous work on the same Pd-alloy [41]. The lattice parameter constant for pure Pd is usually cited in the literature as 3.89 Å [54], which indicates that alloying Pd with 23 wt%Ag increase the unit cell volume [41].

The grain size is estimated by the program and plotted as a function of thickness in Figure 4.13 a) and as a function of the side of the membrane in Figure 4.13 b). The (111) peak were used to quantify the grain size since they were the most intense [41].
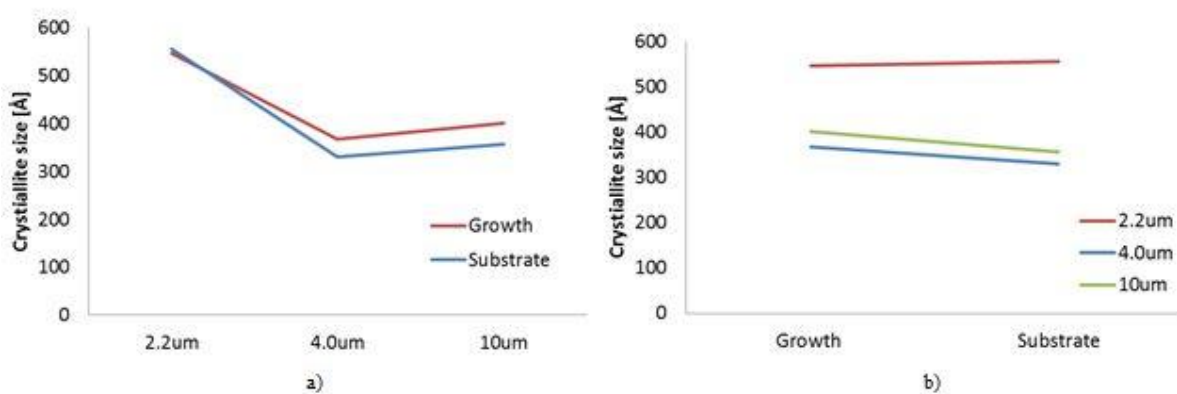


Figure 4.13– The crystallite size [Å] a) vs the thickness for the growth side and permeate side of the membrane b) vs the sides of the membrane for each of the thicknesses.

From Figure 4.13 can it as described be observed that the grain size decrease from the growth side to the substrate side, and that the difference between the sides increases with increasing thickness. This reflects the growth process of the membrane, since the roughness of the surface can be associated with grain size. The Si wafer has a smooth surface that affects this roughness on the substrate side. The grain size at 10 µm is higher than at 4.0 µm in this work, but it is expected to be some variation in the thickness dependency due to previous work [9, 35].

The studied growth and substrate side of the membrane are from the same wafer, but are not the same sample. This means that the sides studied are from different areas on the wafer. This could give some variation in the result due to a gradient in the membrane thickness across the silicon wafer [50].

The literature shows that there are peaks at lower order for Pd-Ag alloys [41]. They are not detected in this work due to the programming. The series was not done again with a more specific scatter angle range for Pd-Ag alloys, but it was change for the Pd-Cu alloys since they are the main focus for this work.

### 4.4.2 Palladium Copper

The Pd-Ag membranes were investigated to observe the difference between the growth and substrate side for membranes with different content of Cu. The grain (crystallite) size and lattice plane was studied. The samples studied in this work had a Cu content of 16.8 at% and 40.5 at%. The scatter angle range was changed to 35-90 degrees to detect the expected lower peaks [41]. The diffractogram for both samples are given in figures below.
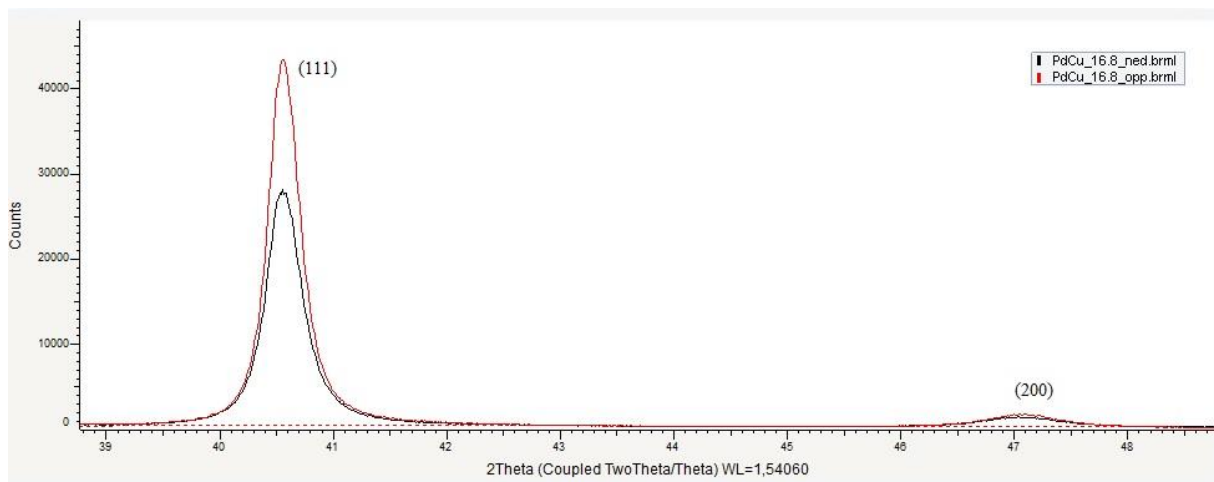


Figure 4.14 – Diffractogram Pd-Cu membrane with a 16.8at% copper content.
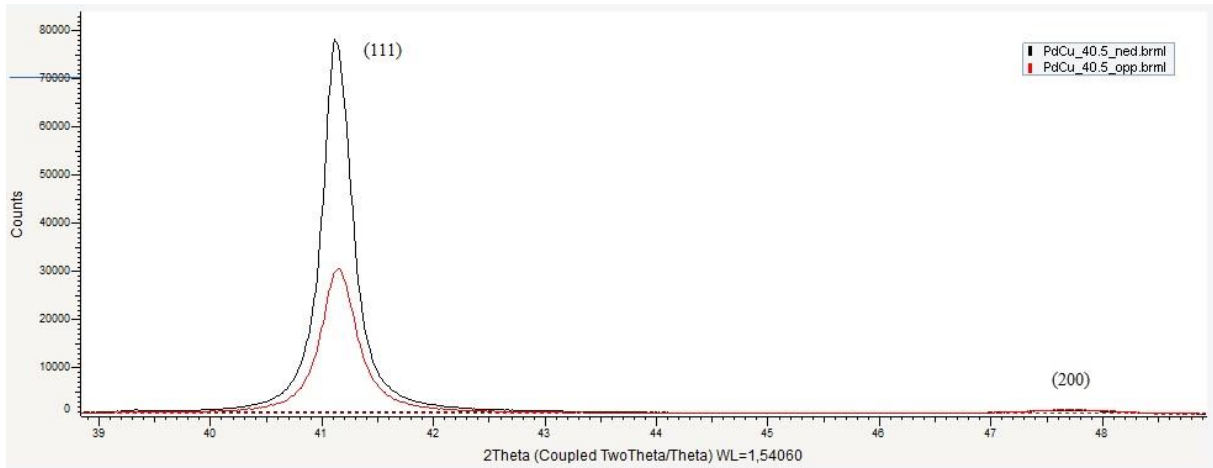
Figure 4.15 – Diffractogram Pd-Cu membrane with a 40.5at% copper content.

These figures are just a segment of the diffractogram and it is given in in its entire form in Appendix G, were also the lower order peaks are shown, i.e. (220), (331) and (222) from fcc reflection. The XRD is performed at as-grown membranes, with a 40 at% copper content and below, in room temperature. They have not been exposed to hydrogen, thus is it probably only the fcc patterns that are indicated [8, 26]. The bbc structure is first present at higher copper content and Peters et al. [49] indicates that it also has to be exposed for higher temperatures. The diffractograms are similar to the reported work done one membranes with the same thickness [49].

The broadening of the diffraction peaks suggest a small increase of grain size at the substrate side of the membrane to the growth side for the Pd-Cu alloy with 16.8 at% of copper, as for Pd-Ag. The estimated value for the grain size for this membrane is actually the same for both sides, 31±0.05nm. While it for the Pd-Cu alloy with 40.5 at% of copper indicates the opposite, a decrease of grain size from the substrate side to the growth side. The estimated value for the grain size for this membrane varies from 27±0.05nm to 36±0.05.

The lattice parameters are determined from the (111) peak and Equation 2.11-12. The measured value in this work is comparable with the previous work on the same Pd-alloy [41, 55], the measured value for Pd-Ag and the lattice parameter constant for pure Pd [54], The lattice parameters are reported in Table 4.8.

Table 4.8 –Lattice parameter constant.

| | Lattice parameter [Å] |
|---|---|
| Experimental value literature  [54] | 3.85 |
| Pd-Ag 23 at% | 3.92 |
| Pd-Cu 16.8at% | 3.85 |
| Pd-Cu 40.5% | 3.80 |

This shows that the lattice parameter for a low content is similar to the reported value for pure Pd, and smaller for the membrane with higher content. This indicates that the alloying Pd copper decrease the unit cell volume. The lattice parameter decrease with increasing content of copper and this is consistent with the literature [49, 55].This decrease in the lattice parameter is most likely causing the reduction in diffusivity and solubility observed in this work [17].

Chapter 6

# CONCLUSION AND FURTHER WORK

The hydrogen permeance and permeability for $Pd_{1-x}Cu_x$ membranes in the range of 5.8 at% - 55.1 at% copper has been obtained upon stabilization under hydrogen and sweep gas, and under pure hydrogen and a total differential pressure. A trend of decreasing permeability with increasing copper content for the membranes was observed. The membranes investigated were in a small thickness range, yet the permeability measured was not constant. This could indicate that there are deviations in the microstructure due to the sputtering technique, and that impurities and time and contamination during the storages can influence the permeability. The possibilities for increased surface area for the membranes exposed to pure hydrogen under total pressure difference could also be an explanation for the slight variation, in addition to experimental uncertainty.

The isotherms from the solubility measurements of hydrogen in $Pd_{1-x}Cu_x$ membranes showed a non-linear trend at high pressure, which affects the reproducibility. The deviation increases with increasing temperature and Cu concentration in the alloy. The deviation could be due to expected phase transitions, or that the material changes in long time perspective. However the solubility through the membrane decreases with temperature and copper content as a consistent trend. Further, the solubility of hydrogen in $Pd_{1-x}Cu_x$ membranes is measured to be lower than for the Pd77%/Ag23%, which influences the diffusivity and thus the estimated activation energy. The activation energy for Pd- Cu with 5.8 at%, 16.8 at% and 40.5 at% is respectively estimated to be 31kJ/mol, 39kJ/mol and 47kJ/mol.

The lattice parameter and grain size of the membranes was studied by X-ray diffraction. The lattice parameter is estimated and compared to pure palladium (3.85Å). The Pd77%/Ag23% membranes display a higher value (3.92Å) and the $Pd_{1-x}Cu_x$ membranes a lower value (3.85Å/3.80Å). This indicates that alloying copper with Ag increases the unit cell volume, while alloying it with Cu decreases it. It is also observed a trend of decrease in the lattice parameter with increasing content of copper. The penetration depth for the measurements is generally too large to obtain precise conclusions on how the grain size varies between the growth and substrate sides. Nevertheless, some weak trends were found. For the Pd77%/Ag23% membrane was it observed a trend of decreasing grain size from the growth

side to the substrate side, and an increase in the difference between the sides with increasing membrane thickness. The Pd-Cu membrane with 16.8 % copper follows the same trend with decreasing grain size from the growth side to the substrate side. This trend could be due to the sputtering technique used to fabricate the films. The Pd-Cu membrane with 40.5 % copper follows the opposite trend with increasing grain size from growth to substrate side.

The sorption measurement for the $Pd_{1-x}Cu_x$ should be examined with the same procedure to qualify how reproducible the measured values are. The same should be done for the experiments measuring the permeation of hydrogen trough the membranes. The permeation through the $Pd_{1-x}Cu_x$ membranes could also be studied in a larger perspective due to the expected resistance to impurities like $H_2S$ and CO. The X-ray diffraction experiments should also be done on $Pd_{1-x}Cu_x$ membranes before and after the permeation experiment to study the possible phase changes. The permeation and X-ray diffraction experiments should also be done with membranes with copper content in the range between and above the investigated membranes in this work, to get an even better understanding of the behavior.

# REFERENCES

1.      Basile, A., *Hydrogen Production Using Pd-based Membrane Reactors for Fuel Cells.* Topics in Catalysis, 2008. **51**(1-4): p. 107-122.

2.      Bredesen, R., et al., *Palladium-based Membranes in Hydrogen Production*, in *Membrane Engineering for the Treatment of Gases, Volum 2: Gas-separation Problems Combined with Membrane Reactors*, G.B. Enrico Drioli, Editor. 2011, Royal Society of Chemistry.

3.      Moulijn Jacob A. , M.M., Van Diepen Annelies, *Chemical Process Technology*. 2001: WILEY.

4.      Nunes Susanna, P.K.-V., *Membrane Technology in the Chemical Industry*. 2006: Wiley-VCH.

5.      Lu, G.Q., et al., *Inorganic membranes for hydrogen production and purification: A critical review and perspective.* Journal of Colloid and Interface Science, 2007. **314**(2): p. 589-603.

6.      Gao, H., et al., *Chemical Stability and Its Improvement of Palladium-Based Metallic Membranes.* Industrial & Engineering Chemistry Research, 2004. **43**(22): p. 6920-6930.

7.      Fazle Kibria, A.K.M. and Y. Sakamoto, *The effect of alloying of palladium with silver and rhodium on the hydrogen solubility, miscibility gap and hysteresis.* International Journal of Hydrogen Energy, 2000. **25**(9): p. 853-859.

8.      Yuan, L., A. Goldbach, and H. Xu, *Segregation and H2 Transport Rate Control in Body-Centered Cubic PdCu Membranes.* The Journal of Physical Chemistry B, 2007. **111**(37): p. 10952-10958.

9.      Vicinanza, N., et al., *Effect of solubility and surface phenomena on the hydrogen transport properties of sputtered Pd77%/Ag23% thin film membranes.* In preparation (2014).

10.     Klette, H. and R. Bredesen, *Sputtering of very thin palladium-alloy hydrogen separation membranes.* Membrane Technology, 2005. **2005**(5): p. 7-9.

11.     Bredesen, R. and H. Klette, *Method of manufacturing thin metal membranes. US Patent 6086729.* 2000 SINTEF, Trondheim: Norway.

12.     Uemiya, S., T. Matsuda, and E. Kikuchi, *Hydrogen permeable palladium-silver alloy membrane supported on porous ceramics.* Journal of Membrane Science, 1991. **56**(3): p. 315-325.

13.     Mejdell, A.L., *Properties and application of 1-5um Pd/Ag23wt.% membranes for hydrogen separation*, in *Chemical Engineering*. 2009, Norwegian University of Science and Technology.

14.     Mejdell, A.L., et al., *Effects of CO and CO2 on hydrogen permeation through a ~3μm Pd/Ag 23wt.% membrane employed in a microchannel membrane configuration.* Separation and Purification Technology, 2009. **68**(2): p. 178-184.

15.     Mejdell, A.L., et al., *Hydrogen permeation of thin, free-standing Pd/Ag23% membranes before and after heat treatment in air.* Journal of Membrane Science, 2008. **307**(1): p. 96-104.

16.     Arild, J.B., *Microchannel Membrane Reactor for production of pure Hydrogen*, in *Department of Chemical Engineering*. 2014, Norwegian University of Science and Technology.

17. Viciananza Nicla, S.I.-H., Næss Live Nova, Peters Thijs A., Bredesen Rune, Borg Anne, Venvik Hilde J, *Thickness dependent effects of solubility and surface phenomena on hydrogen transport of sputtered Pd77%Ag23% thin film membranes.* Journal of Membrane Science, 2014.

18. Ward, T.L. and T. Dao, *Model of hydrogen permeation behavior in palladium membranes.* Journal of Membrane Science, 1999. **153**(2): p. 211-231.

19. Athayde, A.L., R.W. Baker, and P. Nguyen, *Metal composite membranes for hydrogen separation.* Journal of Membrane Science, 1994. **94**(1): p. 299-311.

20. Thomson, W.J., *Introduction to transport phenomena*. 2000, New Jersey: Prentice Hall PTR.

21. Chorkendorff I., N.J.W., *Concepts of Modern Catalysis and Kinetics*. 2007: WILEY-VCH.

22. Hurlbert, R.C. and J.O. Konecny, *Diffusion of Hydrogen through Palladium.* The Journal of Chemical Physics, 1961. **34**(2): p. 655-658.

23. Holleck, G.L., *Diffusion and solubility of hydrogen in palladium and palladium--silver alloys.* The Journal of Physical Chemistry, 1970. **74**(3): p. 503-511.

24. Huang, W., et al., *Thermodynamic modelling of the Cu–Pd–H system.* Calphad, 2007. **31**(3): p. 315-329.

25. Li, M., et al., *A thermodynamic modeling of the Cu–Pd system.* Calphad, 2008. **32**(2): p. 439-446.

26. Decaux, C., et al., *Time and frequency domain analysis of hydrogen permeation across PdCu metallic membranes for hydrogen purification.* International Journal of Hydrogen Energy, 2010. **35**(10): p. 4883-4892.

27. Subramanian, P.R. and D.E. Laughlin, *Cu-Pd (Copper-Palladium).* Journal of Phase Equilibria, 1991. **12**(2): p. 231-243.

28. Roa, F., et al., *Preparation and characterization of Pd–Cu composite membranes for hydrogen separation.* Chemical Engineering Journal, 2003. **93**(1): p. 11-22.

29. Roa, F., M.J. Block, and J.D. Way, *The influence of alloy composition on the H2 flux of composite Pd ・ Cu membranes.* Desalination, 2002. **147**(1–3): p. 411-416.

30. Morreale, B.D., et al., *Effect of hydrogen-sulfide on the hydrogen permeance of palladium–copper alloys at elevated temperatures.* Journal of Membrane Science, 2004. **241**(2): p. 219-224.

31. Viciananza, N., *An investigation of fundamental phenomena affecting the performance of sputtered Pd-alloy film membranes for hydrogen separation* in *Chemical Engineering*. 2014, Norwegian University of Science and Technology.

32. Opalka, S.M., et al., *Hydrogen interactions with the PdCu ordered B2 alloy.* Journal of Alloys and Compounds, 2007. **446–447**(0): p. 583-587.

33. Carradò, A., H. Pelletier, and T. Roland, *Nanocrystalline Thin Ceramic Films Synthesised by Pulsed Laser Deposition and Magnetron Sputtering on Metal Substrates for Medical Applications*. Biomedical Engineering - From Theory to Applications. 2011.

34. Pratibha Pandey, R.S.C., *Membranes for gas separation.* Progress in polymer science 2001. **26**: p. 853-893.

35. Mejdell, A.L., et al., *Performance and application of thin Pd-alloy hydrogen separation membranes in different configurations.* Journal of the Taiwan Institute of Chemical Engineers, 2009. **40**(3): p. 253-259.

36. Tsakoumis, N., et al., *Lecture TKP 4510 Catalyst Characterization by Volometric Chemisorption* 2013.

37.    Demirocak, D.E., et al., *Volumetric hydrogen sorption measurements – Uncertainty error analysis and the importance of thermal equilibration time.* International Journal of Hydrogen Energy, 2013. **38**(3): p. 1469-1477.

38.    Askeland Donald R. , P.P.p., *The science and enineering of materials*. 2008: Cengage Learning.

39.    Mario, B., *Thin film analysis by x-ray scattering*. 2006: WILEY-VCH.

40.    Che Michel, V.J.C., *Characterization of solid materials and heterogeneous catalysts*. Vol. 2. 2012: WILEY-VCH.

41.    Mekonnen, W., et al., *Microstructural characterization of self-supported 1.6μm Pd/Ag membranes.* Journal of Membrane Science, 2008. **310**(1–2): p. 337-348.

42.    Mekonnen, T.W., *Self-supported, thin Pd/Ag membranes for Hydrogen separation* in *Physics*. 2009, Norwegian university of science and technology Norway.

43.    Karl, C.J. *Instrument X-ray Optics* 2006  [cited 2014 24.june]; Available from: http://pd.chem.ucl.ac.uk/pdnn/inst1/optics1.htm.

44.    Braithwaite A. , S.F.J., *Chromatographic methods*. 1996: Blackie Academic & Professional.

45.    Grob Robert L., B.E.F., *Modern Practice of Gas Chromatography*. 2004: John Wiely & Sons.

46.    Zhang, K., S.K. Gade, and J.D. Way, *Effects of heat treatment in air on hydrogen sorption over Pd–Ag and Pd–Au membrane surfaces.* Journal of Membrane Science, 2012. **403–404**(0): p. 78-83.

47.    Venvik, H.J. Autumn 2013: NTNU.

48.    L, M.D., *Method for hydrogen separation and purification*. 1969, Google Patents.

49.    Peters, T.A., et al., *Development of thin binary and ternary Pd-based alloy membranes for use in hydrogen production.* Journal of Membrane Science, 2011. **383**(1–2): p. 124-134.

50.    Viciananza Nicla, S.I.-H., Peters Thijs A., Bredesen Rune, Venvik Hilde J, *New insight to the heat treatment in air procedure for enhancement of the hydrogen transport properties of thin Pd77%/Ag23% membranes.* In preperation, 2014.

51.    Ness, L.N., *Pd-based Membranes for Hydrogen Separation - Membrane structure and Sorption and Permeation Behavior*. 2013, NTNU. p. 113.

52.    Howard, B.H., et al., *Hydrogen permeance of palladium–copper alloy membranes over a wide range of temperatures and pressures.* Journal of Membrane Science, 2004. **241**(2): p. 207-218.

53.    Zhang, X., et al., *Hydrogen transport through thin palladium–copper alloy composite membranes at low temperatures.* Thin Solid Films, 2008. **516**(8): p. 1849-1856.

54.    Mehl, M.J. and D.A. Papaconstantopoulos, *Applications of a tight-binding total-energy method for transition and noble metals: Elastic constants, vacancies, and surfaces of monatomic metals.* Physical Review B, 1996. **54**(7): p. 4519-4530.

55.    Semidey-Flecha, L., C. Ling, and D.S. Sholl, *Detailed first-principles models of hydrogen permeation through PdCu-based ternary alloys.* Journal of Membrane Science, 2010. **362**(1–2): p. 384-392.

Appendix A
# RISK ASSESSMENTS

**Hazardous activity identification process**

| Risikovurdering | Nummer | Dato |
|---|---|---|
| HMS-avd. | HMSRV2601 | 08.10.2013 |
| Godkjent av | Side | Erstatter |

Unit: _Kjemisk prosessteknologi_  Date: 08.10.2013

Line manager: _Edd. A. Blekkan_

Participants in the identification process (including their function): Hilde Venvik (supervisor), Nicla Vicinanza (PhD stipendiat), Bengt Arild Camilla Lindgren (MSc)

Short description of the main activity/main process: Membrane apparatus

| ID no. | Activity/process | Responsible person | Laws, regulations etc. | Existing documentation | Existing safety measures | Comment |
|---|---|---|---|---|---|---|
| 1 | Assembling/use of flamable gases H2/CH4 | Hilde Venvik | | safety data sheet EIGA067A (H2) no number (CH4) | Room detector, local detector, leak testing, gloves, goggles, lab coat. | |
| 2 | Assembling/use of toxic gases CO | Hilde Venvik | | safety data sheet: no number | Room detector, local detector, leak testing, gloves, goggles, lab coat. | |
| 3 | Assembling/use of non toxic and inert gases; CO$_2$/N$_2$/Ar/He | Hilde Venvik | | safety data sheet: no number CO2; EIGA089A N2; EIGA003A Ar, EIGA061A He | Room detector, local detector, leak testing, gloves, goggles, lab coat. | |

# NTNU

HMS/KS

## Risk assessment

| | Utarbeidet av | Nummer | Dato |
|---|---|---|---|
| | HMS-avd. | HMSRV26 03 | 08.10.2013 |
| | Godkjent av | Side | Erstatter |

**Unit:** Kjemisk prosessteknologi **Date:** 08.10.2013

**Line manager:** Edd. A. Blekkan

**Participants in the identification process (including t** Hilde Venvik (supervisor), Nicla Vicinanza (PhD stipendiat), Bengt Arild Johannesen (MSc),
Camilla Lindgren (MSc)

**Signatures:**

| ID no. | Activity from the identification process form | Potential undesirable incident/strain | Likelihood: Likelihood (1-5) | Consequence: Human (A-E) | Environment (A-E) | Economy material (A-E) | Reputation (A-E) | Risk value Human | | Comments/status Suggested measures |
|---|---|---|---|---|---|---|---|---|---|---|
| 1 | Assembling/use of flamable gases H2/CH4 | (a) leakage (b) fire | (a) 3 (b) 1 | (a) A (b) D | (a) A (b) D | (a) A (b) D | | (a) A3 | (b) D1 | Leak testing with noble gases and room and local detectors. Change of gas bottles is to be done by appropriate staff within working hours |
| 2 | Assembling/use of toxic gases CO | (a) leakage (b) fire | (a) 3 (b) 1 | (a) D/E (b) D | (a) A (b) D | (a) A (b) D | | (a) E3 | (b) D1 | Leak testing with noble gases and room and local detectors.Change of gas bottles is to be done by appropriate staff within working hours |
| 3 | Assembling/use of non toxic and inert gases: CO2/N2/Ar/He | (a) leakage | (a) 3 | (a) B | (a) A | (a) A | | (a) B3 | | Leak testing with noble gases and room and local detectors |

## Operating Instructions

| Instrument/Apparatus: | Membrane apparatus | |
|---|---|---|
| Serial Number: | None | Placement Kjemihall D 2nd floor |
| Original Manual: | None | |
| Log book with signature for training & maintenance: | None | |

**Risk Evaluation**

Date: 27/09/2011
Archived:

| Compulsory Protection Equipment: | | Hazards: | |
|---|---|---|---|
| Safety Goggles | x | Fire | x |
| Gloves | x | Chemicals/Gasses | x |
| Hearing Protection | | Electricity/Power | x |
| Protective Clothing | x | Temperature/Pressure | x |
| Breathing Protection | | Cutting/Crushing | |
| Shielding | | Rotating Equipment | |
| Other | x | Hazardous Waste | x |
| None | | Beyond regular working hours | x |
| | | Others | x |
| | | None | |

**Operating Instructions**

(Fill In or Attach Seperate Instructions)

GC manual; Eurothermal manual; HSE - course; leak testing before every experiment.

**Emergency Procedure**

(Emergency Stop Procedure, Image of Switches/Stop Procedure):

Shut down gas bottles and cut power. Then evacuate.

**Maintenance Routines**

Frequency When needed
Service Agreements: None
Maintenance Contact: None
Maintenance Describe None outside maintinence.

| Equipment Responsible: | | Deputy: | |
|---|---|---|---|
| Name: | Hilde Venvik | Name: | Nicla Vicinanza |
| Telephone: | | Telephone | 7359411 |
| Mobile: | 92808787 | Mobile: | 47166722 |
| Signature: | | Signature: | |

| Controlled & Updated: | | | |
|---|---|---|---|
| Date: | Date: | | Date: |
| Date: | Date: | | Date: |

HMS

# Hazardous activity identification process

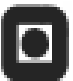| | Risikovurdering | | Nummer | | Dato |
|---|---|---|---|---|---|
| | HMB-avd. | | HMSRV2601 | | 08.10.2013 |
| | Godkjent av | Side | | Erstatter | |

**Unit:** _Kjemisk prosessteknologi_     **Date:**    08.10.2013

**Line manager:** _Edd Blekkan_

**Participants in the identification process (including their function):**
Hilde Venvik (supervisor), Nicla Vicinanza (co-supervisor),
Karin Dragsten (staff engineers, instrument responsible) Camilla Lindgren (master student).

**Short description of the main activity/main process:** Chemisorption instruments, Micromeritics ASAP 2020/2010

| ID no. | Activity/process | Responsible person | Laws, regulations etc. | Existing documentation | Existing safety measures | Comment |
|---|---|---|---|---|---|---|
| 1 | Use of flammable and toxic gasses (H₂, CO). | Room responsible/instrument responsible/ user | AML | MSDS, user manual | Preform leak tests when replacing gas bottles or chaning the gas feed system. Detection system in the room (CO and H2). Mobile gas detectors. | Training is compulsary before changing gas bottles and performing changes in the feed system. CO bottle should be closed when not in use. Pregnant users are not allowed in the lab if CO is in use/sign outside entrance door). |
| 2 | Oven | User | AML | User manual (blue folder) | Warning sign and shield | Cool down sample reactor before disconnecting it. |
| 3 | Liquid (N₂) | User | AML | MSDS, user manual | Danger note in the lab, personal protective equipment available in lab. Trolley with tip. User must have training | |

IV

Unit:

Line manager:

Participants in the identification process (including their function):

Signatures: _(handwritten signature)_

Kjemisk prosessteknologi    Date:    08.10.2013

Edd Blekkan

Hilde Venvik (supervisor), Nicla Vicianza (co-supervisor),

Karin Dragsten (staff engineers, instrument responsible) Camilla Lindgren (master

| ID no. | Activity from the identification process form | Potential undesirable incident/strain | Likelihood (1-5) | Human (A-E) | Environment (A-E) | Economy/material (A-E) | Reputation (A-E) | Risk value Human | Comments/status Suggested measures |
|---|---|---|---|---|---|---|---|---|---|
| 1 | Use of flammable and toxic gasses (H2, CO), | Poisoning/fire/explosion | 2 | B | | | | 2B | Gas detection system in the lab. Changing of the gas bottle will be done by the staff engineer or the gas responsible. |
| 2 | Oven | Skin burn, fire | 2 | B | | | | 2B | Warning sign on the oven |
| 3 | Liquid (N2) | skin irritation, eye contact | 2 | D | | | | 2D | Danger note in the lab, personal protective equipment available in lab. Trolley with tip. User must have training |

v

## Operating Instructions

| Instrument/Apparatus: | Micromeritics ASAP 2020/2010 |
|---|---|
| Serial Number: | Placement K5-441 |
| Original Manual: | Blue folder/white folder placed beside instrument |

| Log book with signature for training & maintenance: |
|---|
| Log book beside the instrument |

**Risk Evaluation**

| Date: | 17.08.2013 |
|---|---|
| Archived: | |

| Compulsory Protection Equipment: | | Hazards: | |
|---|---|---|---|
| Safety Goggles | x | Fire | x |
| Gloves | x | Chemicals/Gasses | x |
| Hearing Protection | | Electricity/Power | |
| Protective Clothing | x | Temperature/Pressure | x |
| Breathing Protection | | Cutting/Crushing | |
| Shielding | x | Rotating Equipment | |
| Other | | Hazardous Waste | |
| None | | Beyond regular working hours | x |
| | | Others | |
| | | None | |

**Operating Instructions**

(Fill In or Attach Seperate Instructions)

Detailed instructions in the user manual beside the instrument. User instruction/procedure beside the instrument. All users will have a copy of these precedures.

**Emergency Procedure**

(Emergency Stop Procedure, Image of Switches/Stop Procedure):

Close the gas bottles and turn of the electricity, main switch on the side. The gas bottles belonging to the instrument are marked with ASAP.

**Maintenance Routines**

Frequency When needed

Service Agreements: Once a year

Maintenance Contact: Mikrotek, Tom Andre Brubak 90838670/ brubak@microtek.no

Mainteinans described in the procedure

| Equipment Responsible: | | Deputy: | |
|---|---|---|---|
| Name: Karin Dragsten | | Name: Magnus Rønning | |
| Telephone 91897245 | | Telephone 94121 | |
| Mobile: 48023837 | | Mobile: | |
| Signature: | | Signature: | |

**Controlled & Updated:**

| Date: | Date: | Date: |
|---|---|---|
| Date: | Date: | Date: |

## Elaboration of the points in the form "Identification of Hazardous Activity"

**What**

**Activity/process**

Identification of activities/processes included in the risk assessment that may entail a risk of human injury or environmental damage, such as machinery, laboratory activities, work in engineering workshops, the use of certain chemicals etc. Break down the whole activity/process into its constituent parts, and give a short description of each of these parts. The participants must come to agreement about the scope of the activities to be risk assessed.

The following aspects must be considered

• "A risk to whom" – employees, the environment, isolated individuals or a group, the enterprise, society?

• "A risk posed by what " – which installation, which activity, what categories of accident?

• "For which time period/duration"- the risk level may vary over time

Risk represents a potential loss, not a loss that has already occurred. Activities/processes that are normally deemed relatively risk-free may involve an increased risk under certain conditions.

**Responsible person**

Who is responsible for each activity/process? Do other units carry responsibility or carry out tasks in relation to reducing the risks? Organisational maps can be used to clarify responsibility.

**Laws, regulations etc.**

What laws, regulations and other official requirements apply to the activity/process? See the HSE handbook, HMSRV-20/01, www.lovdata.no, www.arbeidstilsynet.no, www.hmsetatene.no, and municipal regulations (www.trondheim.kommune.no)

**Existing documentation**

The unit must access existing central and local guidelines, construction drawings, certificates, crane operator licences, forklift operator licences, completed training, service agreements, operation manuals, checklists etc. See also earlier risk assessments and HSE checks, local HSE booklet, lab handbook, NTNUs stoffkartotek etc.

**Safety measures**

What safety measures already exist for the area/equipment? (E.g. ventilation, personal protective equipment, emergency stop device, marking/signposting, partition walls etc.).

# What's A Risk Matrix

A risk matrix is simple graphical tool. It provides a process for combining the chance for an occurance of an event (likelihood) and the cuncequence if the event occured. Use the tool fur everyday judgements and decisions. Know when to accept the risk. Know when to reject the risk.

## RISK ASSESSMENT MATRIX

| | Column1 | Column2 | Column3 | Column4 | Column5 | Column6 |
|---|---|---|---|---|---|---|
| CONSEQUENCE | Very critical | E1 | E2 | E3 | E4 | E5 |
| | Critical | D1 | D2 | D3 | D4 | D5 |
| | Dangerous | C1 | C2 | C3 | C4 | C5 |
| | Relative safe | B1 | B2 | B3 | B4 | B5 |
| | Safe | A1 | A2 | A3 | A4 | A5 |
| | | Minimal | Low | Medium | High | Very high |

Risk Increases In This Direction

LIKELIHOOD

| COLOR | | Describing function |
|---|---|---|
| Red | | Extreme risk – immediate action required |
| Yellow | | Attention needed to develop risk reduction strategies. |
| Green | | Minimal injury requiring no/minimal intervention or treatment. |

## ALARP

Risk will be treated to ensure they are "As Low As Reasonably Practical"(ALARP) or in the "Broadly Acceptable" areas.

Generally Intolerable

ALARP / Tolerable

Broadly Acceptable
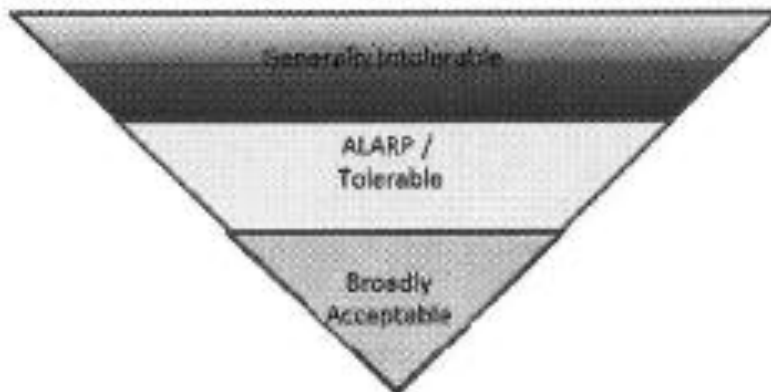
Appendix B
# MICROCHANNEL MOUNTING PROCEDURE

## Polishing

Polish the feed side of the module and the channel in "Sliperom". Use 1200, 2400 and finally 4000 polishing disc. Polish the copper gasket as well with 2400 polishing disc to ensure that the sealing is efficient. A new copper gasket is used for every new module.
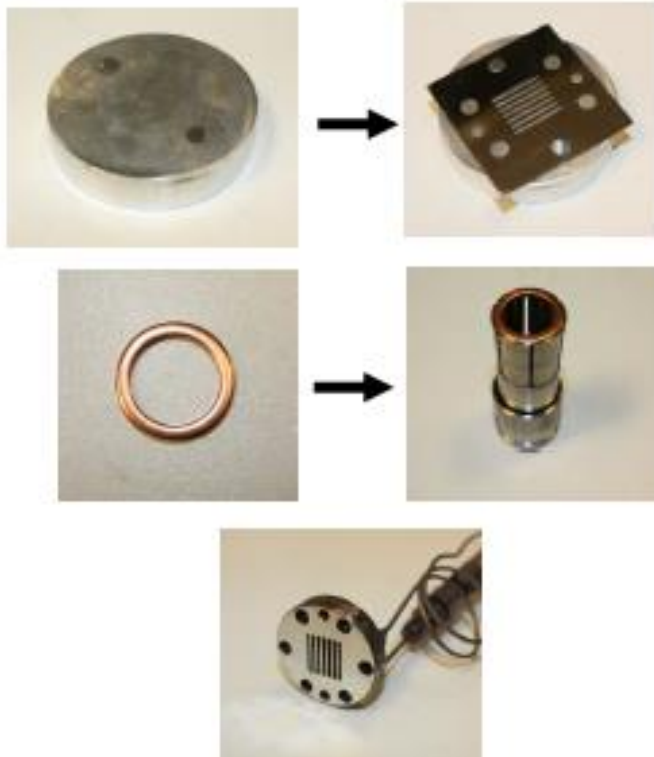


## Cleaning

Pour some ethanol in a beaker then put the beaker in the ultrasound bath. Put both feed and permeate side of the module in ethanol. Let it run for about 10 minutes.

Dry out most of the ethanol from the parts with compressed air, and connect one at a time each tube of the module to the argon tap on the wall to dry the inside of the pipes:

## Assembling the module

The whole module is built-up as shown on this scheme:
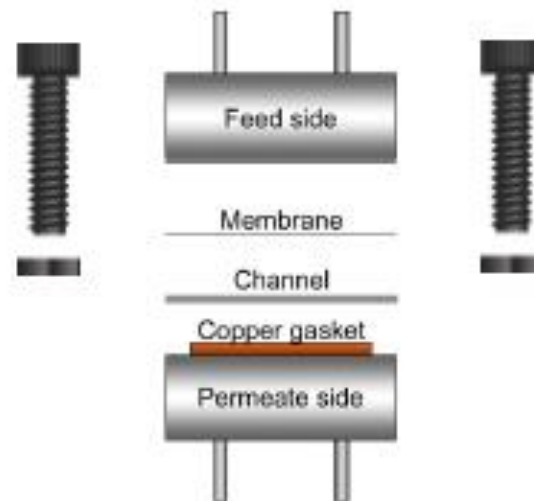


1. First, mount the permeate side of the module and the copper gasket on the vice as depicted below, trying to align the smaller holes with the edge of the vice so that the screw holes are easier to find later on.

2. Put the channel on top and tape it to the vice.
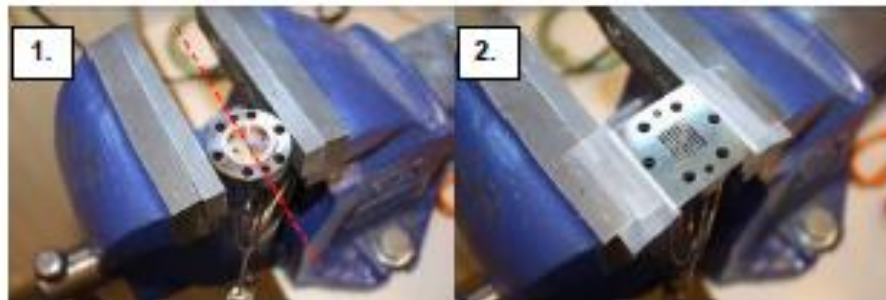


3. Then cut away the membrane from the as-sputtered wafer. Put gloves on and put the wafer with film side up on a dust-free paper. Prepare tape bits approximately the size of the channel side, forming little handles. Stick them on the film so that the tape-free area is approximately that of the channel area and leave some sticky surface free so that it can be stuck on top of the vice.

4. Cut along all edges with a scalpel. Pull away the membrane from one side then from the other side. Pulling from one side only can cause the film to rip from where the other piece of tape is stuck.

5. Lay the film on the channel trying to make it sit flat.
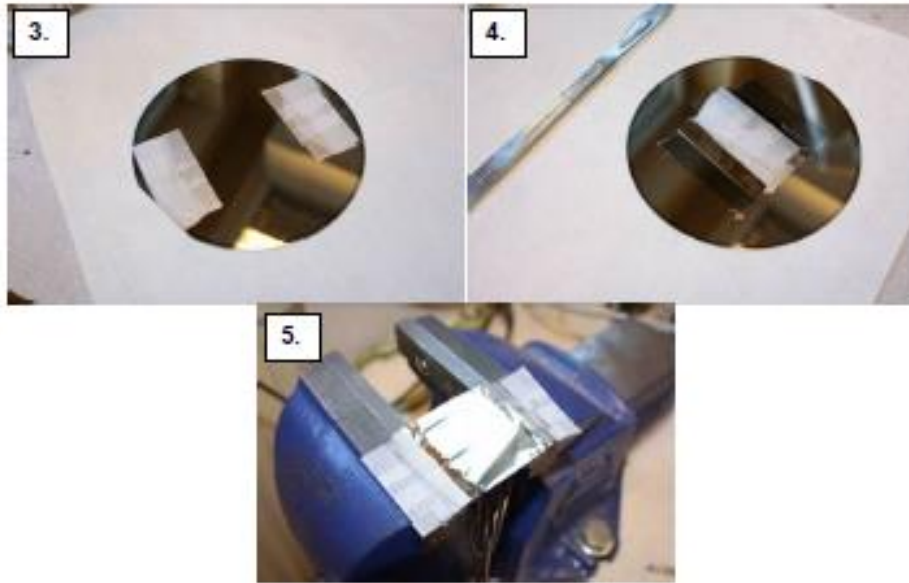
6. Cover it with the feed side of the module. Align it by looking from the sides. If possible, hold the upper tubes by hand or gallows, at least at first, to avoid wrinkling the film. Pierce the first hole with a pointy object like tweezers not to crack the film any further. Put a screw in and drive a bolt on.

7. Repeat this operation for these other holes.
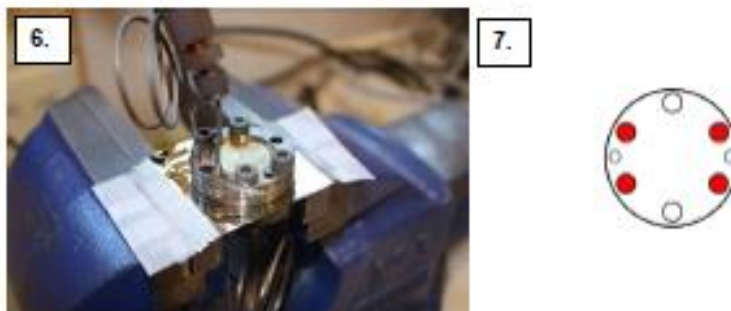




8. Cut away the surplus of film, not too close to the screws area so it does not tear apart. Peel away any remaining tape bit.

9. Screw the bolts on evenly. Undo the vice and rotate the whole module. Tighten the vice and put the last screws in. Screw all the bolts as tight as possible with a hex key and a no. 6 wrench; screws will tend to come loose overtime with high

temperatures. Use force on the wrench not to break the key. Connect the pipes to set-up.



## Unmounting a module after testing

After testing, leave the support feed gas ($N_2$) and sweep gas (Ar) only and shut the rest of the valves on the set-up. Remaining hydrogen should be swept away for about 1 hour at high temperature (300°C or over).

The module should then be cooled down to room temperature. Apply a downward temperature ramp with the oven controller and take the fibreglass rolls off the oven.

Once at room temperature, put the $N_2$ and Ar controller setpoints to 0.0 in LabView / MiniLab and close switches on the set-up.

Undo pipe bolts on the module and unscrew all six bolts. Pick up the copper gasket with pliers.

# Appendix C
# MASS FLOW CONTROLLER CALIBRATION

The mass flow controllers and their specification are given in Table C.1.

Table C.1 – Mass flow controllers

| Channel | Gas type | MFC-nr | Range |
|---------|----------|--------|-------|
| 3 | $N_2$ | 0202022 D | 100nml/min |
| (10) | Ar | 8209668 B | 1000nml/min |
| (11) | $H_2$ | 14202819 A | 1000nml/min |

The flowrate were measured at different set-points and plotted for each gas. The calibration curves are given below in Figure C1.
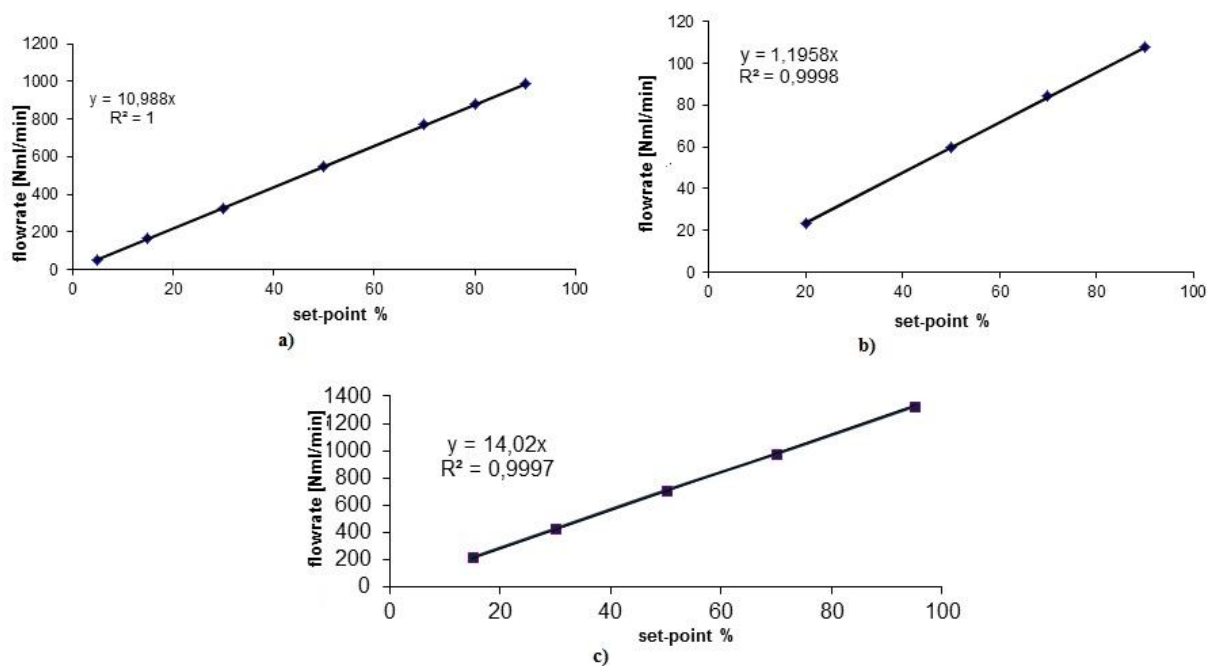


Figure C1 – Calibration curves a) Hydrogen b) Nitrogen and c) Argon

The calibration describes the difference in the set-point and the actual flow, and a trend line gives the slope which is used in laview to correct the flow.

# Appendix D
# HYDROGEN PERMEATION

Hydrogen flux as a function of exposure time at 350 ℃ for $Pd_{1-x}Cu_x$ membranes is presented in Figure D1 and D2.
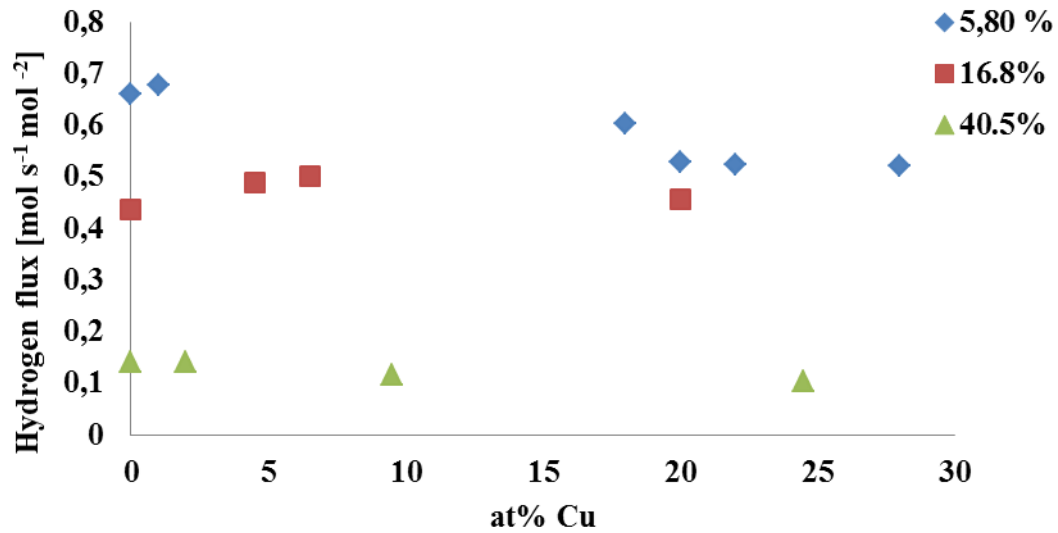


Figure D1 – Hydrogen flux as a function of time at 350 ℃
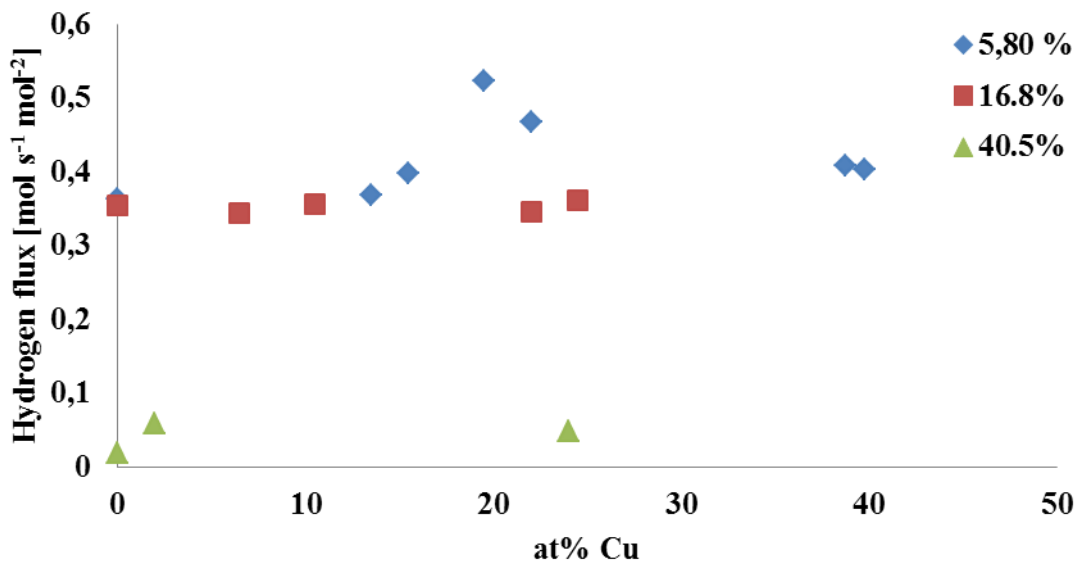


Figure D2 - Hydrogen flux as a function of time at 300 ℃

The permeance and permeability for the membrane with 5.8at% and 16.8at% copper content at various differential pressures for 350℃ and 300℃ is given in Table D1 and D2.

Table D.1 – Calculated permeance and permeability for the $Pd_{1-x}Cu_x$ samples upon stabilization in hydrogen at 350 ℃

| Concentration of Cu [at%] | Pressure difference [Pa] | Permeance [mol m$^{-2}$s$^{-2}$Pa$^{-0,5}$] | Permeability [mol m m$^{-2}$s$^{-2}$Pa$^{-0,5}$] |
|---|---|---|---|
| 5.8 | 0.5 | $3.9 \cdot 10^{-3}$ | $8.5 \cdot 10^{-9}$ |
| | 1.0 | $3.9 \cdot 10^{-3}$ | $8.6 \cdot 10^{-9}$ |
| | 1.5 | $4.3 \cdot 10^{-3}$ | $9.6 \cdot 10^{-9}$ |
| 16.8 | 0.5 | $3.9 \cdot 10^{-3}$ | $6.7 \cdot 10^{-9}$ |
| | 1.0 | $3.8 \cdot 10^{-3}$ | $6.5 \cdot 10^{-9}$ |
| | 1.5 | $3.8 \cdot 10^{-3}$ | $6.5 \cdot 10^{-9}$ |

Table D.2 – Calculated permeance and permeability for the $Pd_{1-x}Cu_x$ samples upon stabilization in hydrogen at 300 ℃

| Concentration of Cu [at%] | Pressure difference [Pa] | Permeance [mol m$^{-2}$s$^{-2}$Pa$^{-0,5}$] | Permeability [mol m m$^{-2}$s$^{-2}$Pa$^{-0,5}$] |
|---|---|---|---|
| 5.8 | 0.5 | $3.0 \cdot 10^{-3}$ | $6.6 \cdot 10^{-9}$ |
| | 1.0 | $3.7 \cdot 10^{-3}$ | $8.2 \cdot 10^{-9}$ |
| | 1.5 | $3.0 \cdot 10^{-3}$ | $6.8 \cdot 10^{-9}$ |
| 16.8 | 0.5 | $3.1 \cdot 10^{-3}$ | $5.3 \cdot 10^{-9}$ |
| | 1.0 | $3.1 \cdot 10^{-3}$ | $5.3 \cdot 10^{-9}$ |
| | 1.5 | $3.0 \cdot 10^{-3}$ | $5.1 \cdot 10^{-9}$ |

# Appendix E
# SORPTION PROCEDURE

## PALLADIUM SILVER

The program sequence for Pd-Ag membranes at different temperatures are given in Figure E.1-3.

Table E.1 – Sequence performed at 300 ℃ Pd-Ag.

| Task | Gas | Temperature [℃] | Rate [℃/min] | Time [min] |
|---|---|---|---|---|
| Evacuation | Helium | 100 | 10 | 30 |
| Evacuation | Helium | 300 | 10 | 15 |
| Evacuation | | 300 | 10 | 120 |
| Leak test | | 300 | 10 | - |
| Evacuation | | 300 | 10 | 60 |
| Flow | $H_2$ | 350 | | 15 |
| Analysis | $H_2$ | 300 | 10 | - |

Table E.2 – Sequence performed at 350 ℃ Pd-Ag.

| Task | Gas | Temperature [℃] | Rate [℃/min] | Time [min] |
|---|---|---|---|---|
| Evacuation | Helium | 100 | 10 | 30 |
| Evacuation | Helium | 300 | 10 | 15 |
| Evacuation | | 300 | 10 | 120 |
| Leak test | | 300 | 10 | - |
| Evacuation | | 300 | 10 | 60 |
| Flow | $H_2$ | 300 | 10 | 15 |
| Analysis | $H_2$ | 350 | 10 | - |

Table E.3 – Sequence performed at 400 ℃ Pd-Ag.

| Task | Gas | Temperature [℃] | Rate [℃/min] | Time [min] |
|---|---|---|---|---|
| Evacuation | Helium | 100 | 10 | 30 |
| Evacuation | Helium | 300 | 10 | 15 |
| Evacuation | | 300 | 10 | 120 |
| Leak test | | 300 | 10 | - |
| Evacuation | | 300 | 10 | 60 |
| Flow | H₂ | 300 | 10 | 15 |
| Analysis | H₂ | 400 | 10 | - |

## TEST PROGRAMS PALLADIUM COPPER

The sequence performed for the two test membranes, 5.8 at% and 40.5 at% of copper, are described. The tables describe the programing at each temperature, and they are order like it was done. The equilibrium interval time, $t_e$, is noted for each test, and the cells were a change is tested, are shaded.

The procedure for tests on a membrane with 5.8 at% copper content is given in Table E4-10.

Table E.4 – Sequence performed at 300 ℃, $t_e$=60s.

| Task | Gas | Temperature [℃] | Rate [℃/min] | Time [min] |
|---|---|---|---|---|
| Evacuation | Helium | 100 | 10 | 30 |
| Evacuation | Helium | 300 | 10 | 15 |
| Evacuation | | 300 | 10 | 120 |
| Leak test | | 300 | 10 | - |
| Evacuation | | 300 | 10 | 60 |
| Analysis | H₂ | 300 | 10 | - |

Table E.5 – Sequence performed at 400 ℃, $t_e$=60s.

| Task | Gas | Temperature [℃] | Rate [℃/min] | Time [min] |
|---|---|---|---|---|
| Evacuation | Helium | 100 | 10 | 30 |
| Evacuation | Helium | 300 | 10 | 15 |
| Evacuation | | 300 | 10 | 120 |
| Leak test | | 300 | 10 | - |
| Evacuation | | 400 | 10 | 120 |
| Flow | H₂ | 400 | 10 | 15 |
| Analysis | H₂ | 400 | 10 | - |

**Table E.6 – Sequence performed at 400 ℃, $t_4$=60s.**

| Task | Gas | Temperature [℃] | Rate [℃/min] | Time [min] |
|---|---|---|---|---|
| Evacuation | Helium | 100 | 10 | 30 |
| Evacuation | Helium | 300 | 10 | 15 |
| Evacuation | | 300 | 10 | 120 |
| Leak test | | 300 | 10 | - |
| Evacuation | | 400 | 10 | 180 |
| Flow | $H_2$ | 400 | 10 | 15 |
| Analysis | $H_2$ | 400 | 10 | - |

**Table E.7 – Sequence performed at 400 ℃, $t_4$=20s.**

| Task | Gas | Temperature [℃] | Rate [℃/min] | Time [min] |
|---|---|---|---|---|
| Evacuation | Helium | 100 | 10 | 30 |
| Evacuation | Helium | 300 | 10 | 15 |
| Evacuation | | 300 | 10 | 120 |
| Leak test | | 300 | 10 | - |
| Evacuation | | 400 | 10 | 120 |
| Flow | $H_2$ | 400 | 10 | 15 |
| Analysis | $H_2$ | 400 | 10 | - |

**Table E.8 – Sequence performed at 300 ℃, $t_4$=60s.**

| Task | Gas | Temperature [℃] | Rate [℃/min] | Time [min] |
|---|---|---|---|---|
| Evacuation | Helium | 100 | 10 | 30 |
| Evacuation | Helium | 300 | 10 | 15 |
| Evacuation | | 300 | 10 | 120 |
| Leak test | | 300 | 10 | - |
| Evacuation | | 300 | 10 | 60 |
| Analysis | $H_2$ | 300 | 10 | - |

**Table E.9 – Sequence performed at 400 ℃, $t_4$=120s.**

| Task | Gas | Temperature [℃] | Rate [℃/min] | Time [min] |
|---|---|---|---|---|
| Evacuation | Helium | 100 | 10 | 30 |
| Evacuation | Helium | 300 | 10 | 15 |
| Evacuation | | 300 | 10 | 120 |
| Leak test | | 300 | 10 | - |
| Evacuation | | 400 | 10 | 120 |
| Flow | $H_2$ | 400 | 10 | 15 |
| Analysis | $H_2$ | 400 | 10 | - |

**Table E.10 – Sequence performed at 400 ℃, $t_4$=10s.**

| Task | Gas | Temperature [℃] | Rate [℃/min] | Time [min] |
|---|---|---|---|---|
| Evacuation | Helium | 100 | 10 | 30 |
| Evacuation | Helium | 300 | 10 | 15 |
| Evacuation | | 300 | 10 | 120 |
| Leak test | | 300 | 10 | - |
| Evacuation | | 400 | 10 | 120 |
| Flow | $H_2$ | 400 | 10 | 15 |
| Analysis | $H_2$ | 400 | 10 | - |

The procedure for tests on a membrane with 40.5 at% copper is given in Table E.11-16.

Table E.11 – A repeated sequence performed at 300 °C, $t_a$=20s.

| Task | Gas | Temperature [°C] | Rate [°C/min] | Time [min] |
|---|---|---|---|---|
| Evacuation | Helium | 100 | 10 | 30 |
| Evacuation | Helium | 300 | 10 | 15 |
| Evacuation | | 300 | 10 | 120 |
| Leak test | | 300 | 10 | - |
| Evacuation | | 300 | 10 | 60 |
| Analysis | H₂ | 300 | 10 | - |

Table E.12 – Sequence performed at 400 °C, $t_a$=20s.

| Task | Gas | Temperature [°C] | Rate [°C/min] | Time [min] |
|---|---|---|---|---|
| Evacuation | Helium | 100 | 10 | 30 |
| Evacuation | Helium | 300 | 10 | 15 |
| Evacuation | | 300 | 10 | 120 |
| Leak test | | 300 | 10 | - |
| Evacuation | | 350 | 10 | 120 |
| Flow | H₂ | 350 | 10 | 15 |
| Analysis | H₂ | 400 | 10 | - |

Table E.13 – Sequence performed at 400 °C, $t_a$=20s.

| Task | Gas | Temperature [°C] | Rate [°C/min] | Time [min] |
|---|---|---|---|---|
| Evacuation | Helium | 100 | 10 | 30 |
| Evacuation | Helium | 300 | 10 | 15 |
| Evacuation | | 300 | 10 | 120 |
| Leak test | | 300 | 10 | - |
| Evacuation | | 400 | 10 | 120 |
| Flow | H₂ | 400 | 10 | 15 |
| Analysis | H₂ | 400 | 10 | - |

Table E.14 – Sequence performed at 400 °C, $t_a$=10s.

| Task | Gas | Temperature [°C] | Rate [°C/min] | Time [min] |
|---|---|---|---|---|
| Evacuation | Helium | 100 | 10 | 30 |
| Evacuation | Helium | 300 | 10 | 15 |
| Evacuation | | 300 | 10 | 120 |
| Leak test | | 300 | 10 | - |
| Evacuation | | 400 | 10 | 120 |
| Flow | H₂ | 400 | 10 | 15 |
| Analysis | H₂ | 400 | 10 | - |

Table E.15 – Sequence performed at 400 °C, $t_a$=20s.

| Task | Gas | Temperature [°C] | Rate [°C/min] | Time [min] |
|---|---|---|---|---|
| Evacuation | Helium | 100 | 10 | 30 |
| Evacuation | Helium | 300 | 10 | 15 |
| Evacuation | | 300 | 10 | 120 |
| Leak test | | 300 | 10 | - |
| Evacuation | | 350 | 10 | 120 |
| Flow | H₂ | 350 | 10 | 15 |
| Analysis | H₂ | 400 | 10 | - |

Table E.16 – Sequence performed at 300 °C, $t_a$=60s.

| Task | Gas | Temperature [°C] | Rate [°C/min] | Time [min] |
|---|---|---|---|---|
| Evacuation | Helium | 100 | 10 | 30 |
| Evacuation | Helium | 300 | 10 | 15 |
| Evacuation | | 300 | 10 | 120 |
| Leak test | | 300 | 10 | - |
| Evacuation | | 300 | 10 | 60 |
| Analysis | H₂ | 300 | 10 | - |

## Appendix F
# ISOTHERM SORPTION RESULTS

The resulting isotherm for each sample at each temperature is presented below.

### PALLADIUM SILVER

The results for 6µm and 8.5 µm Pd-Ag 23wt% membrane is given are Figure F.1, from the procedure described in Table E1-3.



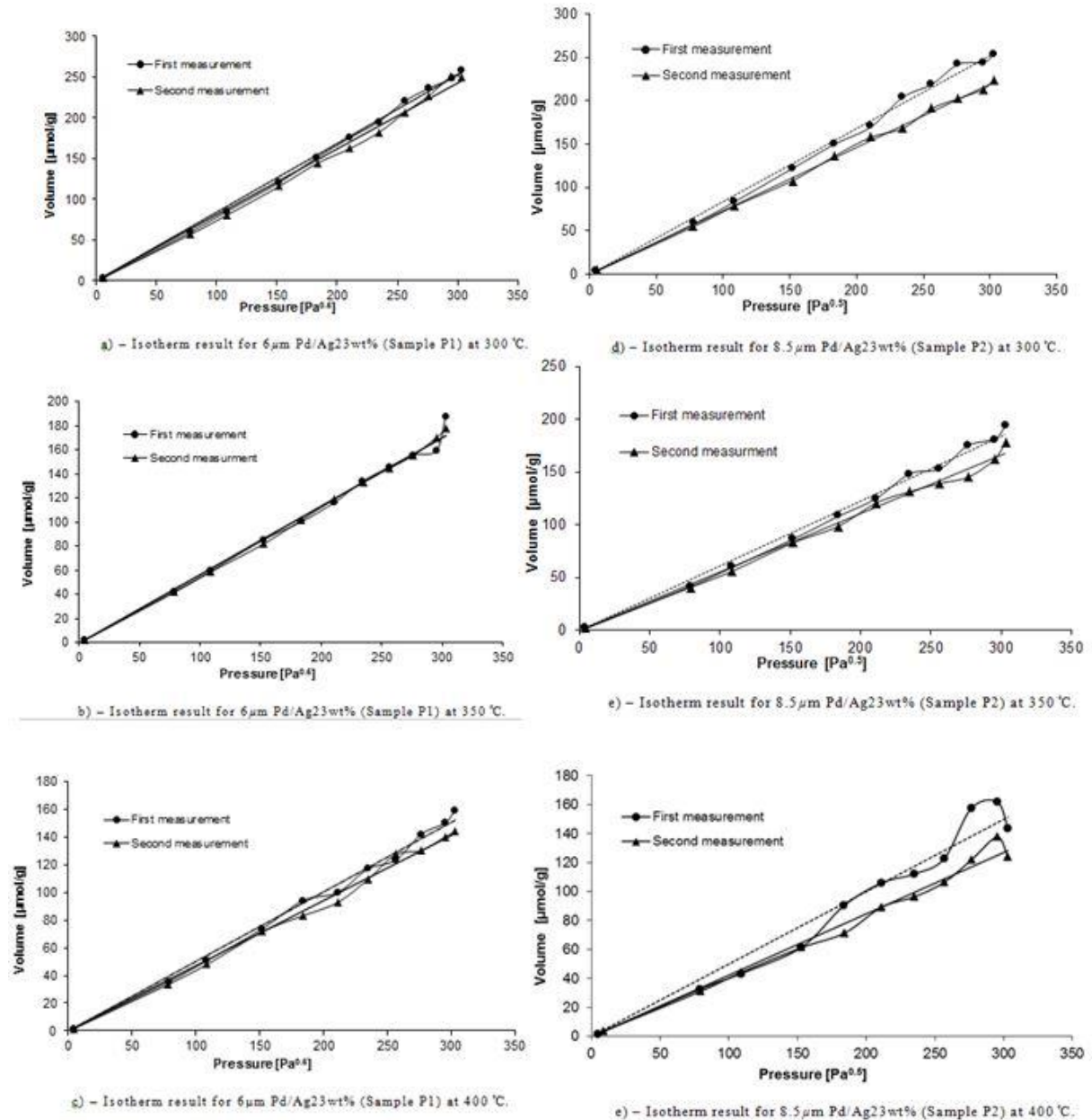Figure F.1 – Equilibrium hydrogen isotherms for 6µm(a-c) and 8.5µm(d-e) Pd-Ag membranes at 300℃, 350℃ and 400℃

## TEST RESULTS

The results for the test on Pd-Cu membrane with 5.8 at% copper is given are Figure F.2.



a) – Isotherm result for Pd-Cu5.8wt% (Sample T1) at 300 ℃.

b) – Isotherm result for Pd-Cu5.8wt% (Sample T1) at 400 ℃.

c) – Isotherm result for Pd-Cu5.8wt% (Sample T1) at 400 ℃.

Figure F.2 – Equilibrium hydrogen isotherms for tests done on Pd-Cu with 5.8at% copper.

- Figure F.2a) present the procedures from Table E.4 and E.8: 300 ℃ before and after 400 ℃ with 60s equilibrium interval time.

- Figure F.2.b) present the procedures from Table E.5 and E.6 with equilibrium time at 60s and various evacuation time (120min and 180min).

- Figure F.2.c) present the procedures from Table E.5, E.7, E.9 and E.10 respectively first, second, third and fourth measurement, with evacuation for 120min and various equilibrium interval time (60s, 20s, 120s and 10s).

The results for the test on Pd-Cu membrane with 40.5 at% copper is given are Figure F.3.



a) – Isotherm result for Pd-Cu40.5wt% (Sample T2) at 300 ℃.

b) – Isotherm result for Pd-C40.5wt% (Sample T2) at 400 ℃

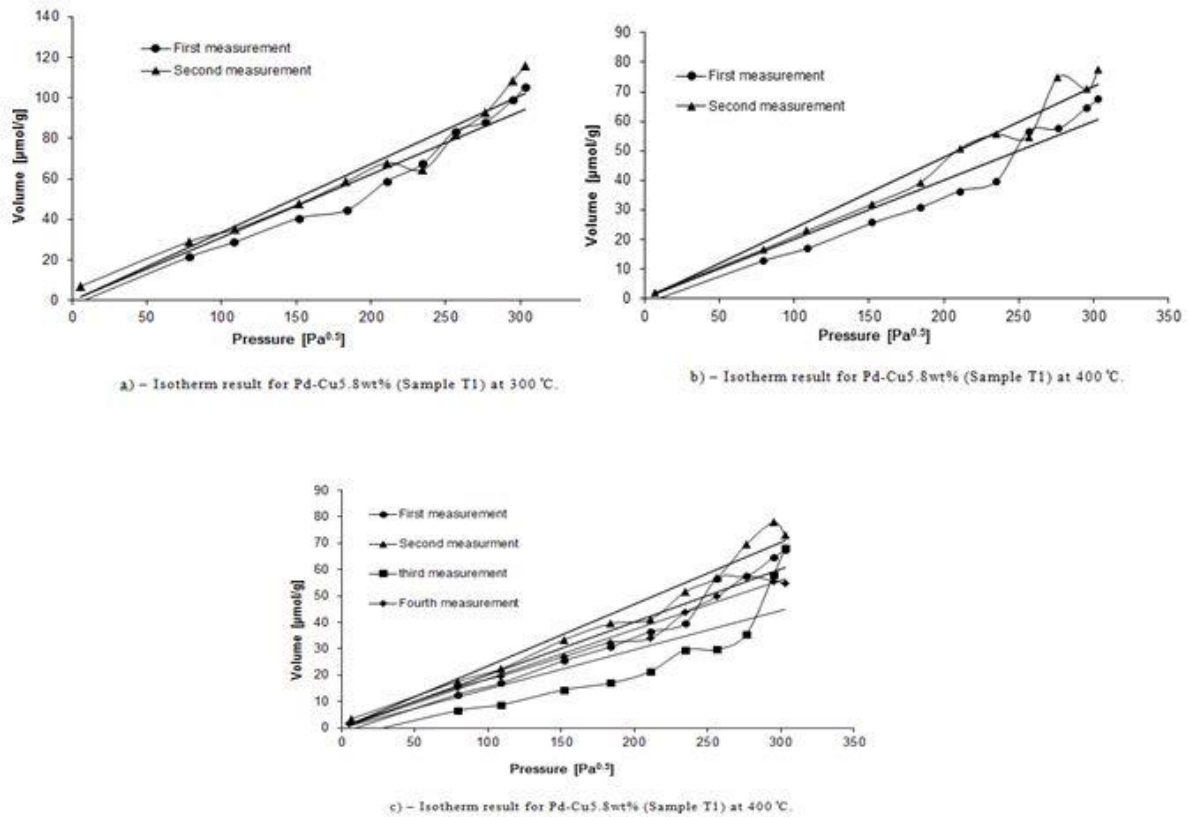c) – Isotherm result for Pd-Cu40.5wt% (Sample T2) at 400 ℃.
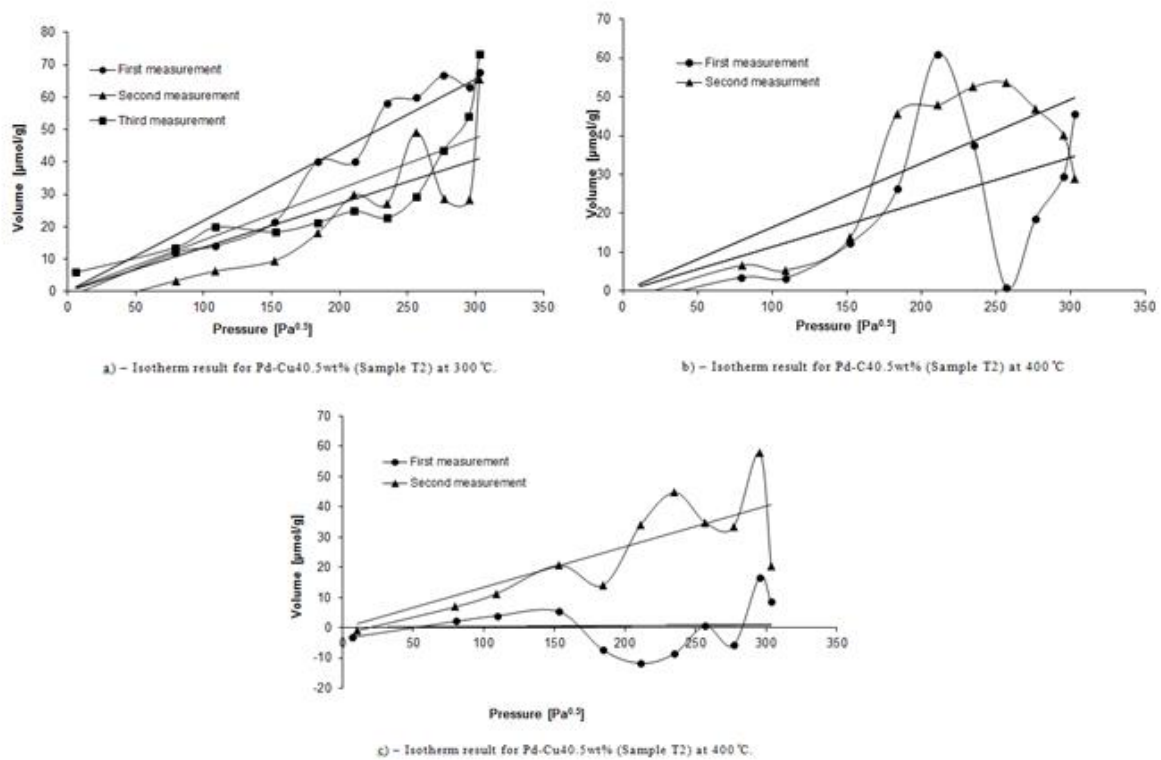
Figure F.3 – Equilibrium hydrogen isotherms for tests done on Pd-Cu with 40.5at% copper.

- Figure F.3a) present the procedures from Table E11 and E16: First and second measurement is programed repeated with no time between, and the third measurement is after some experiments at 400 ℃

- Figure F.3.b) present the procedures from Table E.12 and E.15 which is the same, just with experiments done between. The special with these two is that the evacuation and flow runs at 350 ℃, before the analysis at 400 ℃.

- Figure F.3.c) present the procedures from Table E13 and E.14: where the equilibrium interval time is 20s and 10s.

## PALLADIUM COPPER

The results for Pd-Cu membranes with a copper content of 5.8 at% and 16.8 at% are given are Figure F.4, and described by the procedure in Table E.1-3.



a) – Isotherm result for Pd-Cu5.8wt% (Sample S1) at 300 ℃.

d) – Isotherm result Pd-Cu16.8wt% (Sample S2) at 300 ℃.

b) – Isotherm result Pd-Cu5.8wt% (Sample S1) at 350 ℃.

e) – Isotherm result for Pd-Cu16.8wt% (Sample S2) at 350 ℃.

c) – Isotherm result forPd-Cu5.8wt% (Sample S1) at 400 ℃.

f) – Isotherm result for Pd-Cu16.8wt% (Sample S2) at 400 ℃.

Figure F.4 – Equilibrium hydrogen isotherms for 5.8at% (a-c) and 16.8at% (d-f) copper in Pd-Cu membranes at 300 ℃, 350 ℃ and 400 ℃

The results for Pd-Cu membranes with a copper content of 20.7 at% and 36.9 at% are given are Figure F.5.



a) – Isotherm result for Pd-Cu20.7wt% (Sample S3) at 300 ℃.

d) – Isotherm result for Pd-Cu36.9wt% (Sample S4) at 300 ℃.

b) – Isotherm result for Pd-Cu20.7wt% (Sample S3) at 350 ℃.

e) – Isotherm result for Pd-Cu36.9wt% (Sample S4) at 350 ℃.

c) – Isotherm result for Pd-Cu20.7wt% (Sample S3) at 400 ℃.

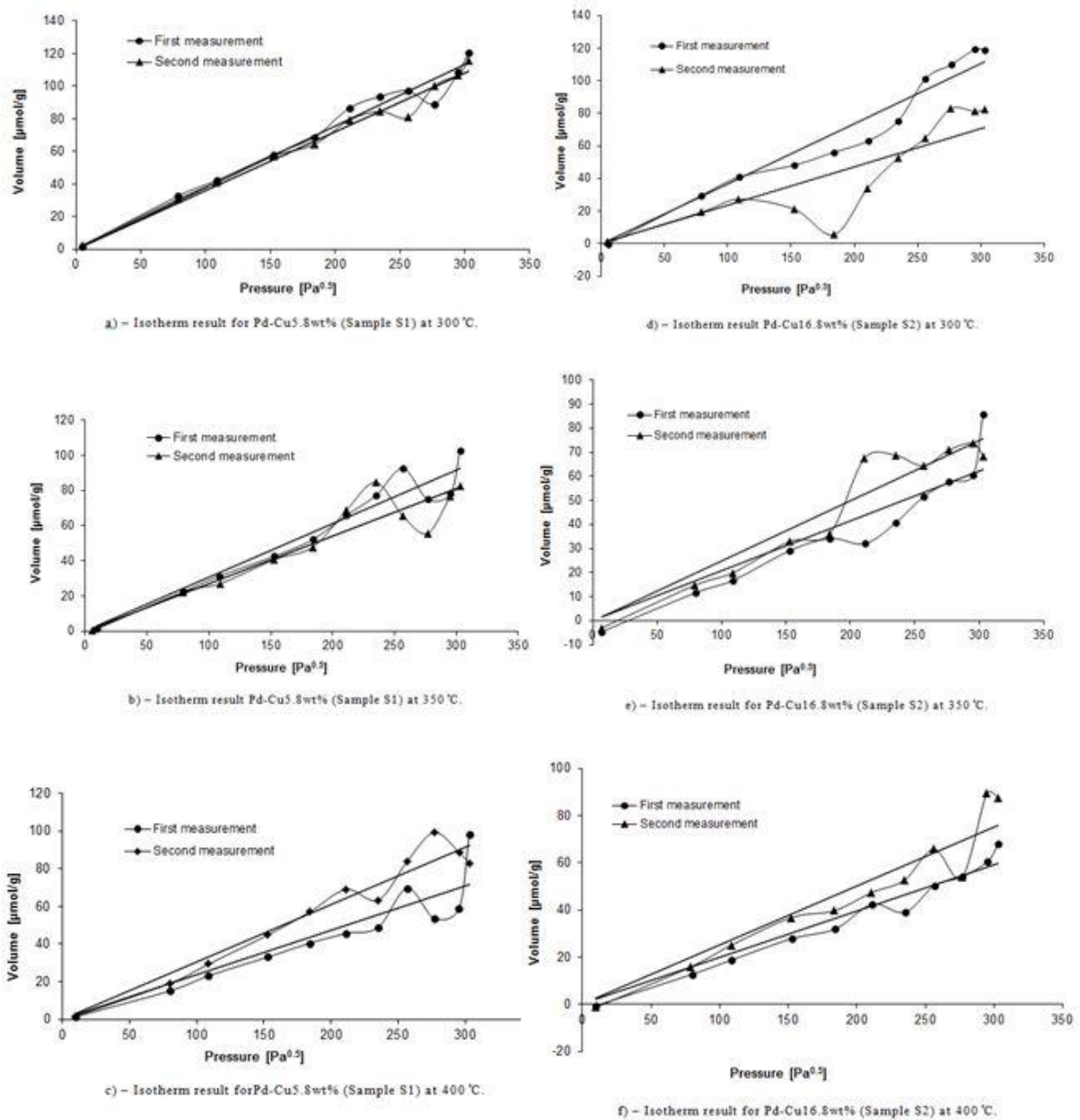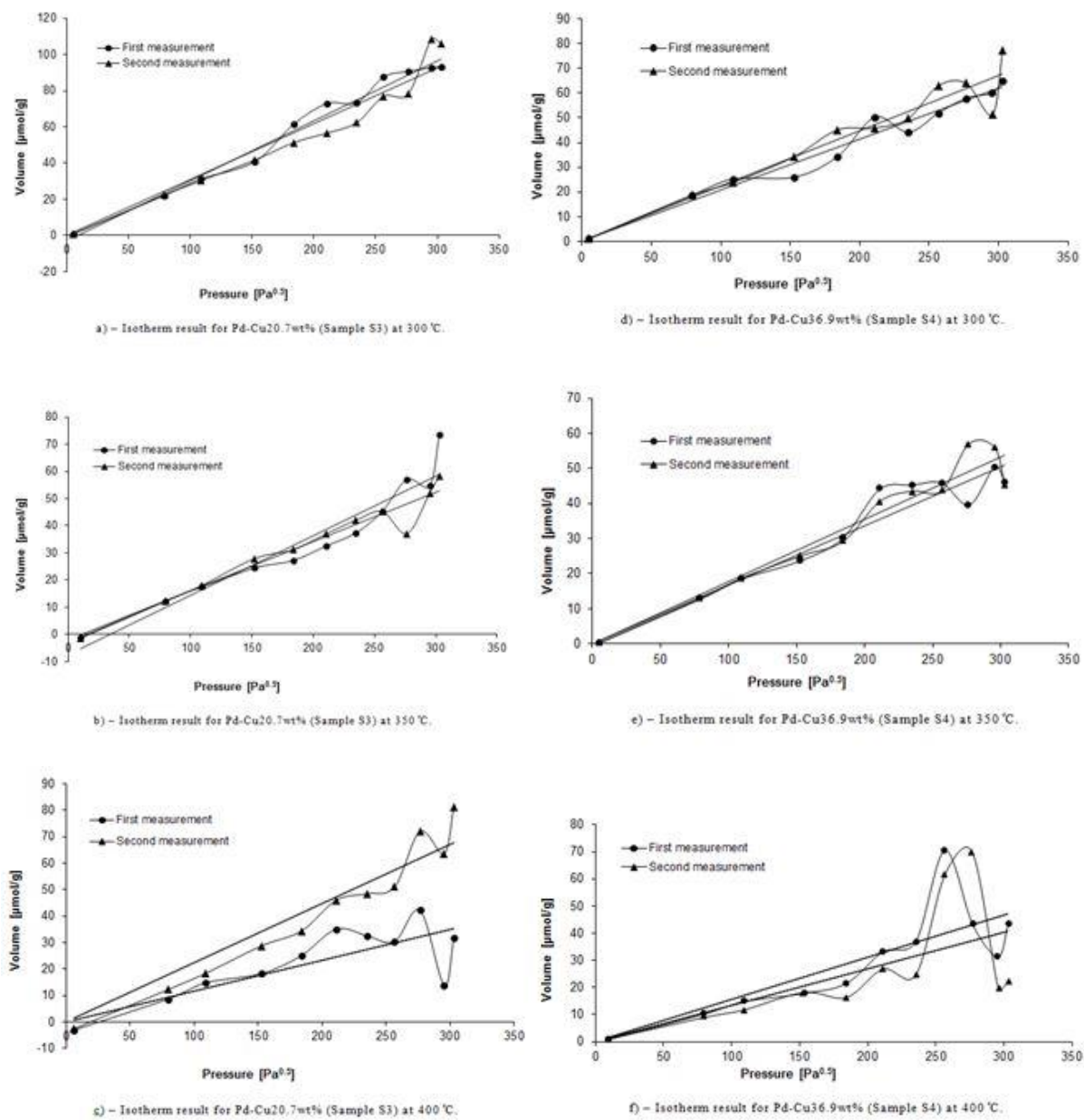f) – Isotherm result for Pd-Cu36.9wt% (Sample S4) at 400 ℃.

Figure F.5 – Equilibrium hydrogen isotherms for 20.7at% (a-c) and 36.9at% (d-f) copper in Pd-Cu membranes at 300 ℃, 350 ℃ and 400 ℃

The results for Pd-Cu membranes with a copper content of 40.5 at% and 55.1 at% are given are Figure F.6.



a) – Isotherm result for Pd-Cu40.5wt% (Sample S5) at 300 °C.

d) – Isotherm result for Pd-Cu 55.1wt% (Sample S6) at 300

b) – Isotherm result for Pd-Cu40.5wt% (Sample S5) at 350 °C.

e) – Isotherm result for Pd-Cu 55.1wt% (Sample S6) at 350 °C

c) – Isotherm result for Pd-Cu 40.5wt% (Sample S5) at 400 °C

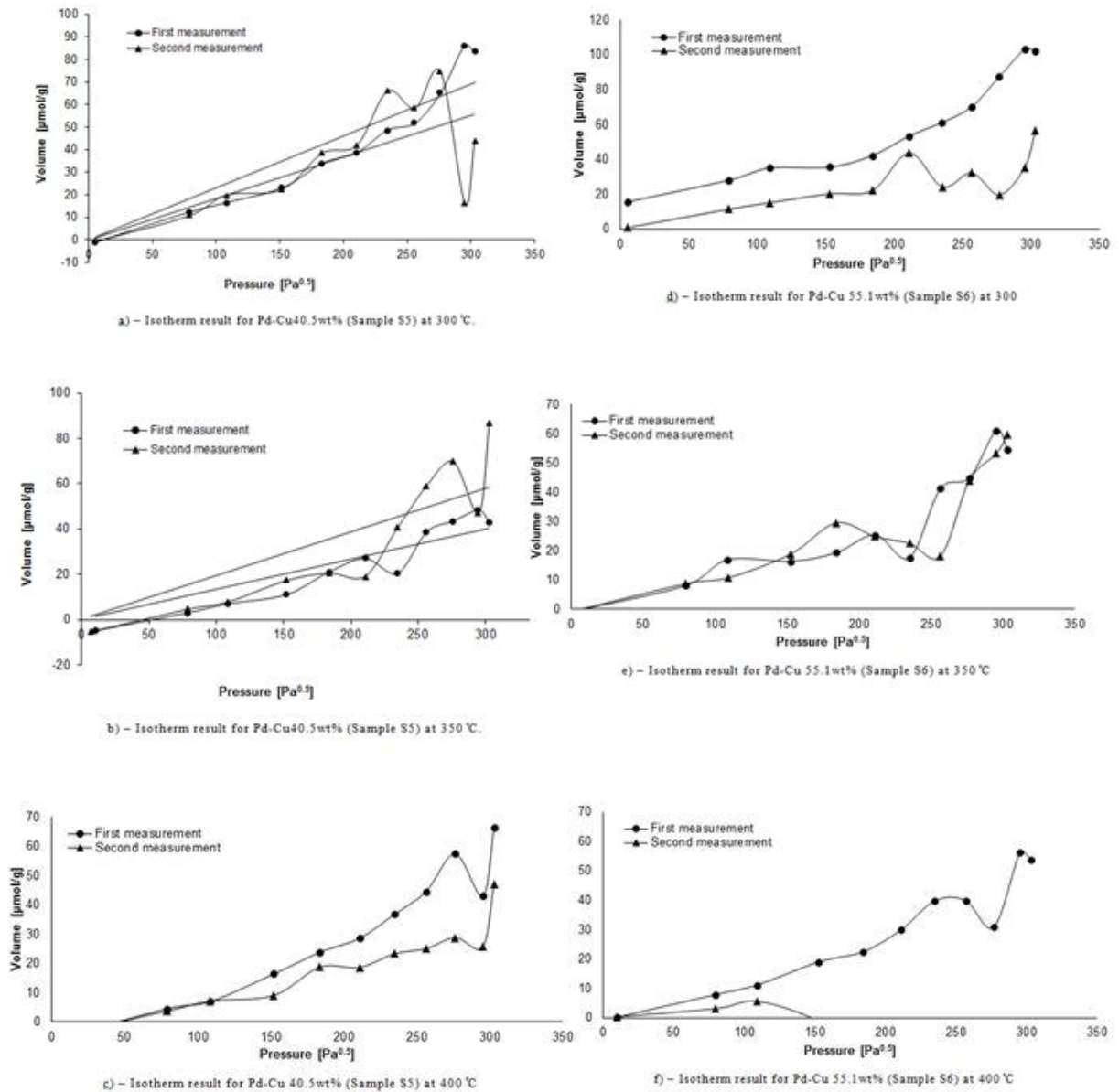f) – Isotherm result for Pd-Cu 55.1wt% (Sample S6) at 400 °C

Figure F.6 – Equilibrium hydrogen isotherms for 40.5at% (a-c) and 55.1at% (d-f) copper in Pd-Cu membranes at 300 °C, 350 °C and 400 °C

## MODIFIED FIT RESULTS

A modified isotherm up to 200Pa$^{0.5}$ is described for each sample at each temperature in the section below.

The results for Pd-Cu membranes with a copper content of 5.8 at% and 16.8 at% are given are Figure F.7.
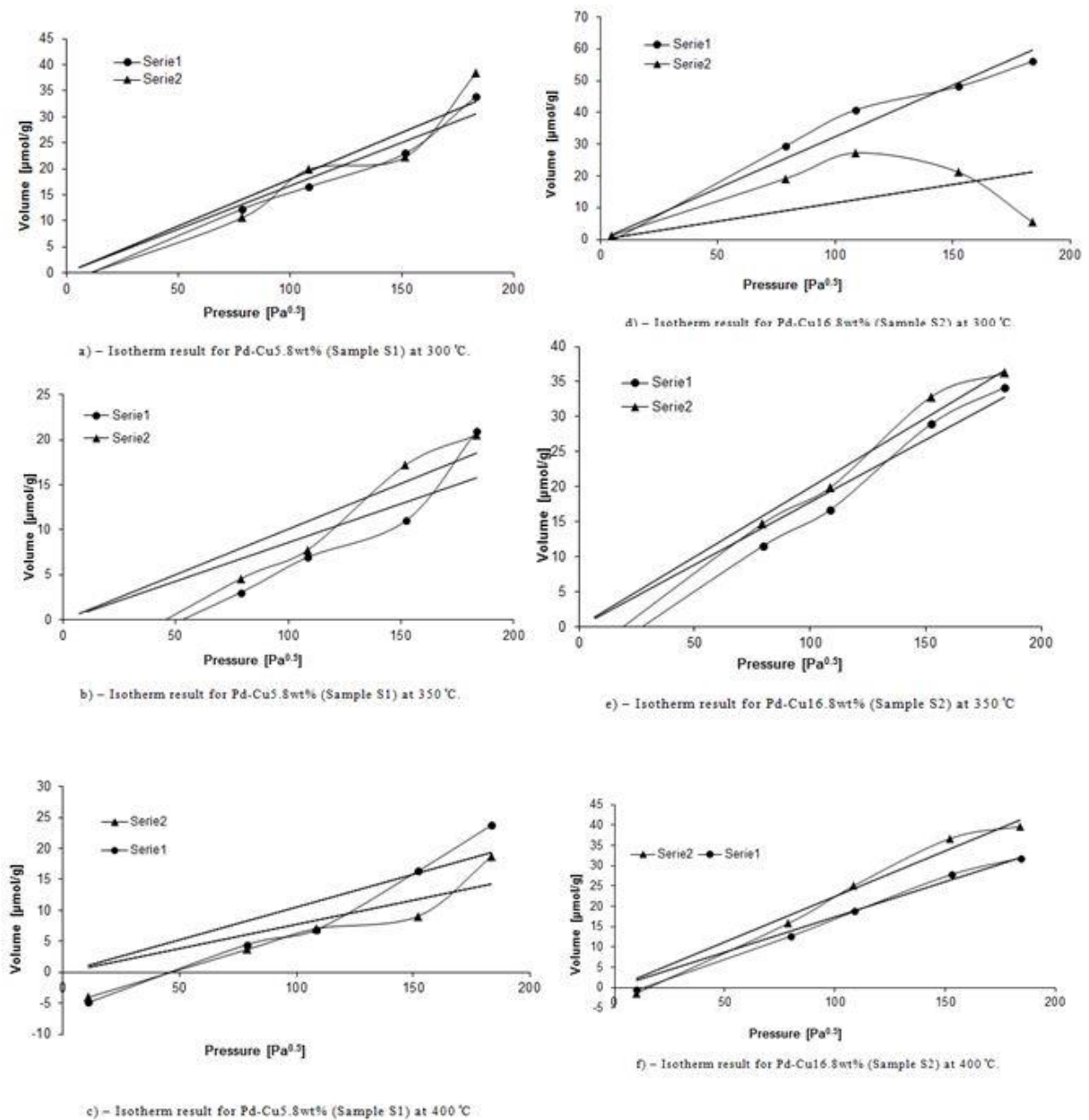


a) – Isotherm result for Pd-Cu5.8wt% (Sample S1) at 300 ℃.

d) – Isotherm result for Pd-Cu16.8wt% (Sample S2) at 300 ℃.

b) – Isotherm result for Pd-Cu5.8wt% (Sample S1) at 350 ℃.

e) – Isotherm result for Pd-Cu16.8wt% (Sample S2) at 350 ℃

c) – Isotherm result for Pd-Cu5.8wt% (Sample S1) at 400 ℃

f) – Isotherm result for Pd-Cu16.8wt% (Sample S2) at 400 ℃.

Figure F.7 – Equilibrium hydrogen isotherms for 5.8at% (a-c) and 16.8at% (d-f) copper in Pd-Cu membranes at 300 ℃, 350 ℃ and 400 ℃

The results for Pd-Cu membranes with a copper content of 20.7 at% and 36.9 at% are given are Figure F.8.



a) – Isotherm result for Pd-Cu20.7wt% (Sample S3) at 300 ℃.

d) – Isotherm result for Pd-Cu36.9wt% (Sample S4) at 300 ℃.

b) – Isotherm result for Pd-Cu20.7wt% (Sample S3) at 350 ℃

e) – Isotherm result for Pd-Cu36.9wt% (Sample S4) at 350 ℃.

c) – Isotherm result for Pd-Cu20.7wt% (Sample S3) at 400 ℃.

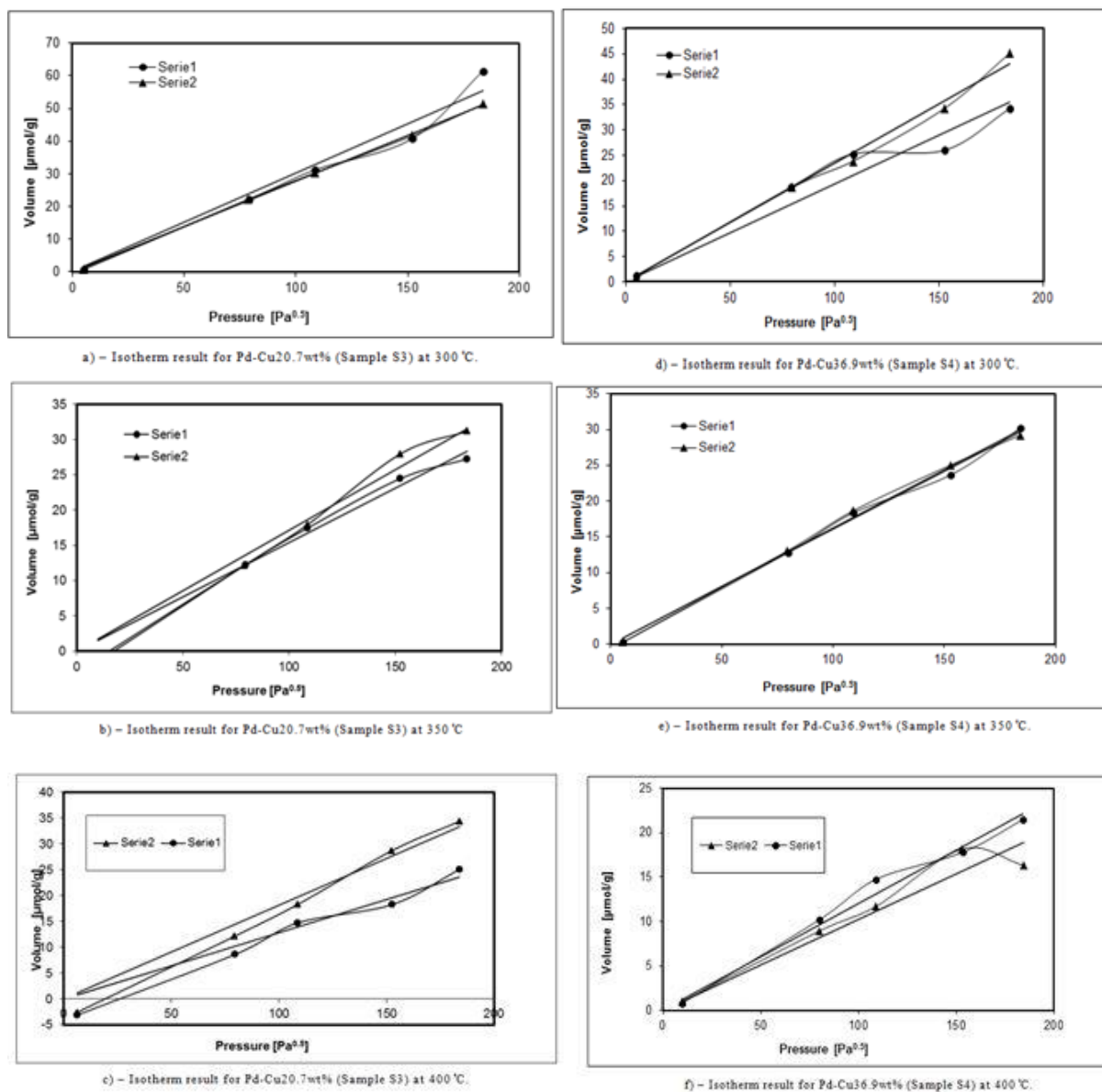f) – Isotherm result for Pd-Cu36.9wt% (Sample S4) at 400 ℃.

Figure F.8 – Equilibrium hydrogen isotherms for 20.7at% (a-c) and 36.9at% (d-f) copper in Pd-Cu membranes at 300 ℃, 350 ℃ and 400 ℃

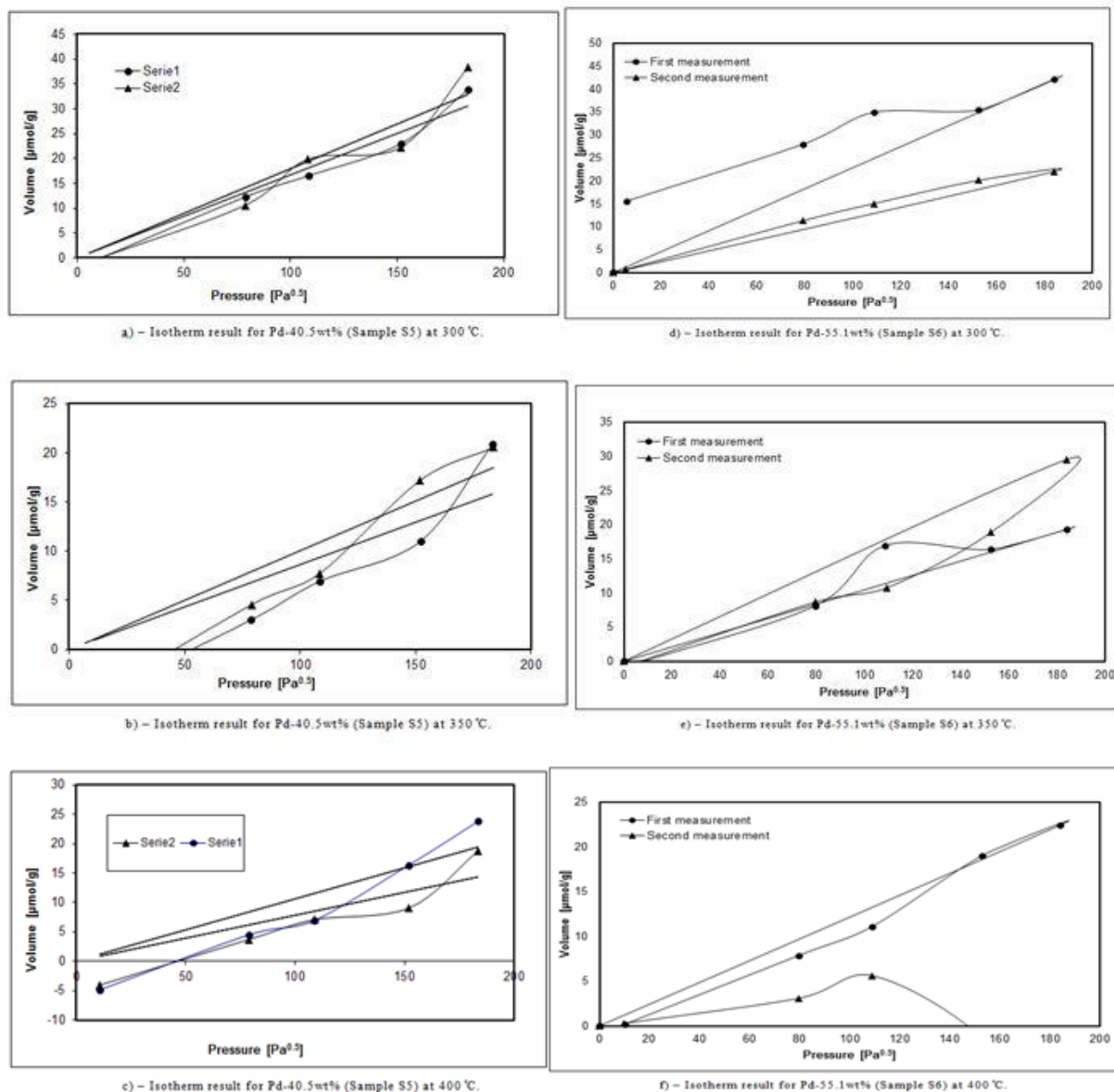The results for Pd-Cu membranes with a copper content of 40.5 at% and 55.1 at% are given are Figure F.9.



a) – Isotherm result for Pd-40.5wt% (Sample S5) at 300 ℃.

d) – Isotherm result for Pd-55.1wt% (Sample S6) at 300 ℃.

b) – Isotherm result for Pd-40.5wt% (Sample S5) at 350 ℃.

e) – Isotherm result for Pd-55.1wt% (Sample S6) at 350 ℃.

c) – Isotherm result for Pd-40.5wt% (Sample S5) at 400 ℃.

f) – Isotherm result for Pd-55.1wt% (Sample S6) at 400 ℃.

Figure F.9 – Equilibrium hydrogen isotherms for 40.5at% (a-c) and 55.1at% (d-f) copper in Pd-Cu membranes at 300 ℃, 350 ℃ and 400 ℃

# Appendix G
# GRAIN STRUCTURE RESULTS

## PALLADIUM SILVER

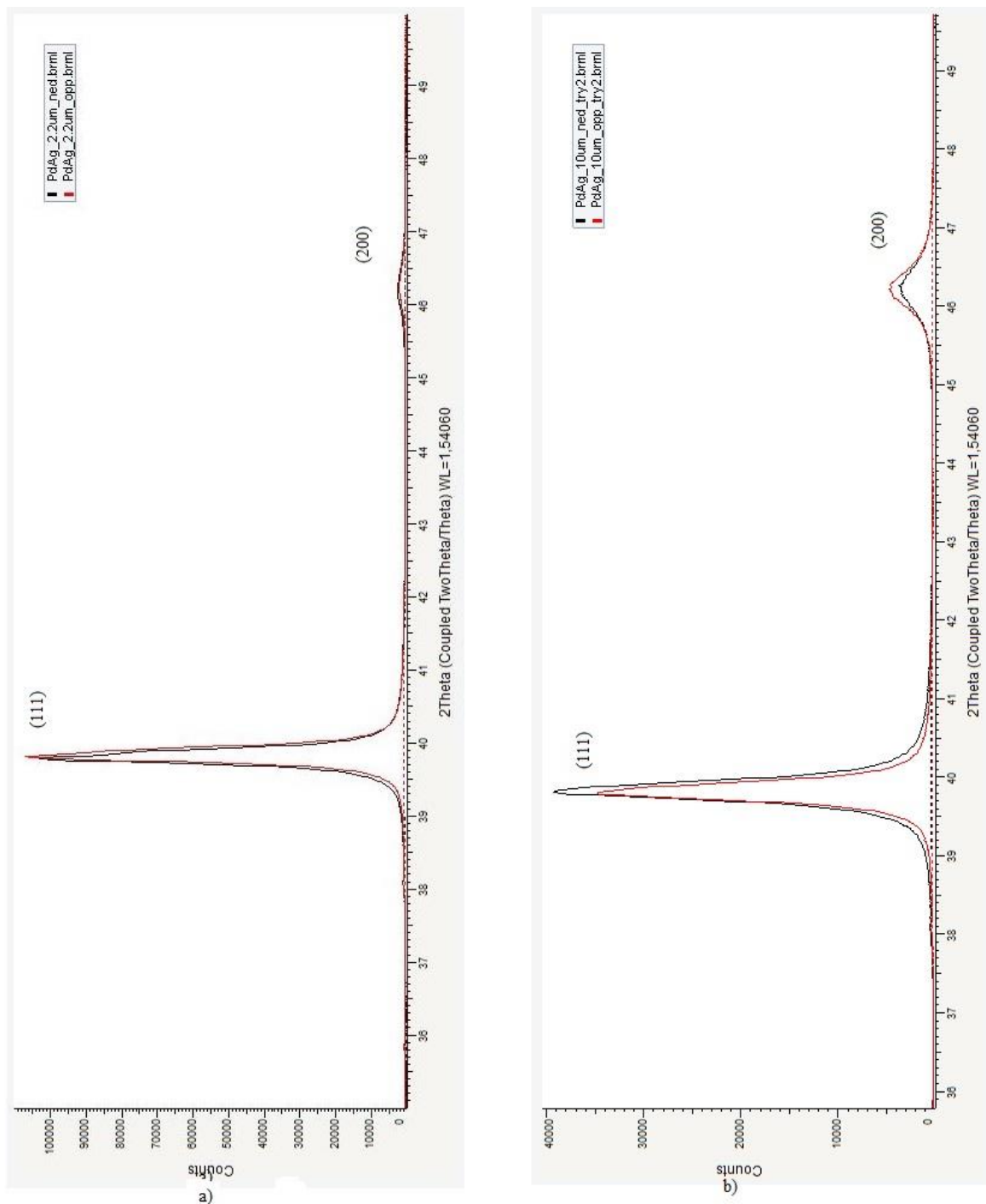The diffractogram for Pd-Ag membranes with different thickness is given below.



Figure G.1 – Diffractogram Pd-Ag a)2.2 µm and b)10 µm

## PALLADIUM COPPER

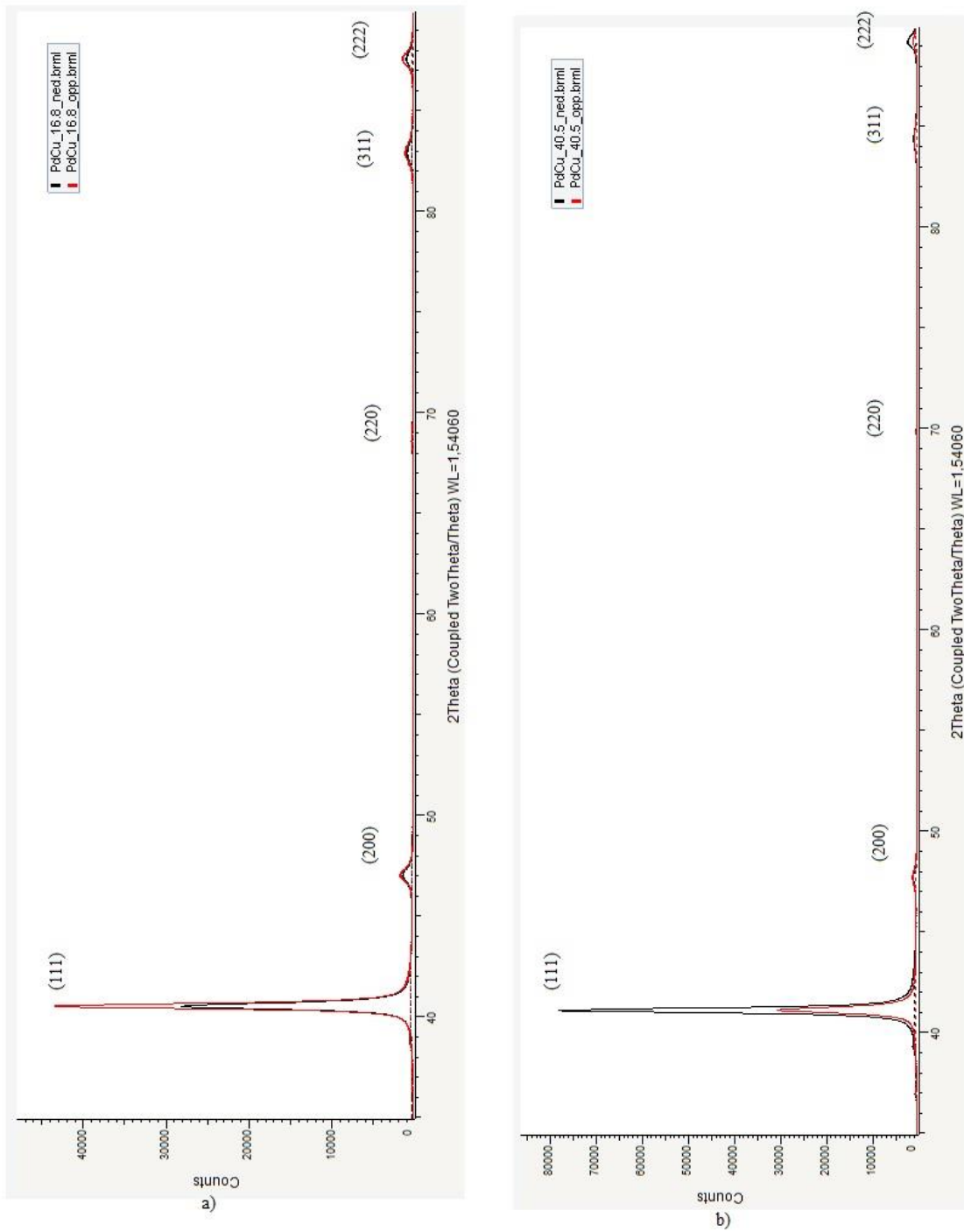The diffractogram for Pd-Cu membranes with different content is given in Figure G.2.



Figure G.2 – Diffractogram Pd-Cu a) 16.8ast% and b) 40.5at%

The crystalline size can be estimated form the size effect that broadens Bragg peaks and can be obtained from the Scherrer equation[40]:

$$D = \frac{K\lambda}{\beta cos\theta} \qquad \text{(G.1)}$$

where $D$ is the crystallite size, $\lambda$ the wavelength, $K$ a dimensionless correction factor, $\theta$ Bragg angle and $\beta$ is the peak width in $2\theta$. The program estimate the crystalline size from an evaluation of Equation G.1 with K=0,9 and the use of the full with at half-maximum of the Bragg peaks.